Multiuser MIMO Indoor Visible Light Communications

A Dissertation
Presented to
the Faculty of the School of Engineering and Applied Science
University of Virginia

In Partial Fulfillment
of the Requirements for the Degree
Doctor of Philosophy in Electrical Engineering

---

by

Jie Lian

December 2017

APPROVAL SHEET

This dissertation is submitted in partial fulfillment of the
requirements for the degree of
PhD in Electrical Engineering

Jie Lian, Author

This dissertation has been read and approved by the examining committee:

Prof. Maite Brandt-Pearce, PhD Advisor

Prof. Stephen G. Wilson , Committee Chair

Prof. Daniel S. Weller

Prof. Malathi Veeraraghavan

Prof. Stephen D. Patek

Accepted for the School of Engineering and Applied Science:

Dean, School of Engineering and Applied Science

December 2017

Abstract

Visible light communications (VLC) is an energy efficient and cost-effective solution for indoor wireless multiple access and a candidate technique to provide high-speed data transmissions. VLC systems are built as dual systems (illumination and data transmission) and have potentially higher privacy than RF communication systems due to the natural character of light. Light emitting diodes (LEDs) that work as transmitters in VLC systems have many advantages, such as ease of modulation, high power efficiency and long life expectancy [1]. Since the radio frequency (RF) spectrum is so congested, and the data transmission rate of RF communications cannot satisfy the huge demand for a high data transmission, VLC has emerged as a possible new technology for the next generation communications.

In this dissertation, we introduce a multi-LED transmitter model and a multi-detector receiver model. Based on these models and the Lambertian law, we derive the impulse response of the indoor channel and the optical power distribution in space.

To support multiple access using VLC, we propose a centralized and four decentralized power allocation algorithms. In the centralized power allocation algorithm, all the LED lamps in the room are coordinated and controlled by a central controller; each LED lamp supports all the users within the indoor area. For standard indoor office illumination level (400 lx), about 40 users can be supported with bit error rates less than 10^{-3} using on-off keying and 70 MHz bandwidth of receivers at 5×10^{-7} W/Hz noise spectral density. The decentralized power allocation algorithms proposed have similar bit error rate performance and less computational burden compared to the centralized algorithm. Compared with the centralized algorithm, the running time of decentralized algorithms is less than 10% of the centralized algorithm. In addition,

some practical considerations, such as shadowing effects, illumination requirements, dimming control and transmitted power quantization are taken into account. From numerical results, the proposed adaptive power allocation algorithms can adjust the transmitted power to reduce shadowing effects and provide an excellent communication performance.

High-speed data transmission is required by modern communication systems. For VLC systems, the transmitted bit rate is also an essential consideration. An adaptive M-ary pulse amplitude modulation (M-PAM) scheme is proposed to provide high bandwidth efficiency for different channel qualities. Given the bandwidth and the power limit characteristics of LEDs, a waveform design algorithm with adaptive M-PAM modulation can be applied for high-speed transmissions. When the 3 dB bandwidth of the LEDs is 20 MHz, and the peak transmitted power is 3 Watts for 3 users, the system can achieve about 200 Mbps bit rate per user using the proposed waveform design algorithm. Channel uncertainty is considered, which can be modeled as a Gaussian random process. Together with the minimum mean squared error filters at the receivers, the optimized waveforms can reduce intersymbol and multiple access interferences together. We then propose an off-line waveform design algorithm to diminish the computational time. For the off-line algorithm, a waveform lookup table can be established in advance, and the proper waveforms can be selected from the table based on the real channel gains in real time. The performance of the off-line algorithm can be estimated by using the channel uncertainty model. Compared with DC-biased optical orthogonal frequency division multiplexing, M-PAM with optimally designed waveforms can provide an 80% higher data rate for single user.

Given the power distribution, we analyze the potential vulnerability of the system from eavesdropping outside the room. By setting up a signal to noise ratio threshold, we define a vulnerable area outside of the room through a window. We compute

the receiver aperture needed to capture the signal and what portion of the space is most vulnerable to eavesdropping. Based on the analysis, we propose a solution to improve the security by optimizing the modulation efficiency of each LED in the indoor lamp. The simulation results show that the proposed solution can improve the security considerably while maintaining the indoor communication performance.

Acknowledgements

First and foremost, I would like to thank my advisor Professor Maïté Brandt-Pearce. Her determination and commitment have always been an inspiration to me. Her deep knowledge of communication theory and her impeccable attitude towards research have greatly helped me to form a rigorous, dedicated, and creative research style for my future career life in the communication engineering field. Her strict requirement towards the quality of publication and presentation also helps me to hold myself to a higher standard.

I would like to thank my dissertation advisory committee members, Prof. Stephen G. Wilson, Prof. Daniel S. Weller, Prof. Malathi Veeraraghavan and Prof. Stephen D. Patek, for their invaluable time and helpful suggestions.

I am grateful to my parents for their patience, help and love. "A journey of one thousand miles begins with one step," my parents always encourage me to take the first step. During the five years, my parents gave me the power to finish the PhD's program. Then, I would thank my lovely wife, who always tells me how good I am when I feel stuck.

I would like to thank the China Scholarship Council for the funding support.

It is a blessing to be surrounded by many colleagues and friends at the University of Virginia. Finally, I am grateful to all my friends in Charlottesville and for making my life at U.Va. enjoyable.

Contents

List of Figures

List of Tables

List of Acronyms

APD: avalanche photo diode

ACO-OFDM: asymmetrically clipped optical OFDM

BER: bit error rate

CSI: channel state information

CDMA: code division multiple access

CM-PAJO: multi-detector PAJO

DEPA: distributed equal power allocation

DCO-OFDM: DC-biased optical OFDM

FOV: field of view

FSO: free space optical

ISI: inter-symbol interference

ITS: intelligent transportation system

JOW: joint optimal waveform

LOS: line of sight

LED: light emitting diodes

LMS-DFE: least mean square decision feedback equalization

MAI: multiple access interference

M-PAM: M-ary pulse amplitude modulation

M-PPM: M-ary pulse position modulation

M-VPPM: M-ary variable pulse position modulation

M-VPM: M-ary variable period modulation

M-PAM: M-ary pulse amplitude modulation

MIMO: multiple input multiple output

MISO: multiple input single output

MMSE: minimum mean squared error

NRZ: non-return-to-zero

OFDM: orthogonal frequency division multiplexing

OFDMA: orthogonal frequency division multiple access

OOC: optical orthogonal code

OOK: on-off keying

OCDMA: optical code division multiple access

PAJO: power allocation joint optimization

PDM-PAJO: partial distributed multi-detector PAJO

PADJO: power allocation disjoint optimization

PPNR: peak radiation power to noise ratio

PAPR: peak power to the average power ratio

PD: photodetector

PPM: pulse position modulation

RGB: red green blue

RZ: return-to-zero

RF: radio frequency

SNR: signal to noise ratio

SINR: signal to interference plus noise ratio

TDMA: time division multiple access

VLC: visible light communication

WDM-PAJO: weighted distributed multi-detector PAJO

ZF: zero forcing

List of Symbols

$\hat{h}_{qk}$: channel gain between LED q and user k

$h_l(t)$: impulse response of LEDs

$h_{qk}(t)$: impulse response from LED q to user k

A_r: area of photodetector

$\sigma^2_{\text{thermal}}$: thermal noise variance

σ^2_{shot}: shot noise variance

σ^2_{h}: channel uncertainty variance

σ^2_{ofdm}: OFDM signal variance

P_r: receiver optical power

P_b: background optical power

$P^{\max}$: peak transmitted optical power

p_{qk}: allocated power from LED q to user k

R_b: transmitted bit rate

R_s: transmitted symbol rate

R_c: transmitted chip rate

M: modulation constellation size

M_{ofdm}: modulation constellation size for OFDM

K: number of users

Q: number of lamps

N_Q: number of total LEDs

N_{sub}: number of subcarriers for OFDM

T_{ofdm}: symbol period for OFDM

V: number of detectors per user

G: gain of PD

L_f: sampling number of waveform

B^{max}: required BER

N_o: noise power spectral density

n_k: additive noise for user k

n_{clip}: clipping noise for OFDM

$\mathbf{P}$: power allocation matrix

$\mathbf{C}$: CDMA code matrix

$\mathbf{w}$: MMSE filter vector

$\mathbf{f}$: waveform vector

$\mathbf{H}$: channel matrix

$\mathbf{F}$: waveform matrix

$\mathbf{W}$: MMSE filter matrix

Ω: optimization thread

$\emptyset$: dimming parameter

ρ: responsivity

τ: SINR weight for WDM-PAJO

Λ: computational burden

γ: signal to interference plus noise ratio

ς reflection coefficient of walls

ϵ: shadowing loss coefficient

η: illumination potential

ϱ/N_{sub}: modulation index for OFDM

ϕ: radiation angle

ψ: incident angle

α: nonlinear distortion coefficient for OFDM

φ transmittance percentage through normal glass

β_q modulation efficiency for LED q

Chapter 1

Introduction

Visible light is defined as the light that is perceptible by the human eye, such as the light from the sun (red, orange, yellow, green, blue, violet, and so on), which has a wavelength ranging from 380 nm to 780 nm. Visible light communication (VLC) is a kind of optical communication that uses the light within the visible wavelength range to transmit signals. Due to the characteristics of light, VLC systems have both advantages and disadvantages over radio frequency (RF) systems. Unlike RF communication systems, there is no spectrum regulation in VLC, and many techniques in RF communications cannot be adopted in VLC directly. In this chapter, we first introduce reasons for developing VLC systems, and then, research achievements contained in this dissertation are summarized.

1.1 Background

With the rapid development of handheld technology, high data rate wireless transmissions are demanded in our daily lives. Considering the spectrum of RF communications is so congested, and that the data transmission rate of RF communications cannot satisfy huge demands for fast data transmissions, VLC has emerged as a new

possible technology for the next generation communications [3]. VLC systems are built as dual systems (illumination and data transmission) and have potentially higher privacy than RF communication systems due to the natural character of light. Light emitting diodes (LEDs) that work as transmitters in VLC systems have many advantages, such as ease of modulation, high power efficiency and long life expectancy [1]. Since LEDs have been widely used in indoor lighting systems, VLC systems are easy to be built based on the existing lighting systems.

From a survey, over 80% of the Internet demands occur in indoor environments. In addition, Wi-Fi systems cannot keep up the increasing demands of data transmissions. Therefore, an alternative indoor high-speed wireless communication method needs to be developed. VLC is a promising communication system that can provide high rate wireless data transmissions and attracts more and more research attention recently.

VLC is not only for indoor communications, but can also be applied to outdoor short-range communications, such as vehicle-to-vehicle communications. As the number of vehicles increases every year, urgent actions are needed to prevent and reduce traffic accidents as well as improving road safety [4]. Since the vehicles' headlights and taillights are usually composed of LEDs, the vehicles can communicate with each other using VLC. Then, an intelligent transportation system (ITS) can be built to improve road safety and traffic flow based on VLC networks [5].

In addition, VLC can be used for many other applications, such as smart lighting, mobile connectivity, healthcare, underwater communications, location-based services, and so on. Applications of VLC have a great potential to increase in the next decades, and these applications can change the pattern of people's lives. According to the latest market research report [6], the VLC market is expected to grow from USD 1.3 Billion in 2017 to USD 14.91 Billion by 2022, at a compound annual growth rate (CAGR) of 62.9% between 2017 and 2022.

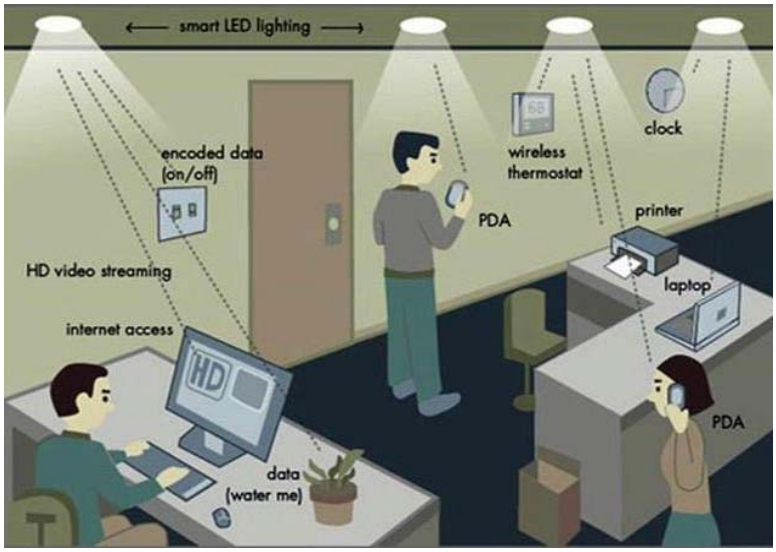

Figure 1.1: Applications for indoor VLC systems.

In this dissertation, we focus on the indoor VLC systems to serve multiple users, providing them high-speed data transmissions. As shown in Fig. 1.1, in an office room, multiple users require wireless connections at the same time, and some may need high data rate transmissions, such as, video chatting, high-definition video downloading, and so on. Therefore, indoor VLC systems are necessary for multiuser applications with a high throughput performance.

Communication systems have both uplink and downlink data transmissions. Considering that users usually require much higher data transmissions over the downlink, this dissertation only discusses the downlink systems.

1.2 Differences Between VLC and RF Communications

Due to the different characteristics between visible light and microwave, there are many differences between VLC and RF systems. In this section, a brief introduction

of these differences is presented.

Modulation

The conventional modulation schemes adopted in RF communications cannot be readily applied in VLC directly because the visible light is non-coherent. For RF systems, amplitude, frequency, and phase can be used to modulate signals. But for VLC systems, since intensity modulation and direct detection should be used, only real non-negative signals can be transmitted. In the following section, some modulation schemes for VLC are introduced.

Flicker and Dimming

Indoor VLC systems are built based on the existing lighting systems; therefore, illumination is a very important function for VLC. For illumination, a non-flickering and dimming controllable system is desired. Flicker and dimming both depend on the light intensity, thus, transmitting data using intensity modulation has an effect on flicker and dimming. When designing indoor VLC systems, dimming control and flicker are two essential considerations to be taken into account.

Limitations of LEDs

For VLC systems, LEDs are usually used as transmitters. High power LEDs are usually required for lighting; however, lighting LEDs have a low rise time that leads to a bandwidth limit. The narrow bandwidth of LEDs limits the data transmission rate.

A forward current drives LEDs, and a higher current should stimulate more optical power. However, LEDs are non-linear devices due to a peak transmitted power constraint. The peak power constraint may distort the signals. When the value of

the signal exceed the constraint, it must be clipped.

1.3 Modulation Schemes for VLC

In this section, some modulation schemes that can be used for VLC systems are introduced. Unlike RF communications, only intensity modulation and direct direction can be used in VLC.

1.3.1 On-Off Keying

On-off keying (OOK) is the simplest technique that can be used in VLC systems. In OOK, the intensity of an optical source is directly modulated by the information sequences which is usually binary. For a sequence, a bit "one" can be represented by an optical pulse, referred to as "on". On the contrary, a bit "zero", referred to as "off", can be represented as a blank duration.

1.3.2 M-ary Pulse Amplitude Modulation

M-ary pulse amplitude modulation (M-PAM) can offer a higher bandwidth efficiency than OOK, since more bits can be transmitted using one pulse in M-PAM. In M-PAM, a pulse is sent in each symbol duration, where the pulse amplitude takes on one of the M possible levels, typically $\{0, \frac{1}{M-1}, \frac{2}{M-1}, \cdots, 1\}$. The number of bits per symbol transmitted is $\log_2 M$.

An example of 4-PAM modulation is given in Figure 1.2 to help us understand the principle of the M-PAM scheme. The data stream ready for transmission is "111001001001" in this figure. For 4-PAM, we divide the stream into groups containing 2 bits. Here, the stream can be divided into "11", "10", "01", "00", "10", "01". Converting these binary numbers into 4-ary ones, we get 0, 1, 3, 2, 1, 3. For 4-PAM,

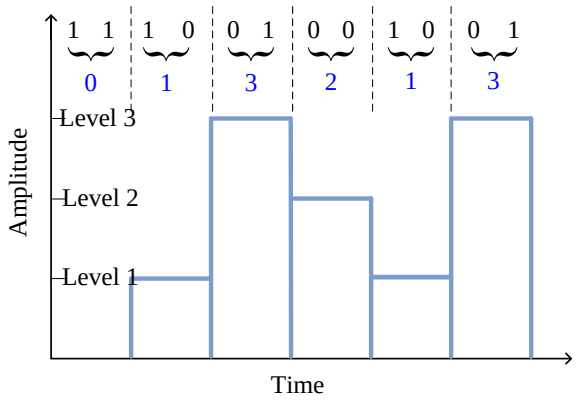

Figure 1.2: 4-PAM modulation

the transmitter just needs to send the corresponding power levels.

1.3.3 Pulse Position Modulation

Pulse position modulation (PPM) that is illustrated in Fig. 1.3 is an orthogonal modulation technique that requires less power than OOK for the same bit rate. The PPM uses the pulse position information to modulate data. The example in Fig. 1.3 shows that the pulse in the 6th time slot in 16-PPM represents the data "0101". To achieve a same bit rate as OOK, since the PPM has more narrow pulse duration than OOK, more bandwidth is required by PPM. Thus, since the LEDs are bandlimited, the PPM scheme may introduce some intersymbol interferences (ISI). ISI is a form of distortion of a signal in which one symbol interferes with subsequent symbols. In addition, PPM requires high synchronization accuracy, which is difficult in practice; therefore, PPM is not considered in this dissertation.

1.3.4 Orthogonal Frequency Division Multiplexing

Orthogonal frequency-division multiplexing (OFDM) is a method of modulating digital data on multiple orthogonal subcarriers as shown in Fig. 1.4. OFDM is a pop-

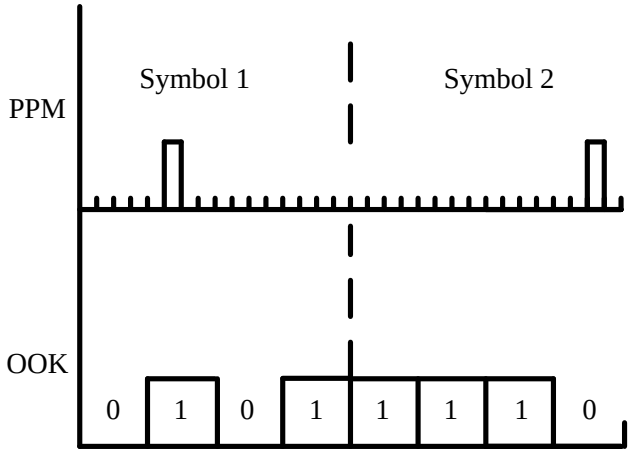

Figure 1.3: Time waveforms for 16-PPM and OOK

ular modulation scheme that has been widely used in RF systems. The conventional OFDM generates complex-valued bipolar signals, which needs to be modified in order to become suitable for VLC systems. A real OFDM signal can be obtained by using Hermitain symmetric data, which reduces the system bandwidth by a half. This approach has been widely accepted in the literature for the generation of a real OFDM signal. The resulting waveform, however, is still bipolar in nature (it has positive and negative parts). A number of techniques have been proposed for the creation of a unipolar signal. For example, a DC bias can be add to the original bipolar signal. This scheme is known as DC-biased optical OFDM (DCO-OFDM) [7]. Another approach is asymmetrically-clipped optical OFDM (ACO-OFDM), which has become popular recently because of its high power efficiency [8]. In this scheme, only the odd-indexed sub-carriers in the OFDM frame are modulated with information.

A characteristic of OFDM is a high peak to the average power ratio (PAPR). A high PAPR results in a severely distorted transmitted signal. Since LEDs have peak transmitted power constraint, the signals that exceed the constraint must be clipped. In this dissertation, the performance of OFDM in VLC systems is discussed.

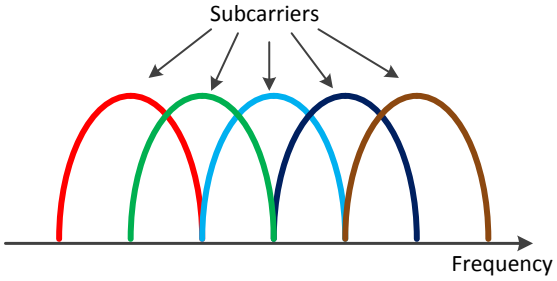

Figure 1.4: Orthogonal subcarriers in OFDM.

1.4 Multiple Access for VLC

For indoor VLC systems, multiuser wireless connection is a big issue that needs to be considered. Often, more than one user needs Internet access simultaneously. Therefore, a reliable multiple access technique is required. Since VLC uses intensity modulation, some multiple access techniques are different than RF. In this section, some multiple access techniques are introduced.

1.4.1 Time Division Multiple Access

Time division multiple access (TDMA) is a conventional multiple access scheme that is used in the digital 2G cellular system such as Global System for Mobile Communications (GSM) in RF. TDMA in VLC is the same as in RF communications. The users in TDMA transmit signals in rapid succession, one after the other, each using its own time slot as shown in Fig. 1.5. The advantages for TDMA are very obvious. The structures of transmitter and receiver can be designed simply. There is almost no multiple access interference (MAI) that is caused by the data for other users if synchronization between different users can be guaranteed.

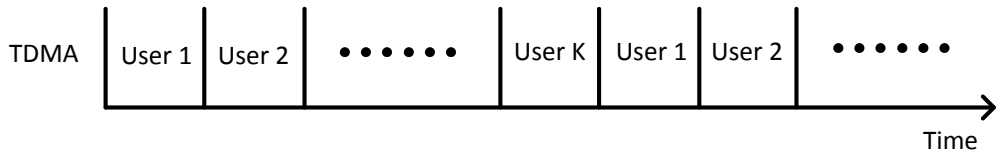

Figure 1.5: A TDMA stream divided into different time slots for different users.

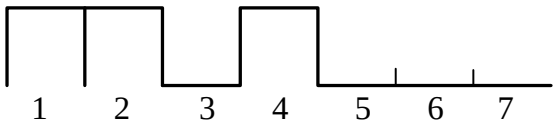

Figure 1.6: An OOC code with the length of 7.

1.4.2 Optical Code Division Multiple Access

Code division multiple access (CDMA) can be employed to provide multiple access for simultaneous users, which has been applied successfully in RF communications for many years. To separate users, each user has a unique code, and the codes for different users can be designed to be nearly orthogonal, therefore, the MAI can be perfectly canceled. For VLC systems, due to intensity modulation, the CDMA codes cannot be orthogonal, and the non-orthogonal codes cannot avoid MAI. To implement the CDMA technique in VLC, choosing the proper optical CDMA (OCDMA) code is a significant step. In this dissertation, we choose optical orthogonal codes (OOC) for OCDMA. Fig. 1.6 shows an example of one of the OOC codes used.

1.4.3 Orthogonal Frequency Division Multiple Access

Orthogonal frequency-division multiple access (OFDMA) is a novel multiple access scheme based on OFDM technique that is used in 4G LTE. As shown in Fig. 1.7, multiple access in OFDMA can be achieved by assigning subsets of subcarriers to individual users, which is a multi-user version of OFDM. Thus, OFDMA also has high PAPR, and the peak power limited LEDs can introduce hard-clipped distortions.

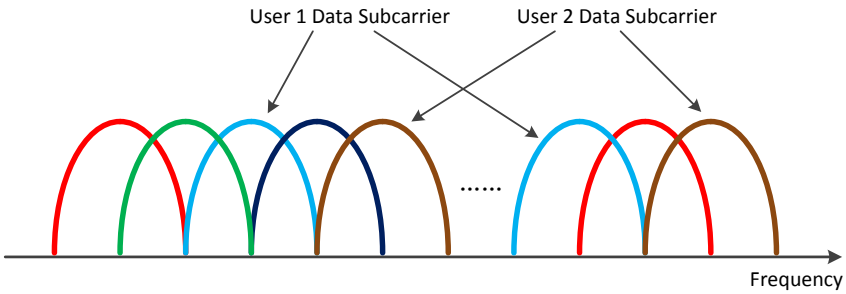

Figure 1.7: Subcarriers for multiple users in OFDMA.

1.5 Literature Review and Dissertation Contributions

For a multiuser VLC system, one of the biggest challenges is how to reduce the MAI and achieve a good communication performance. Three directions have emerged to address this problem. One is to use a multiple input multiple output (MIMO) technique with a precoding algorithm [9], [10], and [11]. However, since only the real non-negative signals can be transmitted by LEDs, the procoding algorithms usually need to add a DC bias. The second direction is to use color-shift-keying modulation over red-green-blue (RGB) LEDs and CDMA to support multiple users [12]. The third trend is to use OFDMA and discrete multi-tone (DMT) modulation to support multiple users [13] and [14]. However, since the OFDMA and DMT have high PAPR, severe distortion may be introduced. In this dissertation, we propose to use OCDMA with resource allocation algorithms for multiple users. For our algorithms, the MAI is minimized by optimizing the signal to interference plus noise ratio.

High-speed wireless data transmission is another hot topic in indoor VLC research [15,16]. To increase the data transmission rate, there are three research trends. One is to use high bandwidth efficiency pulsed modulation schemes, such as M-PAM, M-ary pulse position modulation (M-PPM), M-ary variable pulse position modulation

(M-VPPM) and M-ary variable period modulation (M-VPM) [17–19]. These M-ary modulation schemes have a $(\log_2 M)$-fold increase in data rate compared with OOK. Equalization is the reversal of distortion caused by a bandlimited channel, which is another research trend to reduce the ISI and increase the data rate [20–22]. Using an OFDM technique to increase the bit rate is the third direction [23, 24]. For OFDM, since complex modulation schemes, such as M-ary quadrature amplitude modulation (M-QAM) can be used for subcarriers, the transmission rate can be increased. However, for OFDM, the high PAPR is a drawback. In this dissertation, we propose to use M-PAM and equalization to achieve a high data rate for bandlimited VLC systems.

In general, this dissertation discusses multiuser indoor VLC systems. We propose some algorithms and analyze the performance for indoor VLC systems. The main contributions of this dissertation are listed below, along with the publications in which the work appears:

- Multi-LED lamp and multi-detector receiver models are proposed to support multiuser VLC systems [25].
- Impulse response of indoor VLC channel and received power distributions in the indoor area are discussed [26].
- Centralized and decentralized power allocation algorithms are proposed for multiuser VLC systems [26–28].
- Some practical considerations, such as shadowing effects, illumination requirements, power quantization and computational burden are discussed in this dissertation [28].
- An adaptive M-PAM modulation scheme with power allocation technique for multiuser VLC systems is introduced [29].

- To reduce the ISI and MAI, a waveform design and minimum mean squared error (MMSE) equalizer joint optimization algorithm is proposed [30, 31].
- Imperfect channel state information case is discussed in the waveform design algorithm [31].
- DCO-OFDM is discussed in this dissertation. An optimal modulation index and bit loading technique is applied in DCO-OFDM to maximize the transmission bit rate [32].
- A comparison of the optimized DCO-OFDM and M-PAM modulation is given [32].
- System vulnerability is analyzed [33].

With the help of the multi-LED transmitters and multi-detector receivers, the centralized and decentralized power allocation algorithms can support multiple users and achieve a good performance. Compared with the centralized algorithm, the decentralized algorithms have a much lower computational burden. In addition, some practical considerations are taken into account, and with standard indoor illumination level, many users can be successfully served by using the proposed algorithms. Although the lighting LEDs have limited 3 dB bandwidth, using M-PAM and waveform design algorithm, high data transmissions can still be achieved. Compared with DCO-OFDM, we conclude that using M-PAM and waveform design algorithm can provide a higher bit rate.

1.6 Dissertation Organization

The remainder of the dissertation is organized as follows.

Chapter 2 describes the multi-LEDs transmitter and multi-detector receiver models. Based on these models, the indoor channel impulse response is derived.

In Chapter 3, a centralized and four decentralized power allocation algorithms are introduced to support multiple users in indoor VLC environments. In this chapter, some practical considerations are discussed, such as shadowing effects, illumination requirements, computational burden and power quantization.

In Chapter 4, an adaptive M-PAM modulation scheme is described to support multiple users with the power allocation algorithm. To reduce the ISI caused by the bandlimited LED, a waveform design and MMSE filter joint optimization algorithm is described. MAI can also be reduced by the waveforms. An optimized DCO-OFDM technique is introduced, and a comparison of DCO-OFDM and M-PAM with the waveform design algorithm is discussed.

In Chapter 5, considering the physical characteristics of light, we analyze the interception vulnerability of VLC systems.

Chapter 6 summarizes the dissertation. Conclusion and future work are also described.

Chapter 2

System Description

White LEDs are now widely used as lighting sources for indoor illumination purpose because of their high power efficiency and long life expectancy. For VLC systems, white LEDs can also be used as transmitters. In this chapter, a multi-LED transmitter and a multi-detector receiver models are introduced. With the help of the proposed transmitter and receiver, the system robustness can be improved.

2.1 Transmitter and Receiver Models

We consider a transmitter fixture as illustrated in Fig. 2.1: a multi-LED lamp model consisting of multiple LEDs with different inclination angles [26]. This structure is proposed to cover more illumination area and provide more power to the corner areas. Furthermore, each LED can be configured to transmit light either bearing or not bearing information, giving the system more control.

The multi-detector model used as a receiver is shown in Fig. 2.2, where each photodetector has a different orientation that depends on its inclination angle [2]. The multi-detector receiver can capture the incident light from different directions. If the incident light from one direction is blocked, with the help of this receiver structure,

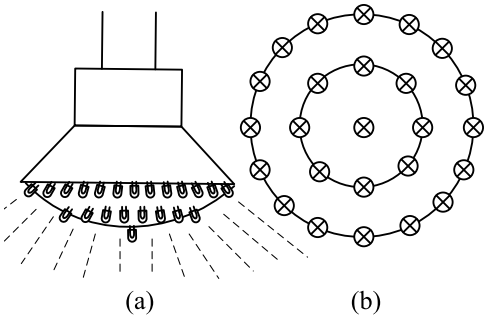

Figure 2.1: Multi-LED lamp model, (a) side view, (b) bottom view

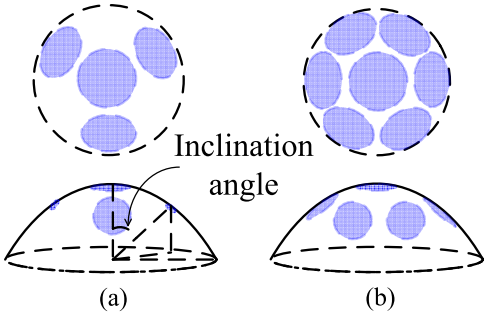

Figure 2.2: Multi-detector model structure, (a) 4-detector model, top and side view, (b) 7-detector model, top and side view (similar to [2]).

the user can still receive light with data from other directions.

2.2 Channel Model

For indoor VLC systems, white LEDs work as transmitters and photo-detectors work as receivers. Since the visible light is non-coherent, intensity modulation and direct detection are employed in VLC systems. At the receiver, the received signal can be represented as

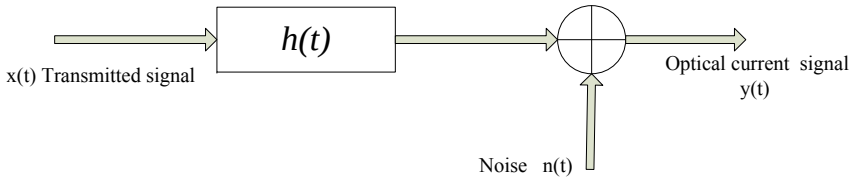

Figure 2.3: Basic indoor VLC channel model

$$y(t) = \rho A_r x(t) * h(t) + n(t), \tag{2.1}$$

where ρ represents the responsivity that measures the electrical output per optical input. A_r is the area of the photodetector. $*$ is convolution, $x(t)$ is the transmitted optical intensity, $n(t)$ is the additive noise, and $h(t)$ is the indoor channel impulse response.

Because of the principles of optics, the light rays from the transmitter can be classified into two parts. They are the line of sight (LOS) rays and diffused rays, as shown in Figure 2.4. These two components cause the multi-path effect in indoor VLC systems. Thus, the indoor VLC channel gain from LED q to user k can be approximated by [34]

$$\hat{h}_{qk} = \hat{h}_{qk}^{(\mathrm{LOS})} + \hat{h}_{qk}^{(\mathrm{Diff})}, \tag{2.2}$$

where $\hat{h}_{qk}^{(\mathrm{LOS})}$ is the contribution due to the LOS, which depends on the distance between transmitter and receiver and on their orientation with respect to the LOS. $\hat{h}_{qk}^{(\mathrm{Diff})}$ is the diffused part, the intensity of which is less than the LOS part. The intensity of the LOS rays and diffused rays follow the Lambertian law. The Lambertian radiant intensity model can be defined as [35]

$$R_0(\phi) = \begin{cases} \frac{m+1}{2\pi}\cos^m(\phi) & \text{for } \phi \in [-\pi/2, \pi/2] \\ 0 & \text{for } |\phi| \geq \pi/2 \end{cases}, \tag{2.3}$$

where m is the Lambertian mode of the light source and ϕ is the radiation angle for the transmitter as shown in Figure 2.5. The maximum radiated power is reached when $\phi = 0$. The Lambertian mode m is related to the LED's semiangle $\Phi_{1/2}$ by

$$m = \frac{\ln 2}{\ln(\cos \Phi_{1/2})}. \tag{2.4}$$

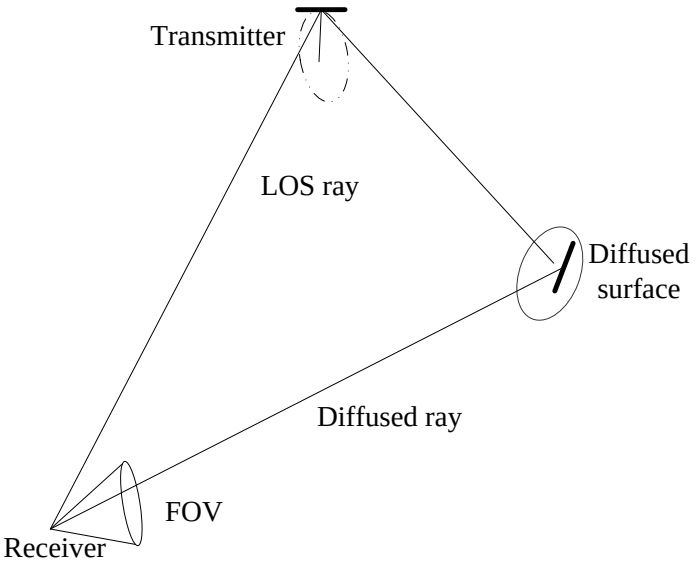

Figure 2.4: Light rays classification.

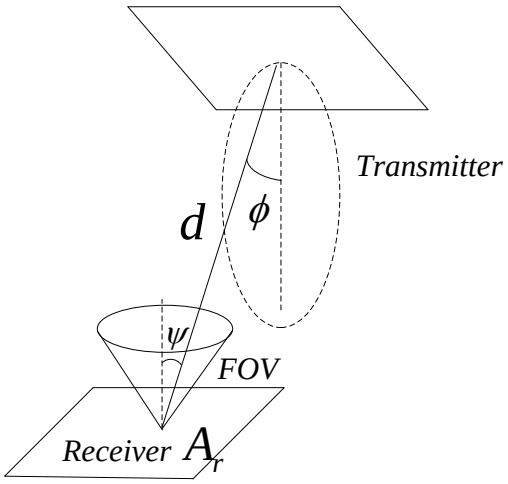

Figure 2.5: LOS light rays model.

The detector effective area can be modelled as a function of the incident angle, ψ, as [35]

$$A_{eff}(\psi) = \begin{cases} A_r \cos\psi & -\pi/2 \leq \psi \leq \pi/2 \\ 0 & \mid \psi \mid > \pi/2 \end{cases}, \tag{2.5}$$

We assume that the detector cannot be active beyond the field of view (FOV) angle Ψ_c. A_r is the area of the photodetector at receiver. Therefore, the LOS link gain

between LED q and user k can be described as

$$\hat{h}_{qk}^{(\mathrm{LOS})} = \begin{cases} \frac{(m+1)}{2\pi l^2}\cos^m(\phi)\cos(\psi) & -\Psi_c \leq \psi \leq \Psi_c \\ 0 & \text{elsewhere} \end{cases}, \tag{2.6}$$

where l is the distance between the transmitter q and the kth receiver. ϕ is the radiation angle, and ψ represents the incident angle. The diffused part can be calculated as

$$\hat{h}_{qk}^{(\mathrm{Diff})} = \prod_{i=0}^{\infty} L_i \varsigma^i, \tag{2.7}$$

where ς is the wall reflection coefficient, and L_i represents the ith bounce link attenuation,

$$\begin{aligned} L_0 &= \frac{(m+1)\cos^m(\phi_0)\cos(\psi_0)}{2\pi l_0^2} \\ L_1 &= \frac{\cos^m(\phi_1)\cos(\psi_1)}{\pi l_1^2} \\ &\vdots \\ L_k &= \frac{\cos^m(\phi_k)\cos(\psi_k)}{\pi l_k^2} \end{aligned}, \tag{2.8}$$

where l_k represents the distance of the kth bounce link. ϕ_k and ψ_k are radiation angle and incident angle at kth bounce's diffusion point, respectively. [36].

2.3 Additive Noise

The noise in this system can be modeled as thermal noise plus shot noise. The thermal noise and shot noise can be represented as

$$\begin{aligned} \sigma_{\mathrm{thermal}}^2 &= 4\kappa T_\kappa R_s / R_L, \\ \sigma_{\mathrm{shot}}^2 &= 2q\rho P_r R_s \end{aligned} \tag{2.9}$$

where q is the electronic charge, κ is Boltzmann's constant, T_κ is the absolute thermodynamic temperature, and R_s is the transmitted symbol rate. R_L is the resistor in the circuit of the receiver. P_r is the received optical power that can be calculated as

$$P_r = P^{\max} A_r \sum_{q=1}^{Q} \hat{h}_{qk} + P_{\mathrm{b}}, \tag{2.10}$$

P_{b} is the received optical power of background light.

2.4 Summary

This chapter introduces multi-LED and multi-detector models and VLC channel model, as well as the VLC channel can be classified into LOS and non-LOS components. Both the LOS and non-LOS follow the Lambertian law.

Chapter 3

Power Allocation Algorithms for Multiuser VLC Systems

In indoor VLC systems, one significant research challenge that has received some attention in recent years is how to support multiple users with high data rates while limiting the multiple access interference (MAI). So far, three popular research trends have emerged. Multiple input and multiple output (MIMO) has been proposed to use in VLC systems as a method for multiplying the capacity [37–39]. MIMO with precoding is proposed to limit the MAI and improve the signal to interference plus noise ratio (SINR) in [40–42]. The second trend is to use color-shift-keying modulation over red-green-blue (RGB) LEDs and code division multiplexing access (CDMA) to support multiple users [12]. The third direction is to use resource allocation schemes to minimize the MAI. In the third trend, orthogonal frequency division multiple access (OFDMA) and discrete multi-tone (DMT) modulation with transmitted power allocation algorithms to limit the MAI were proposed in [14, 43, 44].

Due to the nature of white LEDs (their nonlinearity and the incoherent light they transmit), it is not easy to implement a modulation requiring frequency-domain pro-

cessing. To avoid this problem, intensity modulation and direct detection (IM/DD) with on-off keying (OOK) modulation is applied in this chapter. Then, direct-sequence optical CDMA (OCDMA) with a time-space minimum mean squared error (MMSE) filter is used to support multiple users. OCDMA has considerable advantages compared with the recently popular orthogonal frequency-division multiplexing (OFDM) technique [45–47]. Since OFDM has a high peak to average power ratio (PAPR), some signals with high intensity would be distorted from the nonlinearity of the LEDs. Furthermore, the structure of the receivers is simple for OCDMA systems compared with OFDM.

In this chapter, we propose a centralized power allocation algorithm and several decentralized power allocation algorithms for multiple users in indoor VLC environments. The algorithms we propose in this chapter have the following advantages compared with other approaches

- All the transmitted power is used for both data transmission and illumination (no extra light needed just for illumination).
- Compared with the OFDM technique, our algorithms do not need to address the high PAPR.
- No DC bias is needed for the transmitted signals.
- The structures of transmitters and receivers are simple.

In addition, we propose to model the shadowing effects as path losses in this chapter. Our adaptive algorithms can reallocate the transmit power and recompute the MMSE filters coefficients to reduce the shadowing effects with the help of MIMO processing.

Some of the work presented in this chapter has been published in [26, 27, 29].

3.1 Transmitted and Received Signals

We assume that the indoor VLC network has N lamps, and there are Q LEDs with different inclination angles for each lamp. Therefore, the number of total LEDs is $N \times Q = N_Q$. We also assume that there are K users in the indoor environment, and each user has V PDs with different orientations.

Let $i_k(t)$ be the signal that is intended for user k, which is represented as $i_k(t) = d_k \cdot c_k(t)$, where d_k is the $\{0, 1\}$ data, and $c_k(t)$ is the OCDMA code waveform for user k. The qth LED sends a linear combination of the users' data as

$$x_q(t) = \sum_{k=1}^{K} p_{qk} i_k(t), \tag{3.1}$$

where $p_{qk} \in [0, p^{max}]$ is the transmitted power of the qth LED allocated to transmitting the data of user k. Assuming a peak radiation power limit of p^{max} from each LED, the constraint $\sum_{k=1}^{K} p_{qk} \leq p^{max}$ needs to be applied on the allocated powers. These power levels are organized in a $N_Q \times K$ matrix denoted as $\mathbf{P}$. The elements in matrix $\mathbf{P}$ represent the power allocation from each LED to each user.

The signal received by the vth detector of user k can be written as [25, 26]

$$r_k^{(v)}(t) = \sum_{q=1}^{N_Q} \hat{h}_{qkv} x_q(t) + n_k^{(v)}(t), \qquad \begin{matrix} k = 1, \ldots, K \\ v = 1, \ldots, V \end{matrix} \tag{3.2}$$

where $n_k^{(v)}(t)$ is the noise experienced by the vth detector of user k. $\hat{h}_{qkv}$ is the channel gain from LED q to the vth detector of user k. In this chapter, shot noise from ambient light and thermal noise are considered. Then, after chip matched filtering

and sampling, the ℓth sample of the discrete time signal received by PD v of user k is

$$r_k^{(v)}[\ell] = \sum_{q=1}^{N_Q} \hat{h}_{qkv} x_q[\ell] + n_k^{(v)}[\ell]. \qquad \begin{matrix} k = 1, \ldots, K \\ v = 1, \ldots, V \end{matrix} \tag{3.3}$$

We design a linear time-space MMSE filter for user k, $\mathbf{w}_k = (\mathbf{w}_{k1},\ \mathbf{w}_{k2},\ \cdots,\ \mathbf{w}_{kL})^T$, where $\mathbf{w}_{k\ell} = (w_k[1,\ell],\ w_k[2,\ell],\ \cdots,\ w_k[V,\ell]),\ \ell = 1,\ 2,\ \cdots,\ L$. Therefore, the length of $\mathbf{w}_k$ is VL, where L is the length of the OCDMA code. This time-space MMSE filter can take advantage of the received signal from all the PDs. After the linear MMSE filter, the received decision variable for user k can be represented as

$$y_k = \sum_{\ell=1}^{L} \sum_{v=1}^{V} r_k^{(v)}[\ell] w_k[v,\ell] + b_k, \tag{3.4}$$

where b_k is a constant for the linear MMSE estimator. From (3.1)-(3.4), the decision variable for user k after MMSE filtering can be rewritten in a matrix form as

$$y_k = g(\mathbf{C}^T \mathbf{D} \mathbf{P}^T \mathbf{H}_k^T)^T \mathbf{w}_k + \mathbf{n}_k^T \mathbf{w}_k + b_k, \tag{3.5}$$

where $g(\cdot)$ is a transformation to reshape the matrix into a VL-vector by concatenating the columns. In (3.5), $\mathbf{D} = diag(d_1, d_2, \cdots, d_K)$, and $\mathbf{n}_k$ is the noise vector. $\mathbf{C}$, $\mathbf{P}$ and $\mathbf{H}_k$ are the OCDMA, power allocation, and channel gain matrices, respectively. They are represented as

$$\mathbf{C} = \begin{pmatrix} c_1[1] & c_1[2] & \cdots & c_1[L] \\ c_2[1] & c_2[2] & \cdots & c_2[L] \\ \vdots & \vdots & \ddots & \vdots \\ c_K[1] & c_K[2] & \cdots & c_K[L] \end{pmatrix}, \tag{3.6}$$

$$\mathbf{P} = \begin{pmatrix} p_{11} & p_{12} & \cdots & p_{1K} \\ p_{21} & p_{22} & \cdots & p_{2K} \\ \vdots & \vdots & \ddots & \vdots \\ p_{N_Q 1} & p_{N_Q 2} & \cdots & p_{N_Q K} \end{pmatrix}, \tag{3.7}$$

and

$$\mathbf{H}_k = \begin{pmatrix} \hat{h}_{1k1} & \hat{h}_{1k2} & \cdots & \hat{h}_{1kV} \\ \hat{h}_{2k1} & \hat{h}_{2k2} & \cdots & \hat{h}_{2kV} \\ \vdots & \vdots & \ddots & \vdots \\ \hat{h}_{N_Q k1} & \hat{h}_{N_Q k2} & \cdots & \hat{h}_{N_Q kV} \end{pmatrix}. \tag{3.8}$$

The time-space MMSE receiver in (3.5) can be derived as follows. The mean-squared error J_k for user k is defined as

$$J_k = E_{\mathbf{d},\mathbf{n}}\{(g(\mathbf{C}^T\mathbf{D}\mathbf{P}^T\mathbf{H}_k^T)^T\mathbf{w}_k + \mathbf{n}_k^T\mathbf{w}_k + b_k - d_k)^2\}, \tag{3.9}$$

where $E_{\mathbf{d},\mathbf{n}}$ represents expectation with respect to the data vector $\mathbf{d}$ and the noise $\mathbf{n}_k$. Solving for $\frac{\partial J_k}{\partial b} = 0$, and $\frac{\partial J_k}{\partial \mathbf{w}_k} = 0$, the MMSE receiver can be obtained as

$$\begin{aligned} \mathbf{w}_k &= (\mathbf{G} + \sigma^2\mathbf{I})^{-1} g(\mathbf{C}^T\mathbf{\Sigma}_k\mathbf{P}^T\mathbf{H}_k^T) \\ b_k &= \frac{1}{2} - \frac{1}{2} g(\mathbf{C}^T\mathbf{P}^T\mathbf{H}_k^T)^T\mathbf{w}_k \end{aligned}, \tag{3.10}$$

where $\mathbf{G} = E_{\mathbf{d}}\{g(\mathbf{C}^T\mathbf{D}\mathbf{P}^T\mathbf{H}_k^T)g(\mathbf{C}^T\mathbf{D}\mathbf{P}^T\mathbf{H}_k^T)^T\}$, and $\mathbf{I}$ is the identity matrix. σ^2 represents the noise variance. $\mathbf{\Sigma}_k = E_{\mathbf{d}}\{\mathbf{D}d_k\}$.

From (3.5), the signal after the MMSE estimator consists of three parts: the target (intended data) for user k, the MAI and the noise. Thus, the received signal for user

k after MMSE filtering can be represented as

$$y_k = \underbrace{g(\mathbf{C}^T\mathbf{D}\mathbf{Z}_k\mathbf{P}^T\hat{\mathbf{H}}_k^T)^T\mathbf{w}_k}_{\text{Target}} + \underbrace{g(\mathbf{C}^T\mathbf{D}\hat{\mathbf{Z}}_k\mathbf{P}^T\hat{\mathbf{H}}_k^T)^T\mathbf{w}_k}_{\text{MAI}} + \underbrace{\mathbf{n}_k^T\mathbf{w}_k}_{\text{Noise}} + b, \tag{3.11}$$

where $\mathbf{Z}_k$ is defined as a matrix with a 1 in its (k,k)th element and zeros in all other places, and $\hat{\mathbf{Z}}_k = \mathbf{I} - \mathbf{Z}_k$.

3.2 Centralized Power Allocation Algorithm

In this section, we describe a centralized power allocation joint optimization algorithm (CM-PAJO) and several decentralized algorithms.

For CM-PAJO, we assume that each LED serves all the users in this indoor environment. In order to eliminate the MAI, each lamp needs to exchange information (channel information sent back from users) with other lamps and allocates power to the users jointly.

From (3.11), the SINR for user k can be calculated as,

$$\begin{aligned} \text{SINR}_k &= \frac{\text{Signal}}{\text{MAI} + \sigma^2\mathbf{w}_k^T\mathbf{w}_k} \\ \text{Signal} &= A_r^2\mathbf{w}_k^T E_{\mathbf{d}}\{g(\mathbf{C}^T\mathbf{D}\mathbf{Z}_k\mathbf{P}^T\mathbf{H}_k^T)g(\mathbf{C}^T\mathbf{D}\mathbf{Z}_k\mathbf{P}^T\mathbf{H}_k^T)^T\}\mathbf{w}_k)\cdot \\ \text{MAI} &= A_r^2\mathbf{w}_k^T E_{\mathbf{d}}\{g(\mathbf{C}^T\mathbf{D}\hat{\mathbf{Z}}_k\mathbf{P}^T\mathbf{H}_k^T)g(\mathbf{C}^T\mathbf{D}\hat{\mathbf{Z}}_k\mathbf{P}^T\mathbf{H}_k^T)^T\}\mathbf{w}_k) \end{aligned} \tag{3.12}$$

The bit error rate for user k can be approximated by [34]

$$\text{BER}_k \approx \frac{1}{2}\text{erfc}\left(\sqrt{\frac{\text{SINR}_k}{2}}\right). \tag{3.13}$$

To optimize the transmitted power allocation, we consider two optimization criteria: to minimize the maximum BER among all the users or to minimize the average

of BER for all the users. Through optimization, we obtain the power allocation as

$$\text{Fairness:}\mathbf{P}^* = \arg\min_{\mathbf{P}} \max_k \text{BER}_k \tag{3.14}$$

or

$$\text{Min-BER:}\mathbf{P}^* = \arg\min_{\mathbf{P}} \sum_k \text{BER}_k, \tag{3.15}$$

where $\mathbf{P}^*$ is the optimal power allocation.

Algorithm 1: Optimal power allocation for "Fairness"

$\min \max \text{BER}_k \Rightarrow \min y$, s.t. $\text{BER}_k \leq y, \forall\ k$;

Use method of Lagrange multiplier;

Equivalent objective function $\pounds(\mathbf{P}, y, \lambda_i)$ is created;

while $i \leq R$, *R is number of random initial values* **do**

  Initialization: random initial value $\mathbf{P}_i$;

  SQP begins;

  repeat

    SQP algorithm;

  until $\pounds(\mathbf{P}, y, \lambda_i)$ *converges*;

  Get $\mathbf{P}_i^*$ for initial value $\mathbf{P}_i$;

end

Output: Choose the $\mathbf{P}_i^*$ that yields the smallest value of y

To find the optimal solutions to (3.14) and (3.15), an iterative method, the sequential quadratic programming (SQP) algorithm, can be used. For the "Fairness" optimization in (3.14), the objective function can be reformulated into an equivalent nonlinear programming problem by appending additional constraints of the form $\text{BER}_k \leq y$ for $\forall\ k$, and then minimizing y over $\mathbf{P}$. The method of Lagrange multi-

Table 3.1: Parameters Used for Indoor Environment

Number of lamps for small room	4
Number of lamps for large room	25
Number of LEDs in each lamp	25
PD number per user	$1, 4, 7$
Dimming parameters for all LEDs	$\emptyset = 1$
Responsivity	0.5A/W
Area of the PD	0.01 cm^2
Wall reflection coefficient	0.8
Radiation optical power of each lamp	300 mW
LED semiangle	30^o
Cyclic 7-length OOC code index [48]	{1, 2, 4}
Cyclic 25-length OOC code index [48]	{1, 2, 7} {1, 3, 10} {1, 4, 12} {1, 5, 14}
Minimum access area	$a_m = 9.8$ m^2
Receiver bandwidth	70 MHz

pliers is used to tackle all constraints. Since the two optimizations are non-convex problems, the optimal solution may be a local minimum. Therefore, we randomly choose different initial values for optimization and choose the best solution from all results. The steps for solving the power allocation algorithm for the "Fairness" criteria is described in Algorithm 1. The steps for solving the "Min-BER" criteria are similar.

To test the applicability of the system in different environments, we show results for both small and large rooms. The parameters used to obtain the numerical results are shown in Table 3.1. This is a baseline for all the numerical results in this chapter.

3.2.1 Single Detector Receiver

The single detector receiver case is considered first in this section.

For a small indoor environment, we consider two typical lamp and user positions,

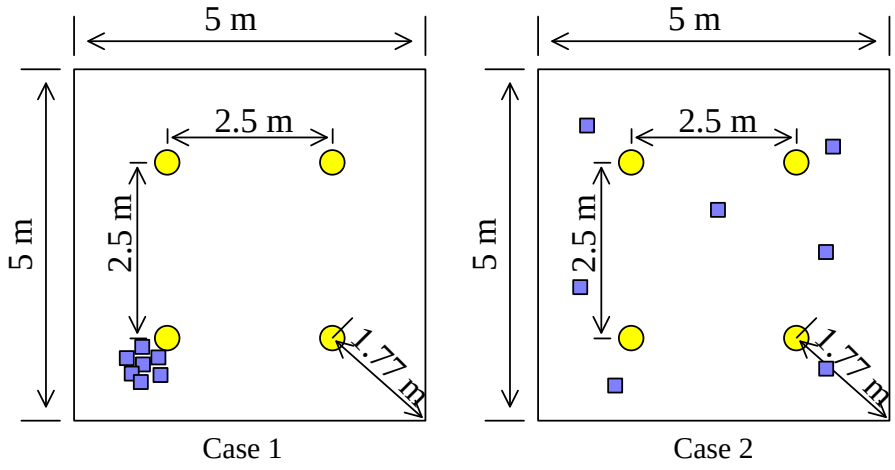

Figure 3.1: Top-down view of the two typical user position cases for the small room. The small circles represent the lamps and the squares represent the users.

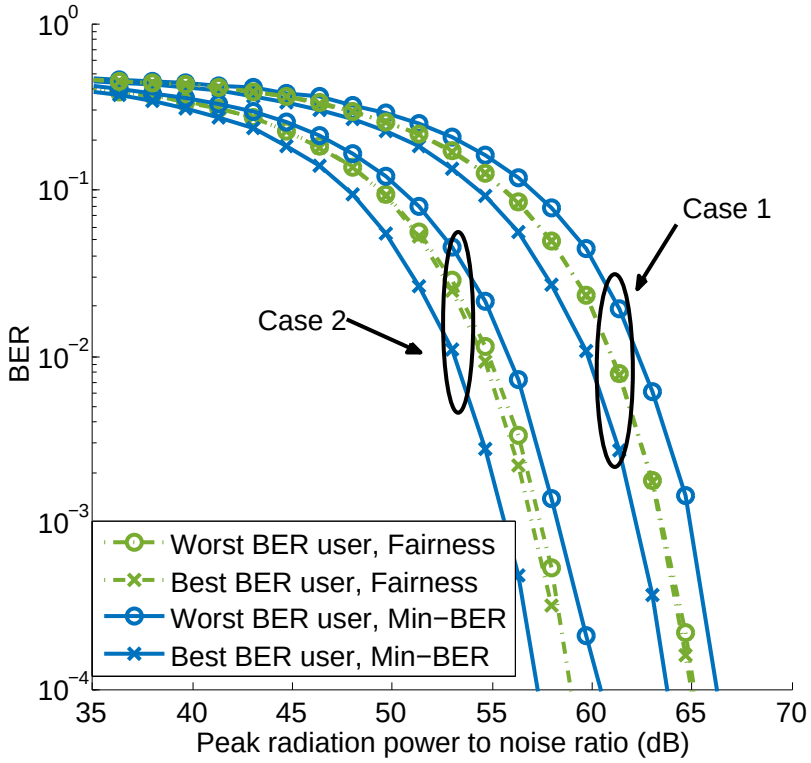

Figure 3.2: BER performance using "Fairness" and "Min-BER" for Case 1 and 2 for CM-PAJO with a single detector and 7-length OOC codes, in the small room.

which are shown in Fig. 3.1. In Case 1, all the users are located in a corner near one of the lamps. In Case 2, all the users are distributed in the room. The numerical results for the BER of the CM-PAJO using the "Fairness" and "Min-BER" optimization criteria from (3.14) and (3.15) for Cases 1 and 2 are shown in Fig. 3.2. The BER curves can be represented as a function of the peak radiation power to noise ratio (PPNR), which is defined as P^{max}/σ^2.[1] Using the "Fairness" criterion, the BER curves for all users are more similar than using the "Min-BER" criterion, as excepted. At a BER of 10^{-3}, there is approximately a 3 dB required transmitted power gap between the best and worst-case users for Min-BER both in Cases 1 and 2. Since the Min-BER method minimizes the average BER for all users, the average BER using Min-BER is slightly better than using "Fairness", by 1 dB. But when equal performance is desired, the "Fairness" method is preferable. Case 2 always has a better BER than Case 1 because the users' locations make better use of all lamps.

3.2.2 Multiple Detector Receiver

In this section, multi-detector receivers are applied and tested.

Fig. 3.3 shows the BER performance of CM-PAJO with different receiver inclination angles from 20 degrees to 60 degrees. We simulated 5 trials of 4 users random distributed in the indoor environment. From the results, the FOV impacts the BER performance more than the inclination angles. In general, with the help of our proposed algorithm, the larger the FOV the better the BER performance for CM-PAJO. In addition, the 7-detector CM-PAJO is always superior to the 4-detector one.

Fig. 3.5 shows that when the number of users increases (selected in the order shown in Fig. 3.4), the BER performances of CM-PAJO become worse, due to an

[1]Note that in VLC systems we use the *transmitted power* to *receiver noise* ratio as an SNR metric, instead of the normal received power to receiver noise ratio [25–27].

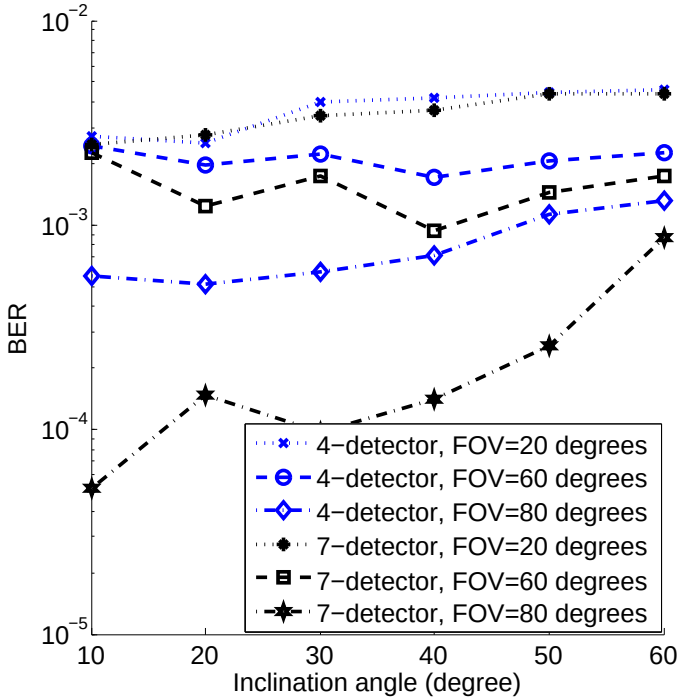

Figure 3.3: Average BER performance of 4 users for CM-PAJO with different inclination angles and different FOV, the peak radiation power to noise ratio is 48 dB.

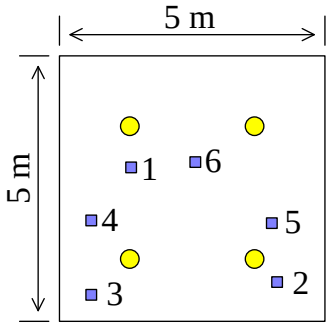

Figure 3.4: Top-down view of indoor environment. The small circles represent the lamps and the squares represent the user 1 to user 6.

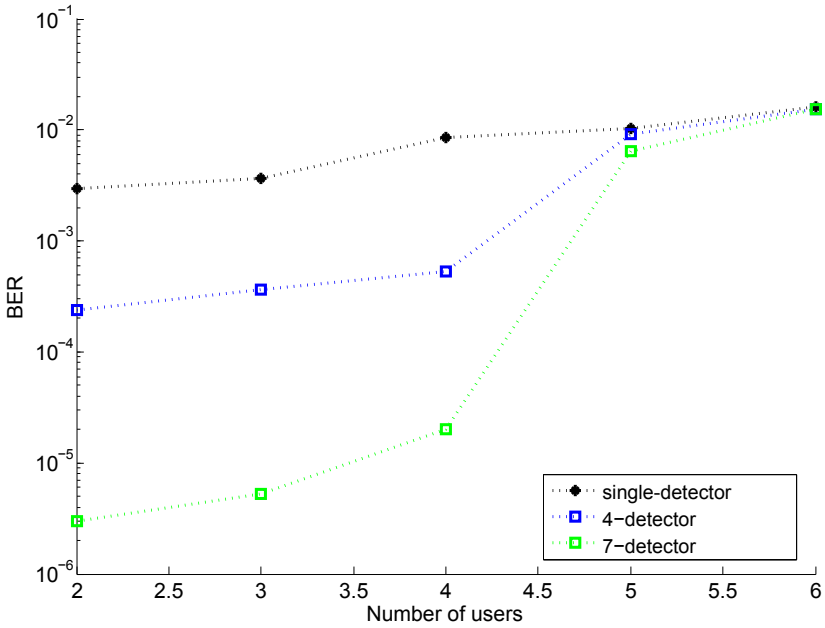

Figure 3.5: Average BER performance of different users for CM-PAJO, with peak radiation power to noise ratio is 48 dB, FOV= 80 degrees.

increase in MAI. Again the 7-detector CM-PAJO has better BER performance than the 4-detector case.

To analyze the performance of the proposed CM-PAJO from a statistical point of view, we simulate 40 trials of 4 users randomly distributed in the indoor environment. The simulation results are shown in Fig. 3.6. For a peak radiation power to noise ratio of 51 dB, more than 75% of the 160 users' BER for both the 4-detector and 7-detector cases are lower than 10^{-3}.

3.3 Decentralized Power Allocation Algorithms

In a large room with many LED lamps, the centralized algorithm presented above becomes prohibitively and unnecessarily complicated. In this section, we describe four decentralized power allocation algorithms better suited to such environments. For the decentralized algorithms, we define a circular *access area* for each lamp,

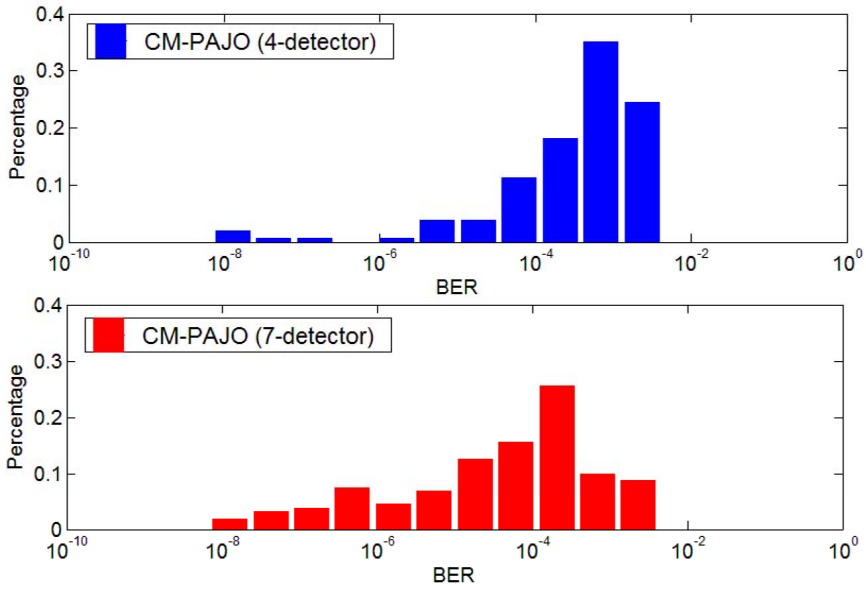

Figure 3.6: Histogram of BER performance for 4 randomly distributed users, with peak radiation power to noise ratio of 51 dB, FOV= 80 degrees

which is shown in Fig. 3.7. This artificially-defined access area is smaller than the actual illumination area of the lamps such that the lamps can serve only the users who are in the access area. To cover the entire indoor area, there may be some overlap of the access areas from different lamps. Each user must be served by at least one lamp, and each lamp can serve more than one user. An example is shown in Fig. 3.8, where there are 4 lamps and 5 users, and each lamp has an access area as drawn. Given the locations of the users, users A and B are in the access area of lamp 1. Users B and C are in the access of lamp 2. User D is in the overlap access area of lamps 3 and 4. User E is in the access area of lamp 3. In this case, since user B is in the overlapping access area of lamps 1 and 2, it can be served by these two lamps. Similarly, user D can be served by both lamps 3 and 4.

Unlike the centralized algorithm, the decentralized VLC optimization can be divided into parallel optimization threads. For each optimization thread, the transmit power allocation and filter design work independently from the other threads. In

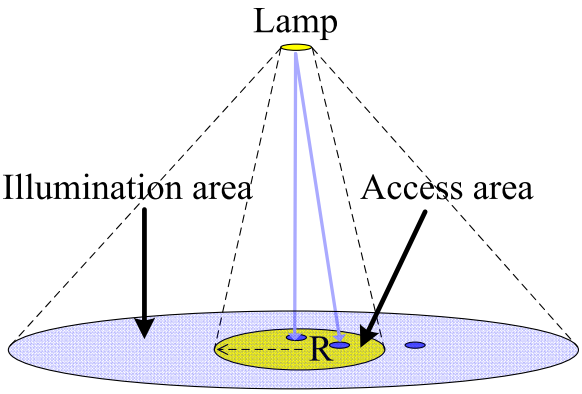

Figure 3.7: Illumination area and access area (the radius is R)

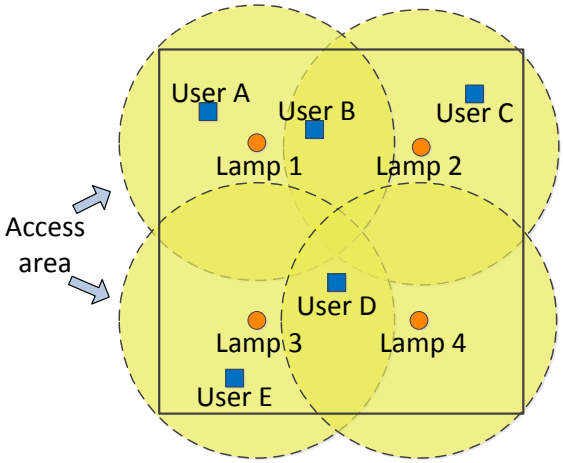

Figure 3.8: Geometry structure of an example.

addition, when we calculate the SINR for each user, we only consider the messages within the thread (so the MAI is assumed to be caused only by the users in the same thread). We use OCDMA as our multiple-access scheme because it can allow each thread to ignore other threads, even if they cause some interference. However, for TDMA and OFDMA, interference can be catastrophic. Since each thread works individually, there is no channel information exchange between the different optimization threads. For all techniques, each lamp must know the data and channel state information for the users in its access area, and all lamps must remain synchronized since a user may receive its signal from more than one lamp.

Decentralized Equal Power Allocation (DEPA)

For DEPA, each lamp works independently and allocates the transmitted power equally to the users in its access area. If there are no users in an access area, the transmitted power is used for lighting only.

In the example displayed in Fig. 3.8, for DEPA, lamp 1 allocates equal transmitted power to users A and B. Similarly, lamps 2 and 3 allocate power to each user in their access areas equally. Since there is only one user in the access area of lamp 4, all the power is allocated to that user.

Power Allocation Disjoint Optimization (PADJO)

All the lamps work independently in PADJO, and each lamp optimizes the power allocated to the users in its own access area using (3.14) or (3.15). Since we assume there are N lamps in the indoor environment, there are N optimization threads, and all threads can work in parallel. Similar to DEPA, there is no channel information exchange between lamps.

Using PADJO, all the lamps and users in the example shown in Fig. 3.8 can be divided into four optimization threads. Thread 1 consists of lamp 1 and users A and B. Thread 2 consists of lamp 2 and users B and C. Thread 3 consists of lamp 3 and users D and E. Thread 4 contains lamp 4 and user D. The four optimization threads work independently. Thus, when the algorithm calculates the SINR for each user in a particular thread, it only consider the messages within the thread.

Weighted Decentralized Multi-detector Power Allocation Joint Optimization (WDM-PAJO)

For WDM-PAJO, all the lamps work independently. They need to know how many access points serve each users, yet there is still no channel information exchange

between lamps. Thus, there are N threads for WDM-PAJO. The SINR for each user is weighted by τ_k to normalize for the extra power received by users that are served by multiple lamps. The algorithm calculates

$$\mathbf{P}^*_{\Omega_{\mathrm{W}}^{(i)}} = \arg\min_{\mathbf{P}} \max_{k\in\Omega_{\mathrm{W}}^{(i)}} Q\left(\sqrt{\tau_k \cdot \mathrm{SINR}_k}\right), \ \forall\ i, \tag{3.16}$$

which is similar to the PADJO, except it accounts for the number of lamps that serve user k, denoted as τ_k. $\Omega_{\mathrm{W}}^{(i)}$ represents the ith WDM-PAJO optimization thread. $\mathbf{P}^*_{\Omega_{\mathrm{W}}^{(i)}}$ is the optimal power allocation matrix for the lamps in the ith thread using WDM-PAJO.

Similar to PADJO, all the lamps and users in Fig. 3.8 can be divided into four optimization threads for WDM-PAJO. In this example, when we optimize the transmitted power in thread 1 using (3.16), $\tau_A = 1$, $\tau_B = 2$ and $\tau_D = 2$, because there are two lamps that serve users B and D. In this case, the optimization threads 1, 2, 3 and 4, can be represented as $\Omega_{\mathrm{W}}^{(1)} = \{\text{lamp 1}, \text{user A}, \text{user B}\}$, $\Omega_{\mathrm{W}}^{(2)} = \{\text{lamp 2}, \text{user B}, \text{user C}\}$, $\Omega_{\mathrm{W}}^{(3)} = \{\text{lamp 3}, \text{user D}, \text{user E}\}$ and $\Omega_{\mathrm{W}}^{(4)} = \{\text{lamp 4}, \text{user D}\}$, respectively.

Partial Decentralized Multi-detector Power Allocation Joint Optimization (PDM-PAJO)

In PDM-PAJO, the lamps and users are divided into different optimization threads depending on the users' locations. Different from PADJO, the lamps that serve the same users can exchange channel information in PDM-PAJO. Therefore, the lamps that work together form an optimization thread.

For PDM-PAJO, the optimization process for a thread is similar to the CM-PAJO

case, which can be described as

$$\mathbf{P}^*_{\Omega_{\mathrm{P}}^{(i)}} = \arg\min_{\mathbf{P}} \max_{k\in\Omega_{\mathrm{P}}^{(i)}} Q\left(\sqrt{\mathrm{SINR}_k}\right),\ \forall\ i, \tag{3.17}$$

where $\Omega_{\mathrm{P}}^{(i)}$ represents the ith PDM-PAJO optimization thread, which contains some lamps and users. $\mathbf{P}^*_{\Omega_{\mathrm{P}}^{(i)}}$ is the optimal power allocation matrix for the lamps in the ith thread using PDM-PAJO.

For the example shown in Fig. 3.8, all the users and lamps can be divided into two optimization threads using PDM-PAJO. Given the locations of the users, the two optimization threads can be represented as $\Omega_{\mathrm{P}}^{(1)} = \{\text{lamp 1},\ \text{lamp 2},\ \text{user A},\ \text{user B},\ \text{user C}\}$, $\Omega_{\mathrm{P}}^{(2)} = \{\text{lamp 3},\ \text{lamp 4},\ \text{user D},\ \text{user E}\}$. Thus, lamps 1 and 2 can work together to support user B by optimizing the transmitted power. When the algorithm calculates the SINR for user A, the MAI is assumed to be caused by the messages from both lamps 1 and 2 to user B. Although users C and A are in the same optimization thread, the algorithm ignores user C when calculating the MAI for user A, since they are not in the same access area.

In general, DEPA, PADJO and WDM-PAJO require no coordination between lamps. PDM-PAJO requires some coordination, and CM-PAJO requires the most, depending on the physical location of the users.

3.3.1 Performance Comparison

We compare the performance of the proposed CM-PAJO and our four decentralized algorithms using the multi-detector model. We test a large indoor environment described in Table 4.2 to compare the CM-PAJO, PDM-PAJO, WDM-PAJO, PADJO and DEPA. In this chapter, we consider the minimum access area case[2] for all the

[2]The minimum access area means the minimum value of the access area for which the entire indoor floor surface is covered. The access area of all lamps is assumed equal.

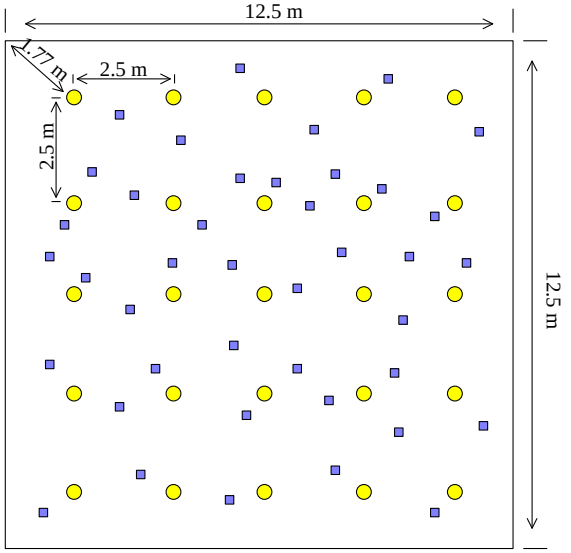

Figure 3.9: Top-down view of the positions of lamps and users in a large indoor environment. The small circles represent the lamps and the squares represent the users.

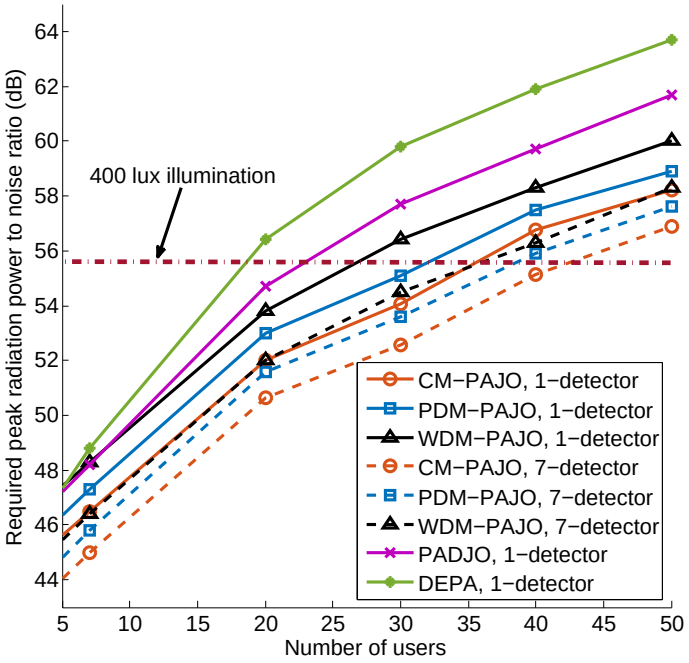

Figure 3.10: Peak radiation power to noise ratio (PPNR) required for a BER of 10^{-3} in the large indoor environment using the minimum access area needed cover the room with 25-length OOC codes.

algorithms. [27] discusses the effect of the size of the access area on some of these algorithms. The geometric position of the lamps and users are shown in Fig. 3.9. From the results in Fig. 3.10, we see that the optimized algorithms do much better than DEPA in general, showing the advantage of resource optimization. CM-PAJO is the optimal power allocation algorithm that can spend about 10 dB less transmitted power than DEPA to achieve the same BER performance. For decentralized algorithms, PDM-PAJO and WDM-PAJO only need 2 dB more power than the CM-PAJO to get the same BER. In addition, using 7 PDs can save as much as 2 dB transmitted power for both centralized and decentralized algorithms over single PD cases. If there is no background light, when the proposed VLC system satisfies standard 400 lx illumination,[3] it can support up to 40 users when using the 7-detector CM-PAJO algorithm.

The BER of the proposed PDM-PAJO technique for different access area radii in the small indoor environment is shown in Fig. 3.11. We also show the BER performance of the CM-PAJO algorithm for comparison. From the simulation results, when the radius increases from 1.77 m to 2.26 m, the BER of PDM-PAJO converges to the CM-PAJO. When $R = 1.77$ m (the minimum radius of the access area), the PDM-PAJO has less than a 2 dB power penalty compared with CM-PAJO.

Fig. 3.12 shows the BER of the WDM-PAJO technique with different access area radii, also in a small indoor environment, compared with PDM-PAJO and CM-PAJO. When the access areas have a small radius, the BER performance of WDM-PAJO and PD-PAJO are almost the same, both yielding less than a 2 dB power penalty compared with CM-PAJO. However, as the radius of the access areas increases, the BER curves diverge. The weight τ_k for all k in (3.16) approaches K, and when all the weight are the same the WDM-PAJO algorithm ceases to work well.

[3] 400 lx is a standard illumination level for office spaces [49]. The conversion between illuminance and power can be found in [50].

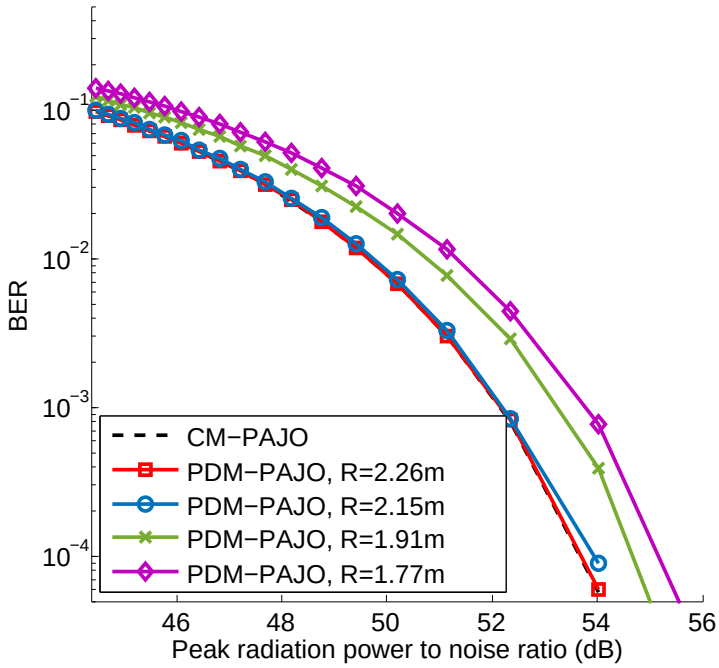

Figure 3.11: Average BER of 4 users for CM-PAJO and PDM-PAJO for different radii of access area in the small indoor environment with single detector.

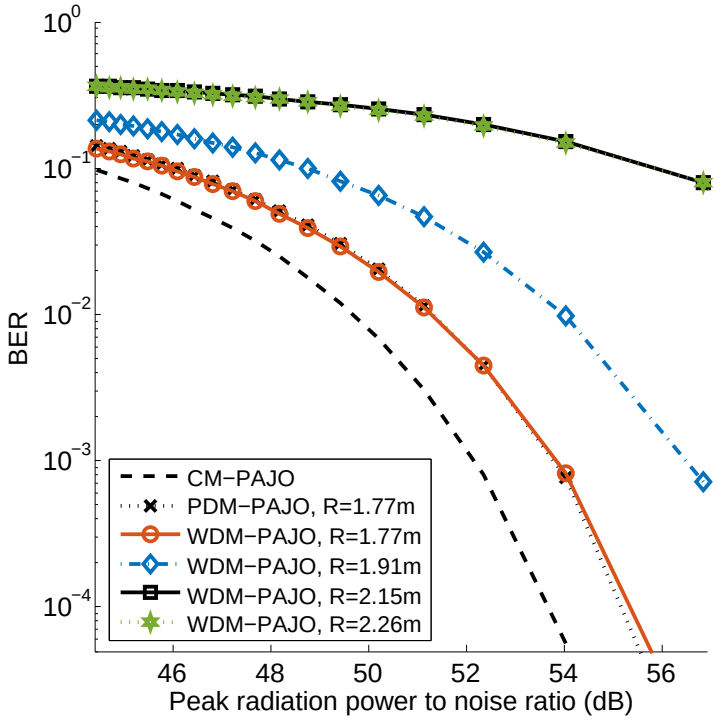

Figure 3.12: Average BER of 4 users for CM-PAJO and WDM-PAJO for different radii of access area in the small indoor environment with single detector.

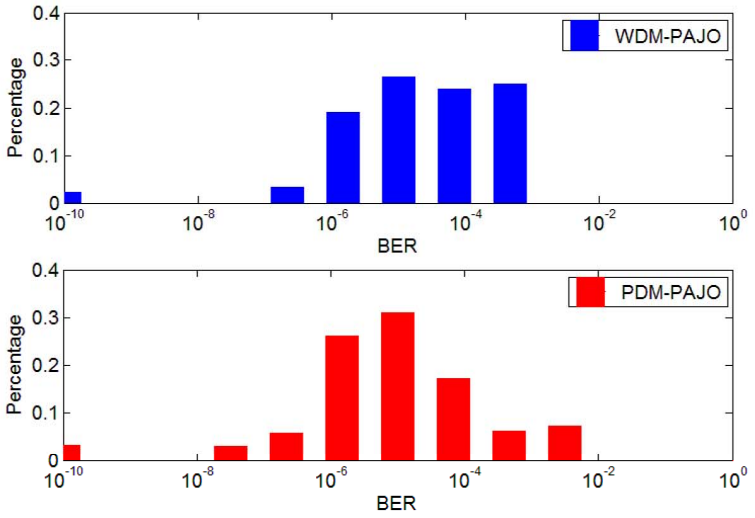

Figure 3.13: Histogram of BER performance for 4 randomly distributed users, with peak radiation power to noise ratio of 61 dB

To analyze the performance of the proposed PDM-PAJO and WDM-PAJO from a statistical point of view, we simulate 40 trials of 4 users randomly distributed in the small room. From the simulation results shown in Fig. 3.13, more than 75% of the 40 trials' BER for PDM-PAJO and WDM-PAJO are lower than 10^{-4}. Since some of the lamps in the PDM-PAJO algorithm exchange feedback information from the users, while in WDM-PAJO there is no information exchange, PDM-PAJO is better able to allocate power to users and often results in a lower BER.

3.4 Computational Burden Comparison

The goal for seeking a decentralized power allocation algorithm is to reduce the computational burden of the centralized algorithm, CM-PAJO, especially for a large indoor environment. To estimate the computational burden, we use the maximum number of variables per thread (optimization problem size) as the metric. The variables to be calculated per thread are the power allocated from the LEDs to the users and the time-space MMSE filter coefficients, which are represented as p_{qk} and $w_k[v, \ell]$

(defined in (3.1) and (3.4), respectively). The number of variables in each thread is the size of the optimization problem, which implies the computational burden.

Since in CM-PAJO all lamps need to share the channel feedback information from all the users and work together to solve for the power allocation, there is only one optimization thread. Therefore, the optimization problem size for CM-PAJO can be derived as

$$\Lambda_{CM} = (N_Q + VL)K. \tag{3.18}$$

Since the proposed decentralized algorithms use parallel processing, the computational burden per thread for them is much lower than for CM-PAJO. The actual optimization problem size depends on the users' positions in the indoor environment. In this chapter, we consider the users to be uniformly distributed in the indoor environment. The optimization problem size of the decentralized algorithms also depends on the access area. We consider the minimum access area case for calculating the computational burden.

For DEPA, the transmitted power for each user is the same. Thus, the optimization problem size is smaller than the other decentralized algorithms because there is no need to calculate the transmitted power for each user, only the filter coefficients at the detectors. The optimization problem size of DEPA can be calculated as

$$\Lambda_{DEPA} = \frac{VLK}{N}. \tag{3.19}$$

Since for both PADJO and WDM-PAJO, the lamps all work independently, and there is no channel information shared among the lamps, the optimization problem

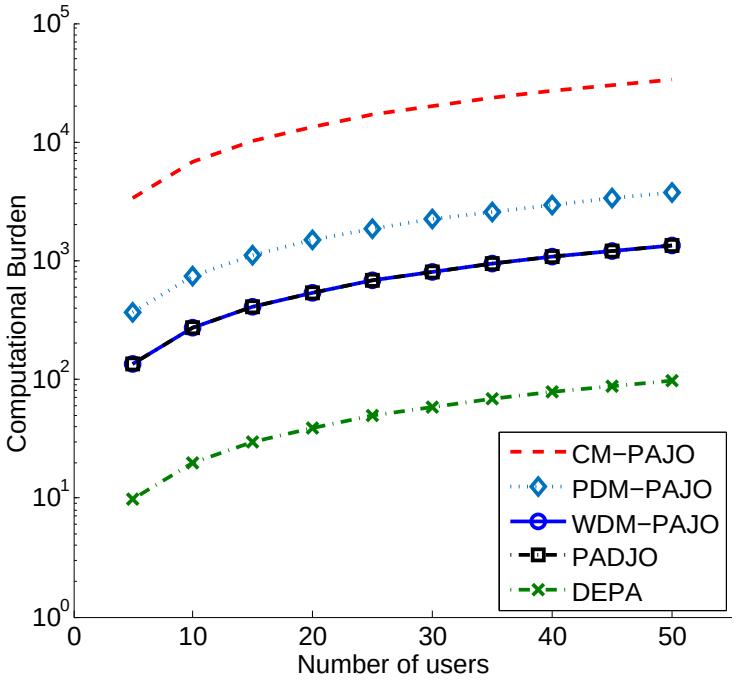

Figure 3.14: Computational burden with the minimum access area in the large indoor environment, 7 PDs per user, and length of OCDMA code of 7.

size of PADJO and WDM-PAJO can be assumed to be the same. Thus

$$\begin{aligned}\Lambda_{PADJO} &= \Lambda_{WDM} \\ &= \frac{(N_Q + VL)K}{N} = \frac{1}{N}\Lambda_{CM}.\end{aligned} \tag{3.20}$$

The optimization problem size per thread for PDM-PAJO can be written as

$$\begin{aligned}\Lambda_{PDM} &= \frac{KN_Q}{N} + VLK \\ &= \Lambda_{WDM} + \frac{(N-1)VLK}{N}\end{aligned} \tag{3.21}$$

Numerical results on optimization problem size are shown in Fig. 3.14. With the help of parallel processing, the four decentralized algorithms have much lower computational burden than the CM-PAJO algorithm. As the number of users increases, the advantage of using a decentralized algorithm becomes more obvious.

Table 3.2: Time consumption comparison of centralized and decentralized algorithms in the large room with 50 users.

	Running Time/Thread, s
CM-PAJO	2.62×10^4
PDM-PAJO	1.93×10^2
WDM-PAJO	8.65×10^0
PADJO	1.02×10^1
DEPA	1.65×10^{-2}

We compare the running time per thread for the centralized and decentralized optimization algorithms. The optimization is performed using the SQP solver in MATLAB running on a PC with an Intel i5 processor and a 2G memory. The 50 uniformly distributed users case is tested. The results, which are the average of 5 trials, are shown in Table 3.2. We find that the decentralized algorithms need much less time than the centralized algorithm. Since there is no optimization for DEPA, the time consumed for DEPA is smallest. PADJO and WDM-PAJO need a similar running time that is about 0.04% of the centralized algorithm. PDM-PAJO takes about 25 more time than WDM-PAJO and PADJO since the optimization threads for PDM-PAJO usually contain more lamps and users; for WDM-PAJO and PADJO, each thread only contains a single LED. Taking into consideration the computational burden and BER performance of the centralized and decentralized algorithms we propose, PDM-PAJO and WDM-PAJO both provide a reasonable trade-off between BER performance and computational burden.

3.5 Practical Considerations

In this section, several practical considerations of our proposed VLC design such as shadowing effects, illumination requirements, dimming control, beamwidth selection,

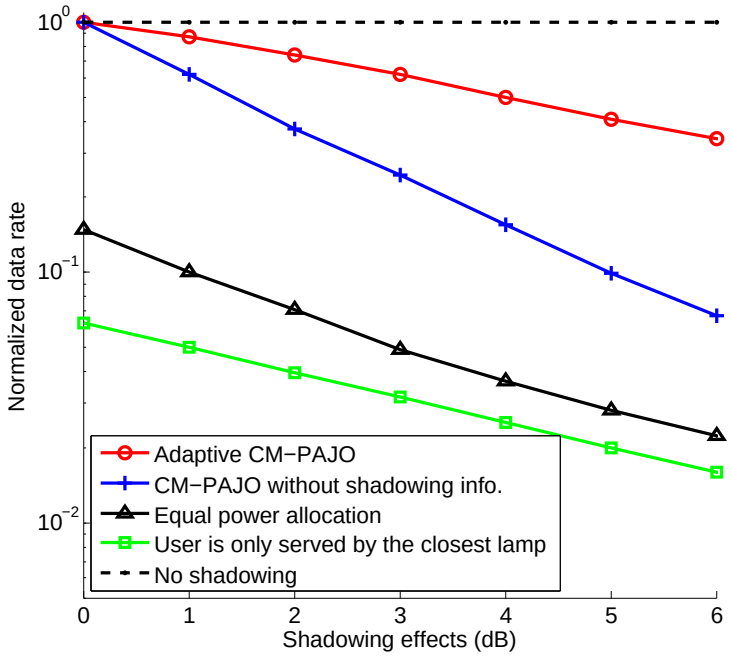

Figure 3.15: Normalized data rate of the user that is blocked under different shadowing conditions for a BER = 10^{-3}. 4 users are in the small indoor environment, and a single detector is used with length-7 OOC codes.

and nonlinear effects of LEDs are discussed.

3.5.1 Shadowing Effects

Shadowing is a common phenomenon that can be regarded as a kind of path loss as in RF communication systems [51]. In our work, we assume that the shadowing effects in VLC systems are caused by objects that block the light. Since the light can be partially blocked, we define the shadowing effects as a power loss. We assume the shadowing losses are generated from the one lamp that is closest to the user. The shadowing loss coefficient for user k is denoted as $\epsilon_k \in [0, 1]$. When $\epsilon_k = 0$ the light is totally blocked, and when $\epsilon_k = 1$ there is no shadowing for user k. In this work, we represent the power loss due to ϵ_k in dB.

To test the effects of shadowing on our system, we assume a 4 users system

in the small indoor environment, and only one of them is affected by shadowing. Fig. 3.15 shows the maximum data rate of the affected user normalized to that of the non-shadowed case. In this chapter, we design our algorithms to be adaptive, so the system reallocates the transmitted power when the environment and users' positions change. Fig. 3.15 compares the adaptive CM-PAJO, the CM-PAJO without shadowing information, the DEPA, and the case that each user is only served by the closest lamp. From the numerical results, although the data rate of all schemes decreases with increasing shadowing effects, the adaptive CM-PAJO has significantly better performance.

For the decentralized algorithms, if the shadowed users are supported by more than one lamp, the decentralized power allocation algorithms can also adjust the power assignment to provide those users good communication service. However, if a user is only served by one lamp, the decentralized algorithms cannot alleviate the shadowing effect. We can usually adjust the size of the access area to make sure each user can be served by more than one lamps using the decentralized algorithms.

3.5.2 Illumination Requirements and Dimming Control

Dimming can be used to satisfy different illumination requirements for different purposes. The effective dimming level depends on the radiation power and the ratio of the OCDMA code weight to the code length, η, which determines the illumination potential. In this work, we assume the OCDMA codewords have been specified (not adaptive), and η is fixed. Thus, the dimming level can only be adjusted by changing the radiation power. The Illumination Engineering Society of North America provides some illumination level standards for indoor environments [49]. For example, the illumination level for an office building should be greater than 400 lx. For hotels and restaurants, 100 lx illumination is enough.

To ensure the room is uniformly illuminated in space, we assume that there are K_v virtual users uniformly distributed in the room, and the virtual users need illumination only (no communications). Thus, the total number of users is $K_{tot} = K + K_v$, where K is the number of real users who need both data and illumination. Under this assumption, we can define the illumination tolerance at user k as Δ_k, and require that

$$|A_r \eta \hat{\mathbf{h}}_k^T \mathbf{p}_{dim}^{max} + P_b - P_{req}| \leq \Delta_k, \tag{3.22}$$

where $\hat{\mathbf{h}}_k = (\hat{h}_{1k1}, \hat{h}_{2k1}, \ldots, \hat{h}_{N_Qk1})^T$. We denote $\hat{h}_{qk1}$ as the channel gain from LED q to the detector of user k that is pointed towards the ceiling. $\mathbf{P}_{dim}^{max}$ is the dimmed peak power vector, which can be represented as $\mathbf{P}_{dim}^{max} = \underline{\emptyset} P^{max} = P^{max}(\emptyset^{(1)}, \emptyset^{(2)}, \ldots, \emptyset^{(N_Q)})^T$, where $\underline{\emptyset} = (\emptyset^{(1)}, \emptyset^{(2)}, \ldots, \emptyset^{(N_Q)})$, and $\emptyset^{(q)}$ is the dimming parameter for LED q. To satisfy specific illumination requirements, the dimming parameters can be adjusted in the range of $[0, 1]$ for dimming control. Thus, the peak power constraint for different LEDs may be different. P_b and P_{req} represent the received power from background light and the required illumination, respectively. The tolerance Δ_k limits the difference between the required illumination and the actual illumination.

To make sure the illumination throughout the room is as spatially constant as possible, the dimmed transmitted power of each LED can be controlled to minimize the illumination tolerance among all the users (real and virtual). Thus, the optimal dimming parameters $\underline{\emptyset}^*$ can be found by

$$[\underline{\emptyset}^*] = \arg \min_{\underline{\emptyset}} \max_k \Delta_k. \tag{3.23}$$

Then, the dimmed peak power vector $\mathbf{p}_{dim}^{max}$ can be used as a peak power constraint for each LED, in either the centralized or one of the decentralized power allocation algorithms described above.

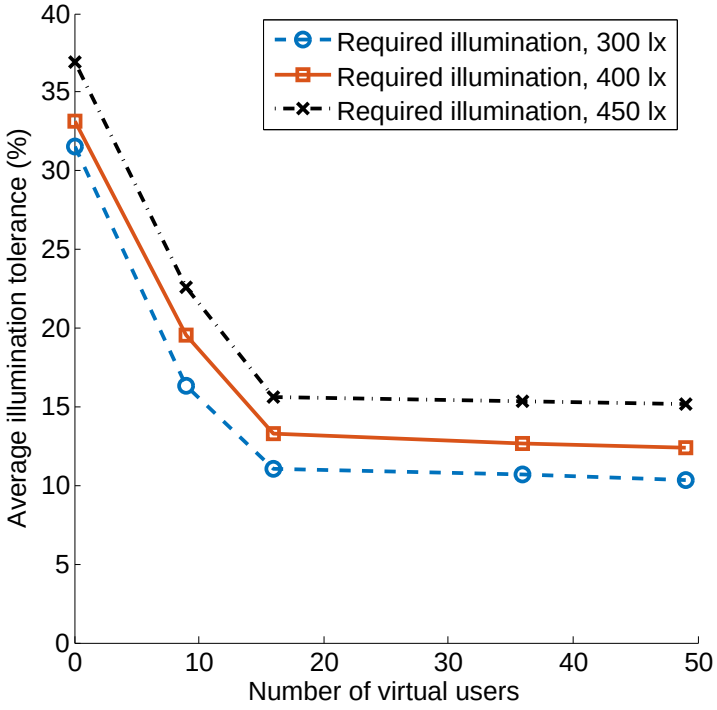

Figure 3.16: Average illumination tolerance for different number of virtual users.

The illumination tolerance can be used as a criterion to evaluate how uniformly an illumination can be provided by the VLC system. Numerical results on the average illumination tolerance of all the indoor area with different numbers of uniformly distributed virtual users are shown in Fig. 3.16. As expected, the more virtual users, the lower the average illumination tolerance that can be achieved, since more virtual users can represent the space in the room more fully. However, more virtual users can introduce more computational burden when we calculate the illumination tolerance. For this result, we conclude that 16 uniformly distributed virtual users can fully represent the entire space in the small indoor environment.

The illumination tolerance Δ_k affects the BER performance in multiuser indoor VLC systems, which is assumed to be in the range of 9% to 60%. From the simulation results, we observe that if the tolerance of illumination increases, the BER performance curve converges to the no-illumination-constraint case. Simulations are

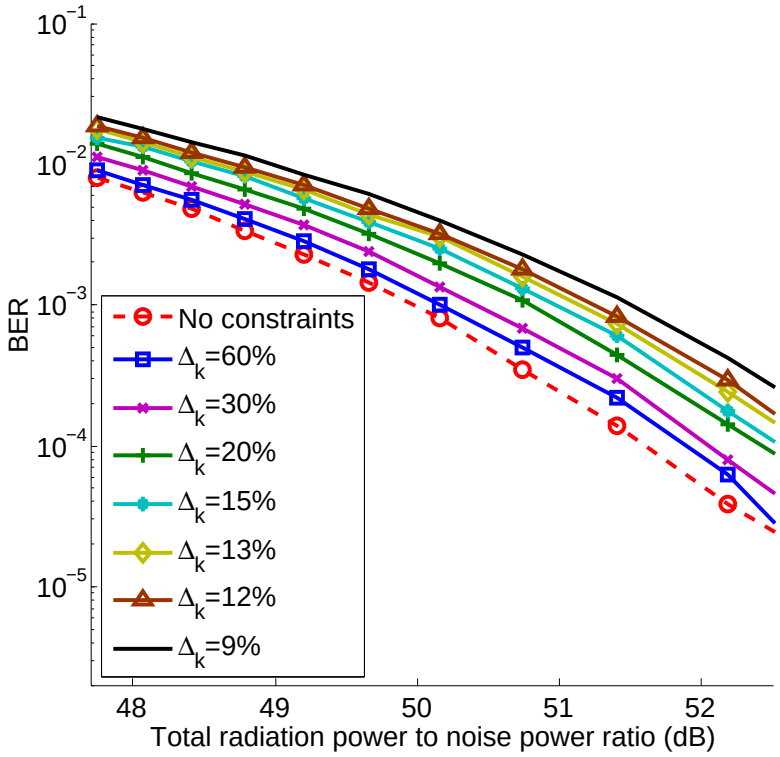

Figure 3.17: BER comparison with different lighting tolerances, with 4 users and 16 virtual users for the 25-LED lamp case, 400 lx illumination requirements

shown for 4 users with data and illumination requirements and 16 virtual users with only illumination requirement in Fig. 3.17. From these results, the BER with 60% tolerance is quite close to the BER without constraints. Note that this variation in the room lighting may be unpleasant for a human eye. The evaluation of this aspect of the design is beyond the scope of this dissertation.

Fig. 3.18-(a) shows a contour plot of the illumination distribution for 4 users with both data transmission and illumination requirements, plus 16 virtual users with illumination requirements only. Fig. 3.18-(b) shows the illumination distribution without data transmission requirements. Comparing these two figures, the illumination distribution in (a) is still smooth and flat. That is to say, setting illumination constraints prevents the lighting system from creating too dark and too bright spots in the room, and the illumination requirements at all the user locations are satisfied.

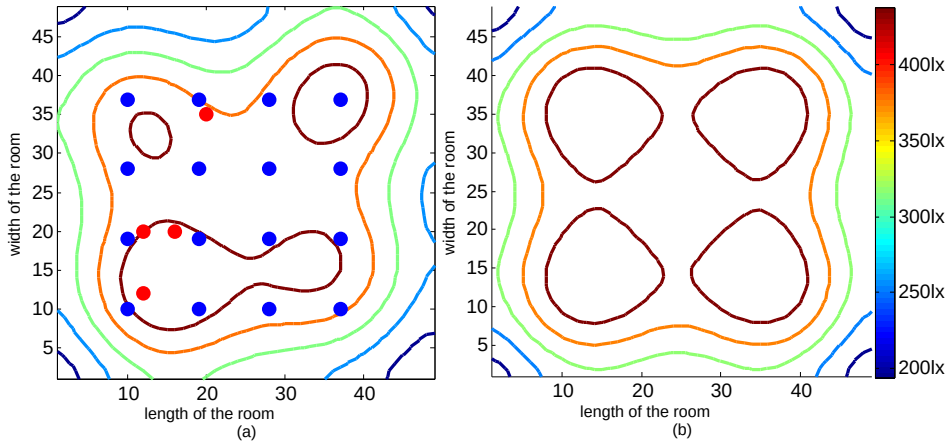

Figure 3.18: Illumination distribution comparison of (a) data transmission case and (b) no data transmission case. The red dots identify the real users, and the blue dots represent the virtual users, with 10% tolerance.

The semiangle of the LEDs is another factor that affects the dimming control accuracy. In Fig. 3.19, we compare the optimal illumination tolerances for different semiangles using our multiple-LED lamp and a single-LED lamp in which there is only one LED per lamp. For small semiangle LEDs (less than 15 degrees) in the multiple-LED case, the beam width of the LEDs is too narrow, and all the area on the floor cannot be illuminated. Thus, some areas of the floor would be very dark, and other areas would be bright. Because of that, the illumination tolerance defined in (3.22) is large. If large semiangle LEDs are used, the illumination area of each LED is relatively large, but the intensity of the illumination would not be as high as in the small semiangle cases. It is not easy to control the illumination level for a particular area as accurately with large semiangle LEDs. Therefore, to make sure the illumination distribution is uniform for different requirements, the semiangle of the LEDs cannot be too large or too small. From the numerical results in Fig. 3.19, a 20-degree semiangle LED is the best choice for the proposed multiple-LED lamp model to have the lowest illumination tolerance if 16 uniformly distributed virtual users are modeled in the small room. The single-LED lamp has a similar behavior as

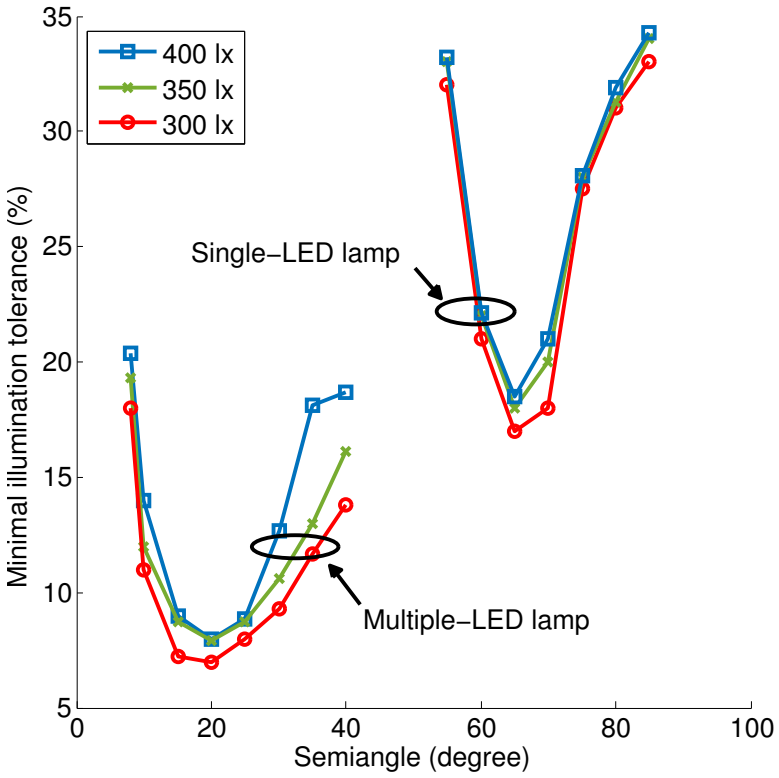

Figure 3.19: Minimum illumination tolerance under different illumination requirements for different LED's semiangle in the small indoor environment; 16 virtual users.

the multiple-LED lamp case. There is an optimal choice for the semiangle, which is around 60 degrees for the single-LED lamp. Compared with the multiple-LED lamp, the single-LED lamp cannot provide high accuracy illumination control.

We also take the background illumination (BI) in the indoor environment into account in the form of background power P_b in (3.22). We assume that the background power also introduces shot noise. If the required illumination level in the room is assumed to be fixed around 400 lx [49], the more background light there is, the less radiation power the LED lamps need to emit. Fig. 3.20 shows the BER performance of the CM-PAJO algorithm under different background light conditions. In this result, we assume the background light is uniformly distributed, and the background illumination on different PDs is the same. We note that increasing the background light decreases the number of users the system can support.

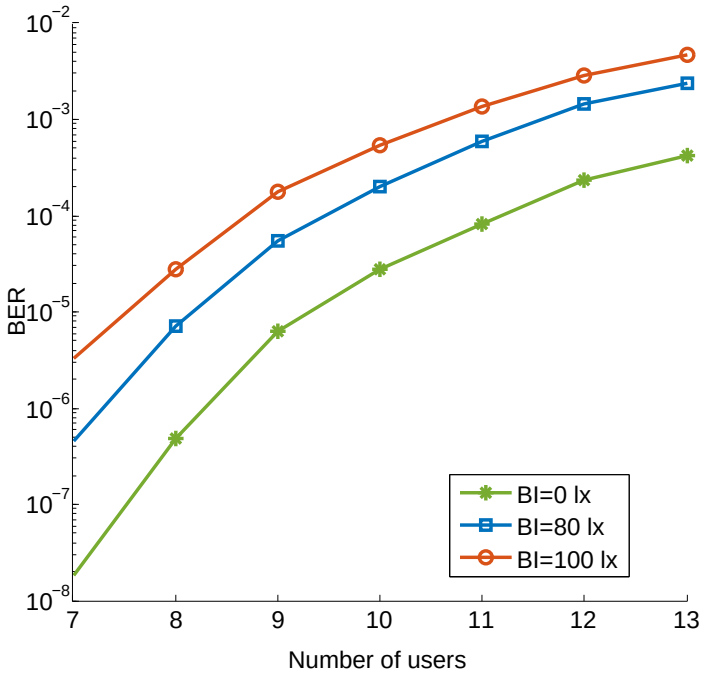

Figure 3.20: BER performance for CM-PAJO under different background light illumination conditions in the small indoor environment with 400 lx required illumination and 7-detector model, 4 users with length-7 OOC codes.

If the background light comes from a window or another room, our multiple PDs system has advantages over the single PD case. Since we take advantage of the signals from different PDs, the space-time MMSE filter can improve the SINR. We now model the background light from a window as a point light source on a wall. We suppose the window is located on one wall of the small room at (0, 2.8, 2.8). Numerical results for this case are shown in Table 3.3. In this case, there are four randomly distributed users, and the background light adds shot noise. The results indicate that our multi-detector system is robust against background light interference from a window by using our MIMO technique.

Table 3.3: BER performance for CM-PAJO with 400 lx required illumination.

BER$\times 10^{-5}$	BI=0 lx	BI=80 lx	BI=100 lx
Number of PDs, $V = 1$	11.3	57.3	132
Number of PDs, $V = 4$	2.19	2.39	2.57
Number of PDs, $V = 7$	1.54	1.67	1.81

3.5.3 Transmitted Power Quantization

Although we assume on-off CDMA coding and OOK modulation, since each LED transmits the sum of signals meant for the various users, the signal itself is no longer on-off pulsed. In this section, we assume each LED of the multiple-LED lamp is a LED-array that is composed of many micro-LEDs (μLED) [52].

The optical power from the LEDs is driven by an input electrical signal that carries information. Due to the structure of the LEDs and the principles of generating light, the relation between the output optical power and the input current can be modeled as a nonlinear function. To diminish the effect of the nonlinearity of LEDs on our system, each μLED in the LED-arrays can only be controlled as on or off, and these μLEDs can be clustered into different groups, where each group can be controlled to be on or off. For example, if the μLEDs in an LED-array can be divided into 7 groups with the same number of μLEDs, there are 8 levels of intensity that can be emitted, from level 0 to level 7. For level 0, no group is lit; for level 7, all the groups are switched on. A design trade-off needs to be found between the quantization errors and the structural complexity, which is outside the scope of this study. Fig. 3.21 shows a possible LED grouping scheme for 8 quantization levels. In this figure, the LEDs in the LED-array are divided into 7 groups with the same number of LEDs. Thus, there are 8 levels of intensity that can be emitted, from level 0 to level 7. For level 0, no group is; for level 7, all the groups are switched on. A design trade-off

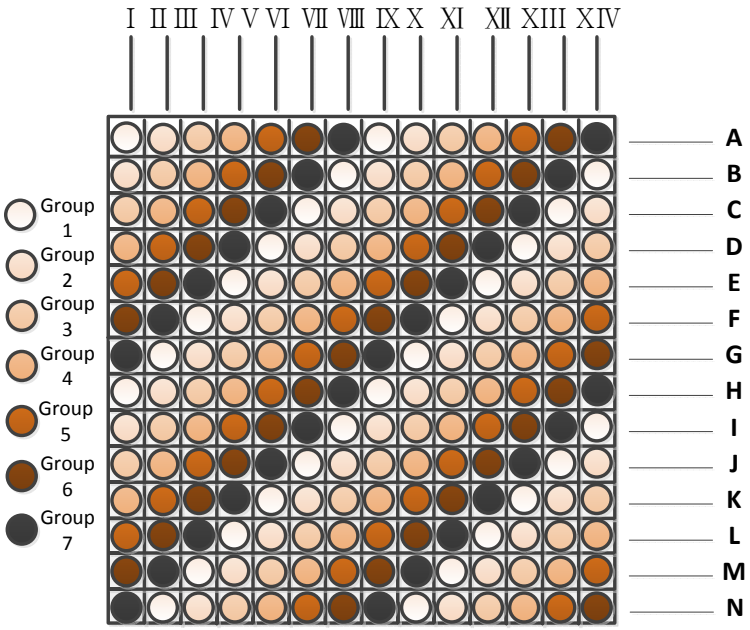

Figure 3.21: LED grouping scheme for 8 quantization levels

needs to be found between the quantization errors and the structural complexity, which is outside the scope of this study.

Numerical results for the system performance of different quantization levels are shown in Fig. 3.22. For the same scenario as shown in Fig. 3.1, Case 2, we conclude that 8 quantization levels are sufficient in our system.

3.6 Summary

In this chapter, we present a multiuser MIMO indoor visible light communication system that is robust against shadowing, dimming, background radiation, and LED nonlinearity. In this system, a centralized power allocation scheme and four decentralized algorithms are proposed. To enhance the SINR for each user, a multiple PDs model is employed at the receiver. The BER performance and computational burden of the algorithms are analyzed. Compared to the centralized power allocation algorithms, the four proposed decentralized power allocation algorithms all have much

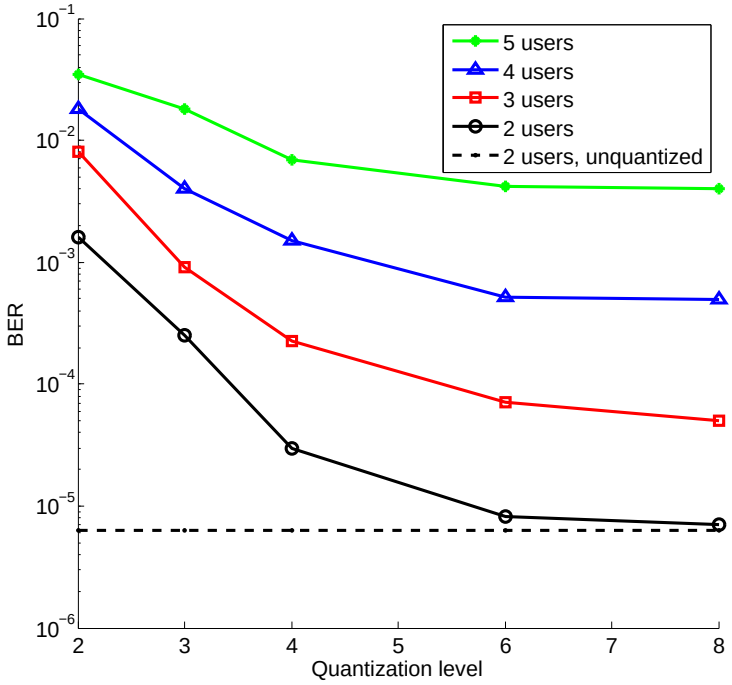

Figure 3.22: The average BER performance for different quantization levels with 2, 3, 4 and 5 users using length-7 OOC codes in the small environment, semiangle is 30 degrees, no dimming control.

lower computational burden. Considering the BER performance of the centralized and all decentralized algorithms, PDM-PAJO and WDM-PAJO are the best choices. When some users are affected by shadowing, our proposed adaptive MIMO power allocation algorithms can reallocate the transmitted power to reduce the shadowing effects. From the simulation results, the data rate of the shadowed user using adaptive CM-PAJO is about twice as high as the algorithm without knowing the shadowing information when the shadowing loss coefficient α_k is 3 dB. The algorithms proposed in this chapter can adjust the dimming parameters for each LED to accommodate the illumination requirements. From the numerical results, our proposed MIMO algorithm can support multiple users with high communication performance in both small and large indoor environments within strict illumination requirements. In addition, the nonlinearity of LEDs is also considered in this chapter and can be solved by using

micro-LED arrays.

Chapter 4

Modulation Schemes for VLC Systems

In this chapter we first propose a robust and high-rate multiuser system design based on M-PAM. Since light emitted from LEDs is non-coherent, an M-ary intensity modulation that has a high bandwidth efficiency such as M-PAM is a good choice [17]. Then, a joint optimization of waveform and MMSE filter is proposed to reduce ISI and MAI simultaneously. In the end, a comparison between DCO-OFDM and M-PAM with designed waveform is given.

The proposed algorithm can adjust the modulation constellation size for each user to maximize the bit rate under different channel environments such as shadowing, light dimming, and the impact of multiple access interference. In our MISO approach, multiple LED lamps coordinate to provide users with maximum data rates. We compare OCDMA using our adaptive M-PAM with TDMA. The OCDMA technique can offer a higher bit rate when the number of users is larger than the length of the OCDMA code.

To increase the transmission throughput, ISI is one of the biggest challenges. We

propose a joint optimal waveform design for visible light communication system using M-ary pulse amplitude modulation to support multiple users. The transmitted waveforms and minimum mean squared error filters are jointly optimized to minimize the intersymbol and multiple access interferences. Based on different channel conditions, the designed waveforms and modulation constellation size can be adaptively adjusted to guarantee the highest data rate.

A comparison between our optimized M-PAM and DCO-OFDM for LED-based communication systems is given. Considering the bandwidth limit and constrained peak transmitted power characteristics of LEDs, bit loading with an optimized modulation index is used for the DCO-OFDM.

Part of the work presented in this chapter has been published in [30, 53].

4.1 Adaptive M-PAM for Multiuser MISO Indoor VLC Systems

4.1.1 Background

To support multiple users, MISO processing and OCDMA can be applied [45, 54–56]. Multiple LED lamps transmit CDMA coded signals in a coordinated manner to support multiple users, making the system robust against channel shadowing. In addition, to diminish the MAI and improve the SINR, the transmitted power from each LED can be optimally allocated to users and optimally detected using a MMSE filter at the receivers, as presented in Section 3.2. In this section we adopt an adaptive M-PAM modulation scheme instead of the OOK previously used. The adaptive M-PAM modulation algorithm selects a different constellation size for each user to optimize the transmitted data rate in a fair manner. Users with better channel

downlink quality can benefit from a larger modulation constellation size and/or be allocated a lower portion of the total LED power so that all users can maintain a preset communication performance level. We show that CDMA is able to provide higher data rates than TDMA for the same performance when the number of users is larger than the code length.

Recently, some significant research has been directed towards designing modulation schemes for VLC systems [17]. M-PAM was explored in [57] to yield a $(\log_2 \mathrm{M})$-fold increase in the data rate compared with OOK. Instead, OFDM can be used to increase the data rate and efficiently combat ISI [24, 58]. Furthermore, researchers have proposed adaptive modulation schemes for VLC based on OFDM [59]. The drawback of OFDM is that it has a relative high PAPR, making it more sensitive to the nonlinear distortion of the LEDs than pulsed techniques such as PAM. An M-ary variable period modulation (MVPM) scheme for VLC was proposed in [19]; MVPM has been proven capable of reducing the slot duration to increase the data transfer rate in VLC system. However, it is difficult to keep all the users synchronized. In addition, the narrow time slot may introduce ISI from multipath in the indoor channel. A MIMO-PPM technology was proposed in [60] to improve the data rates without reducing the reliability of the link. However, the multiuser case was not considered in [60]. Furthermore, PPM is bandwidth inefficient and very sensitive to external interference that may cause a complete data corruption. To alleviate these drawbacks, we propose a MISO CDMA VLC system using an adaptive M-PAM modulation scheme with synchronized symbol rate across users and LED lamps. Channel state information at the transmitter is assumed known perfectly so that when the downlink channel conditions change due to motion or shadowing, the proposed algorithm can adjust the modulation constellation size to optimize the bit rate adaptively.

4.1.2 Adaptive M-PAM

We assume all LED lamps are synchronized with each other and all contribute to the data transmission for all users in the access area of interest. The VLC channel between LED q and user k is completely characterized by $\hat{h}_{qk}$ and known at the transmitters. Using M-PAM modulation, we assume the amplitude of the transmitted symbol for user k is $s_k \in \{0, \frac{1}{M_k-1}, \frac{2}{M_k-1}..., 1\}$, and each symbol carries $\log_2 M_k$ bits, where M_k is the modulation constellation size for user k. Since we assume the binary data is equally likely, the a_k are uniformly distributed. Thus, the transmitted signal for the qth LED can be represented as

$$x_q(t) = \sum_{k=1}^{K} p_{qk} s_k c_k(t), \tag{4.1}$$

where p_{qk} is the power allocated to the qth LED for user k and $c_k(t)$ is the OCDMA codeword for user k. Similar to the work in Section 3.2, the received signal for user k after MMSE filtering can be represented as

$$y_k = \mathbf{s}^T \mathbf{B}_k \mathbf{C} \mathbf{w}_k + \mathbf{n}_k^T \mathbf{w}_k, \tag{4.2}$$

where $\mathbf{s} = (s_1, s_2, \ldots, s_K)^T$ is the transmitted symbol vector; the MMSE filter for user k is defined as $\mathbf{w}_k$; $\mathbf{C}$ represents the CDMA code matrix, which can be represented as $\mathbf{C} = (\mathbf{c}_1, \mathbf{c}_2, \cdots, \mathbf{c}_k)^T$, where $\mathbf{c}_k$ is the CDMA code for user k; $\mathbf{n}_k$ is the noise at the user k, which can be modeled as Gaussian distributed noise with variance σ^2. To

facilitate the formulation, we define the matrix $\mathbf{B}_k = \text{diag}\left(\hat{\mathbf{h}}_k^T \cdot \mathbf{P}\right)$, where

$$\mathbf{P} = \begin{pmatrix} p_{11} & p_{12} & \cdots & p_{1K} \\ p_{21} & p_{22} & \cdots & p_{2K} \\ \vdots & \vdots & \ddots & \vdots \\ p_{Q1} & p_{Q2} & \cdots & p_{QK} \end{pmatrix} \tag{4.3}$$

represents the power allocation matrix. After some calculations, the MMSE filter for user k can be represented as

$$\mathbf{w}_k = \left(\mathbf{C}^T\mathbf{B}_k\mathbf{\Sigma_s}\mathbf{B}_k\mathbf{C} + \sigma^2\mathbf{I}\right)^{-1}\mathbf{C}^T\mathbf{B}_k\mathbf{q}_k, \tag{4.4}$$

where $\mathbf{I}$ is the identity matrix of the same size as the OCDMA code matrix $\mathbf{C}$, and $\mathbf{\Sigma_s}$ is the correlation matrix for the transmitted symbol, which can be calculated as

$$\mathbf{\Sigma_s} = \begin{pmatrix} E\{s_1 \cdot s_1\} & E\{s_1 \cdot s_2\} & \cdots & E\{s_1 \cdot s_K\} \\ E\{s_2 \cdot s_1\} & E\{s_2 \cdot s_2\} & \cdots & E\{s_2 \cdot s_K\} \\ \vdots & \vdots & \ddots & \vdots \\ E\{s_K \cdot s_1\} & E\{s_K \cdot s_2\} & \cdots & E\{s_K \cdot s_K\} \end{pmatrix}, \tag{4.5}$$

and

$$\mathbf{q_k} = \left(E\{s_k \cdot s_1\}, E\{s_k \cdot s_2\}, \cdots, E\{s_k \cdot s_K\}\right)^T, \tag{4.6}$$

where $E\{s_k \cdot s_v\}$ can be calculated as

$$E\{s_k \cdot s_v\} = \begin{cases} \frac{2M_k^2 - M_k}{6(M_k - 1)} & k = v \\ \frac{1}{4} & k \neq v \end{cases}. \tag{4.7}$$

The SINR for user k can be represented as [27][1]

$$\gamma_{\mathrm{k}} = \frac{A_r^2 \mathbf{w_k}^T \mathbf{C}^T \mathbf{B}_k \mathbf{Z}_k \mathbf{\Sigma_s} \mathbf{Z}_k \mathbf{B}_k^T \mathbf{C} \mathbf{w}_k}{\mathbf{w}_k^T \mathbf{C}^T \mathbf{B}_k \hat{\mathbf{Z}}_k \mathbf{\Sigma_s} \hat{\mathbf{Z}}_k \mathbf{B}_k^T \mathbf{C} \mathbf{w}_k + \sigma^2 \mathbf{w}_k^T \mathbf{w}_k}, \tag{4.8}$$

where the matrix $\mathbf{Z}_k$ is defined as a matrix with a '1' in its (k,k)th element and zeros in all other places, and $\hat{\mathbf{Z}}_k = \mathbf{I} - \mathbf{Z}_k$.

From (4.5)-(4.8), we conclude that the SINR for user k depends on the power allocation scheme and the M-ary modulation constellation size of all users. Therefore, the SINR is a function of $\mathbf{M} = (M_1, M_2, \cdots, M_K)^T$ and the power allocation matrix $\mathbf{P}$.

The bit error rate (BER) for user k when using M-PAM can be represented approximately as [34]

$$\mathrm{BER_k} \approx \frac{M_k - 1}{M_k \log_2 M_k} \mathrm{erfc}\left(\sqrt{\frac{\gamma_{\mathrm{k}}}{(M_k-1)^2}}\right) \approx \frac{1}{\log_2 M_k} \mathrm{erfc}\left(\sqrt{\frac{\gamma_{\mathrm{k}}}{(M_k)^2}}\right). \tag{4.9}$$

In this chapter, our adaptive M-PAM scheme can adjust the modulation constellation size for different users, i.e., choose the optimal constellation size to optimize the throughput for all users. The bit rate for user k can be represented as

$$R_b^{(k)} = R_s \cdot \log_2 M_k, \tag{4.10}$$

where R_s is the symbol rate, assumed to be the same for all users. To optimize the throughput fairly, the optimization cost function we use is given by

$$[\mathbf{P}^*, \mathbf{M}^*] = \arg \max_{\mathbf{P},\mathbf{M}} \min_k R_b^{(k)}, \tag{4.11}$$

[1]For all SINR expressions in this chapter, the responsivity of the receiver is ignored. It is nonetheless accounted for in the simulation results.

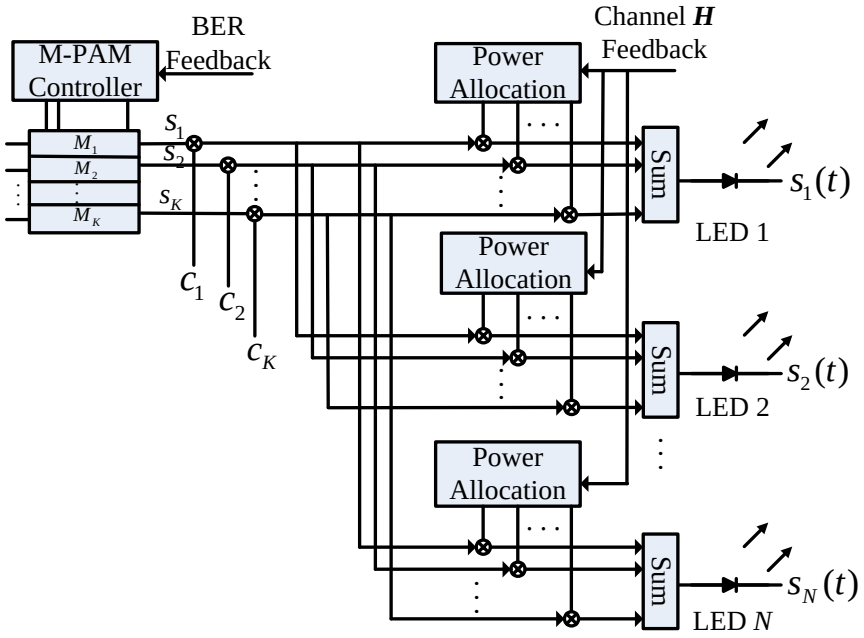

Figure 4.1: Block diagram of the proposed adaptive M-PAM algorithm using our MISO technique

where $\mathbf{P}^*$ and $\mathbf{M}^*$ are the optimal solutions for power allocation and modulation constellation size, respectively. When doing the optimization, a peak transmitted power constraint must be considered. To satisfy the communication quality, a constraint on the BER should also be taken into account. Thus, the optimization constraints can be represented as

$$\sum_{k=1}^{K} p_{qk} \leq P^{max} \text{ and } p_{qk} \geq 0 \ \ \forall q, \quad \text{and} \quad \text{BER}_k \leq B^{max}, \tag{4.12}$$

where P^{max} is the peak transmitted power. B^{max} is the desired BER for each user, which guarantees the communication quality. Usually B^{max} is chosen as 10^{-3}, since forward error correction (FEC) can then be applied to lower it to within application-specific standard values [61].

A block diagram of the proposed adaptive M-PAM algorithm is shown in Fig. 4.10.

The power allocation $\mathbf{P}$ and the M-ary modulation constellation size vector $\mathbf{M}$ is computed jointly. Depending on the channel state information and BER fed back from the users, the central controller optimizes these to maximize the bit rate for each users. The binary data $\mathbf{d} = (d_1, d_2, \ldots, d_K)$ are M-ary modulated , then modulated with OCDMA codes $(c_1, c_2, \ldots, c_K)$, and finally transmitted by the LEDs. If the channel or BER feedback information is changed, the controller adaptively adjusts the constellation size to maintain the desired performance.

4.1.3 OCDMA vs TDMA using M-PAM

Since the OCDMA codes are not perfectly orthogonal, it is not evident *a priori* whether OCDMA is a more efficient method to support multiple users in indoor VLC systems than an orthogonal multiple-access scheme, such as TDMA [62]. In this section, we analyze the throughput achievable with our optimized adaptive M-PAM algorithm using OCDMA vs. TDMA. We compare the SINR, modulation constellation size and the bit rate achievable using OCDMA and TDMA. To keep the comparison fair, we assume the OCDMA and TDMA options use the same bandwidth, i.e., the pulse width, T_c, for both OCDMA and TDMA is the same, as shown in Fig. 4.2. For TDMA, if the number of users increases, the symbol rate for each user decreases, since each time slot can only be used by one user at a time. For OCDMA, the symbol rate for each user only depends on the length of the codeword L. Thus, we can write the symbol rate $\widehat{R}_s$ and $\widetilde{R}_s$ using TDMA and OCDMA, respectively, as

$$\widehat{R}_s = \frac{1}{K \cdot T_c}, \quad \widetilde{R}_s = \frac{1}{L \cdot T_c}. \tag{4.13}$$

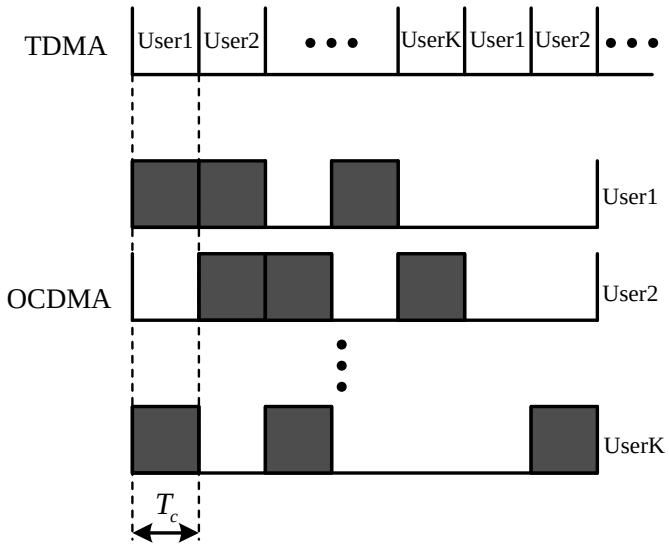

Figure 4.2: OCDMA and TDMA comparison using M-PAM, $K < L$ case ($L = 7$ and $K = 5$).

Therefore, the bit rate for user k using TDMA and OCDMA can be expressed as

$$\hat{R}_b^{(k)} = \frac{\log_2 \hat{M}_k}{K \cdot T_c}, \quad \tilde{R}_b^{(k)} = \frac{\log_2 \tilde{M}_k}{L \cdot T_c}, \tag{4.14}$$

where $\hat{M}_k$ and $\tilde{M}_k$ are the modulation constellation sizes for user k using TDMA and OCDMA, respectively.

To compare the SINR for TDMA and OCDMA, in the following analysis we assume the average transmitted power is $\bar{P}$, and the channel gain $\hat{h}$ from the lamp to all users is the same. Then, we can roughly represent the SINR for each user using TDMA as

$$\hat{\gamma} = \frac{A_r^2 \hat{h}^2 \bar{P}^2}{\sigma^2}. \tag{4.15}$$

Similarly, the SINR for each user using OCDMA can be roughly represented as

$$\tilde{\gamma} = \frac{A_r^2 \hat{h}^2 \bar{P}^2 \omega}{(K-1)\hat{h}^2 \bar{P}^2 \lambda + \sigma^2 K^2 L}, \tag{4.16}$$

where λ is the upper-bound on the cross-correlation value for OCDMA codes used, and ω is the code weight. Note that this expression is a worst case since the MMSE filter would remove much of the MAI.

From (4.15) and (4.16), we obtain

$$\frac{\tilde{\gamma}}{\hat{\gamma}} = \frac{\sigma^2}{\frac{(K-1)\hat{h}^2 \bar{P}^2 \lambda}{\omega} + \sigma^2 \frac{K^2 L}{\omega}}. \tag{4.17}$$

Since $K \geq 1$ and $\omega < L$, we conclude $\tilde{\gamma} < \hat{\gamma}$. In other words, the modulation constellation size for TDMA is greater than or equal to that of OCDMA.

From (4.14), we see that the bit rate is related to the number of users K and the length of the code L for TDMA and OCDMA, respectively. Comparing the bit rate, we get

$$\frac{\tilde{R}_b}{\hat{R}_b} = \frac{K}{L} \cdot \frac{\log_2 \tilde{M}_k}{\log_2 \hat{M}_k}, \tag{4.18}$$

and thus

$$K \underset{\text{TDMA}}{\overset{\text{OCDMA}}{\gtrless}} \xi \cdot L \quad \text{where } \xi = \frac{\log_2 \hat{M}_k}{\log_2 \tilde{M}_k}. \tag{4.19}$$

Since for both $\tilde{M}_k$ and $\hat{M}_k$ can be chosen from small values such as $\{2, 4, 8, 16\}$, we can safely assume that $\xi \approx 1$. Therefore, we can conclude that, when the number of users is larger than the length of OCDMA code, the OCDMA technique can offer a higher bit rate than using TDMA. The highest data rate is achieved when the minimum length code needed to support the number of users is chosen.

Table 4.1: Parameters Used for Large Indoor Environment

Size of room	12.5 m × 12.5 m × 3 m
Semiangle of LEDs	60^o
Area of PD, A_r	1 cm^2
Peak optical power per lamp	300 mW
Noise variance	$\sigma^2 = 2$ μW
Modulation constellation sizes	$2, 4, 8, 16$
B^{max}	$\leq 10^{-3}$
OOC code index	$L = 25$: {1, 2, 7} {1, 3, 10} {1, 4, 12} {1, 5, 14}
	$L = 19$: {1, 2, 6} {1, 3, 9} {1, 4, 11}
	$L = 13$: {1, 2, 5} {1, 3, 8}

4.1.4 Numerical Results

In this section, the performance of the proposed adaptive M-PAM algorithm is shown using simulation. To test the applicability of the algorithm in different scenarios, we show results for different users cases in a large indoor environment, i.e., an empty and unfurnished room. Unless otherwise noted, the parameters used to obtain the numerical results are shown in Table 4.2. We assume the users are randomly dispersed in the room. The geometric position of the lamps and users ($K = 40$ case) is shown in Fig. 4.3.

The shadowing effects are also taken into account in this dissertation, since it is common for objects such as furniture and pedestrians to partially block the light from an LED lamp. We model the shadowing effect as an optical power loss from the one lamp that is closest to the user. Define $\epsilon_k \in [0, 1]$ as the shadowing loss coefficient for user k. When $\epsilon_k = 0$ the light is totally blocked, and when $\epsilon_k = 1$ there is no shadowing effects for user k. In this work, we represent the power loss due to ϵ_k in dB. A feedback channel from each user to the LED controller informs the system of the channel gain experienced so that the algorithm can adjust the M-PAM modulation

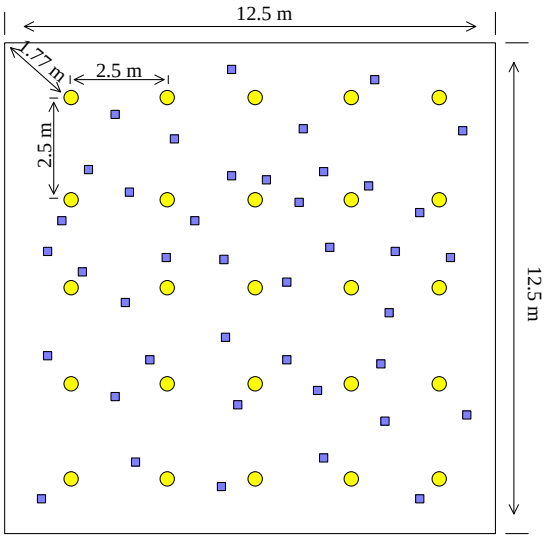

Figure 4.3: Top-down view of indoor environment. The small circles represent the lamps and the squares represent the users.

constellation size adaptively to optimize the bit rate when the channel is experiencing shadowing.

Simulation results under different shadowing conditions are shown in Fig. 4.4. We compare the average modulation constellation size for OCDMA and TDMA under different shadowing loss assuming one quarter of all users are suffering from the shadowing effect. The average modulation constellation size for TDMA is uniformly higher than using OCDMA, as expected due to the lower SINR of OCDMA because of the MAI it experiences.

For higher quality communications, a lower desired BER can be used, inevitably leading to a smaller modulation constellation size, as evident from (4.9). Simulation results in Fig. 4.5 show the performance for various values of B^{max}. As expected, the algorithm must sacrifice data rate to obtain a better BER performance.

Although Fig. 4.6 shows that TDMA has a larger modulation constellation size than OCDMA, the throughput also depends on the relation between the bit rate and the symbol rate, given in (4.10). Numerical results showing the average bit rate using

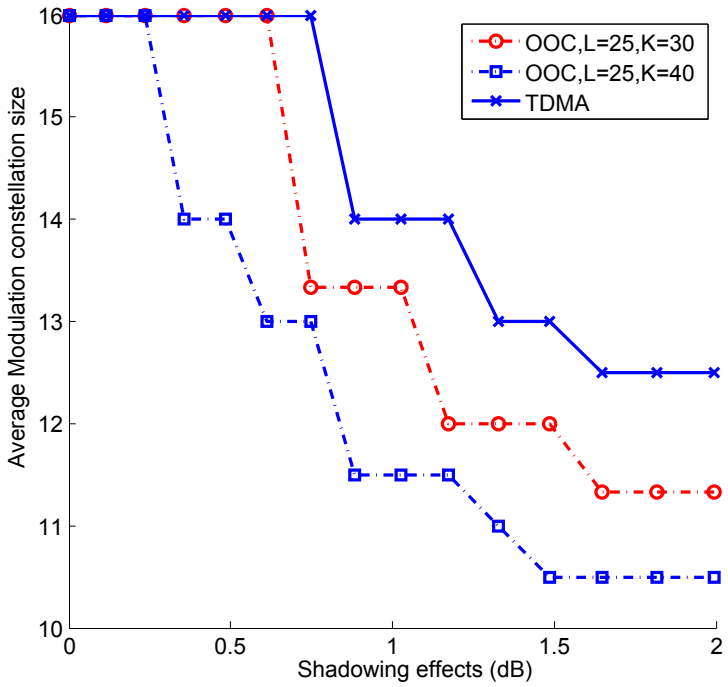

Figure 4.4: Average modulation constellation size for adaptive M-PAM for 30 and 40 user cases with shadowing effects.

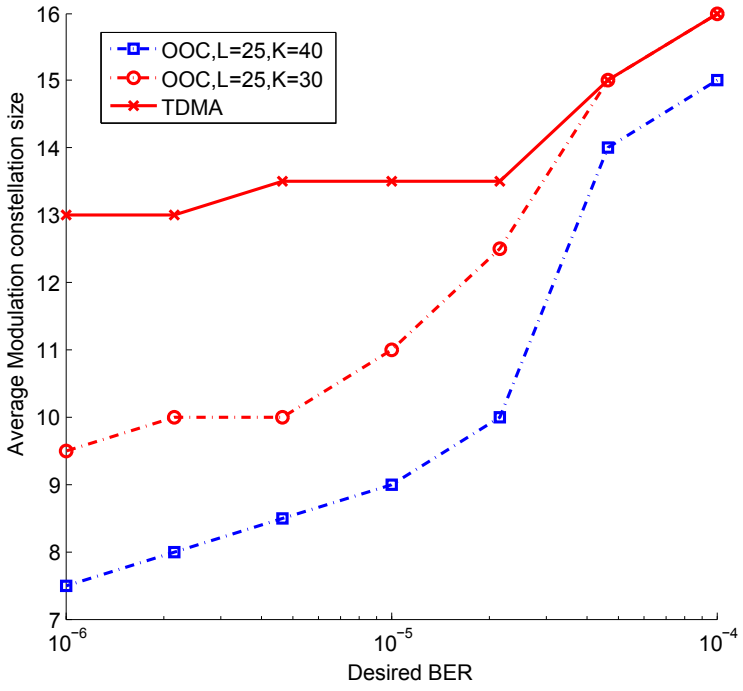

Figure 4.5: Average modulation constellation size for adaptive M-PAM modulation for 30 user and 40 user cases with different desired BER values, no shadowing effects.

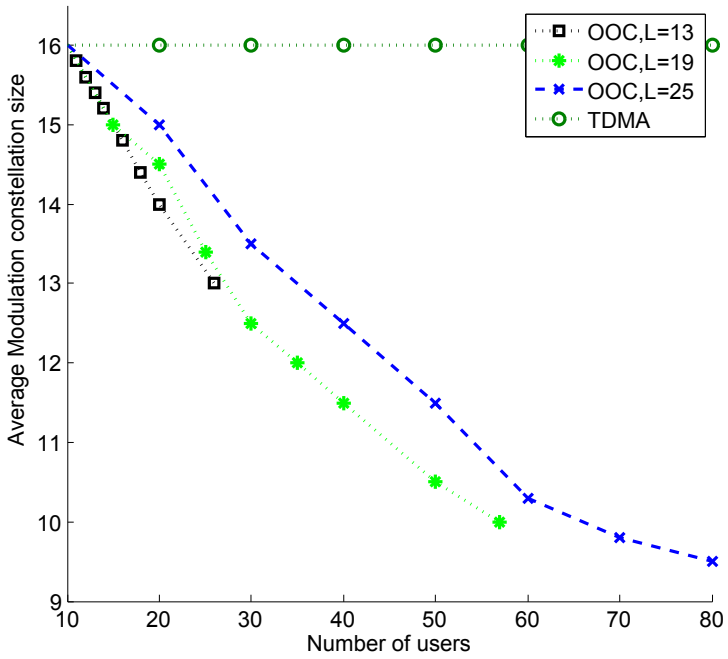

Figure 4.6: Average modulation constellation size for different numbers of users with OCDMA and TDMA techniques, no shadowing effects.

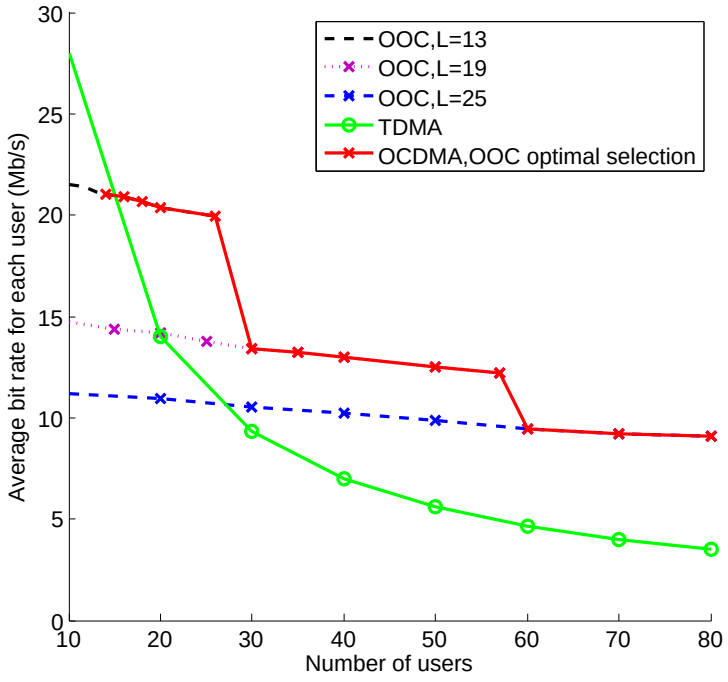

Figure 4.7: Average bit rate for different numbers of users with OCDMA and TDMA techniques; no shadowing effects.

OCDMA and TDMA are given in Fig. 4.7, and prove that we can obtain a higher bit rate using OCDMA if we choose the best OCDMA code. In this chapter, we use OOC codes with length 13, 19 or 25 to support multiple users. These OOC codes can support up to 26, 57 and 100 users, respectively [48]. The results show that the average bit rate for OCDMA is higher than TDMA when the number of users is larger than 15, 20, and 28 when using the length 13, 19 and 25 OOC codes, respectively. We can get a higher bit rate using OCDMA than TDMA by choosing the right OCDMA codes. The highest throughput obtainable for this scenario is labeled 'OCDMA, OOC optimal selection' in Fig. 4.7.

4.2 M-PAM Joint Optimal Waveform Design for Multiuser VLC Systems over ISI Channel

4.2.1 Background

ISI is one of the biggest challenges for high-speed data transmissions. The low rise-time of lighting LEDs and multi-path propagation are two factors leading to ISI. For indoor VLC systems, multi-path propagation comes from reflections of the light from the ceiling, walls, furniture and other reflective surfaces and limits systems operating at bandwidth above 100 MHz [63]. The 3 dB modulation bandwidth of commercial lighting LEDs is limited to a few tens of MHz [64]. Thus, the bandlimited LED is the dominant factor to introduce ISI.

Equalization that can be realized by either hardware or software is an attractive solution to mitigate ISI and obtain a high data rate. Some researchers have proposed a pre-equalization circuit to increase the data rate and have achieved up to 340 Mb/s transmission using OOK with a BER of 2×10^{-3} [65]. Using red-green-blue LEDs and

a hardware equalization circuit, Gb/s data rate can be achieved [64]. As for software equalizers, the zero forcing (ZF) algorithm is a popular signal processing method to mitigate the effects of ISI in RF communications [66, 67]. ZF has also been applied in optical wireless communication [68]. A least mean squared error equalizer using a training sequence for indoor VLC systems was proposed in [20], and both linear and decision feedback equalizers were discussed.

A high bandwidth efficiency modulation, such as M-PAM is a good choice to provide high-speed connections for VLC systems since the light emitted from the LEDs is non-coherent, and intensity modulation should be used. Using M-PAM, a $(\log_2 M)$-fold increase in the data rate compared to OOK can be achieved. Recently an adaptive M-PAM scheme was proposed to provide higher data rate for multiuser VLC systems [21, 53, 69–71]. Instead, OFDM can be used to increase the data rate while combating ISI [23, 24]. However, optical OFDM systems experience a relative high peak to average power ratio (PAPR) that can result in a severe nonlinear distortion of the transmitted signals because of the LED peak transmitted power constraint. Researchers have shown that M-PAM with equalization can provide better performance than OFDM for VLC systems [32, 70].

Another important research topic in indoor VLC is how to choose a multiple access technique. MAI can be a factor limiting the throughput of multiuser systems. TDMA is one approach that can be used due to its small operational complexity [72, 73]. A SDMA technique using angular diversity of the transmitters to support and separate multiple users in indoor VLC environments was proposed in [62], but the bandlimited characteristic of the LEDs was not considered. Recently, we proposed an OCDMA indoor VLC system using a resource allocation algorithm to support multiple users and reduce the MAI [27].

In this section, we solve both problems, high-speed transmission and multiple

access, by using a joint optimal waveform (JOW) design algorithm for MISO multiuser systems. Recently, we proposed a waveform design algorithm in [30], yet MAI was not considered. In this chapter, we expand on this idea to design waveforms capable of reducing both ISI and MAI. In this system, unique waveform designs and MMSE filters for different users are optimized jointly. In addition, to achieve a high data rate, an M-PAM modulation scheme is applied. In this work, the proposed JOWs have two functions: separating users and reducing ISI. Similar to OCDMA, the proposed JOWs are discrete time sequences that are unique to users. But superior to OCDMA, JOWs combat ISI and MAI simultaneously and can be adaptively redesigned when the channel state changes. The JOWs can be optimized for different transmitted symbol rates by maximizing the SINR. For a fixed required BER, by changing the JOW and M-ary modulation constellation size, we can find the maximum data rate. The JOWs can be designed to allow dimming of the light by changing the illumination level, determined by the average waveform power. However, the illumination level is difficult to change in OCDMA or TDMA. Channel state information (CSI) uncertainty is taken into account in this chapter by modeling the channel impulse response as a Gaussian random process.

To address the real-time computational complexity of performing the requisite optimization, an off-line waveform design algorithm is then proposed, using a pre-established waveform table. In practice, the proper waveforms can be selected from the table based on the real channel gains. The performance of the off-line algorithm can be estimated by using the channel uncertainty model.

4.2.2 Channel Model

In a typical indoor VLC system, LEDs are used to transmit data and illuminate the indoor area at the same time. Since the light from the LEDs is non-coherent,

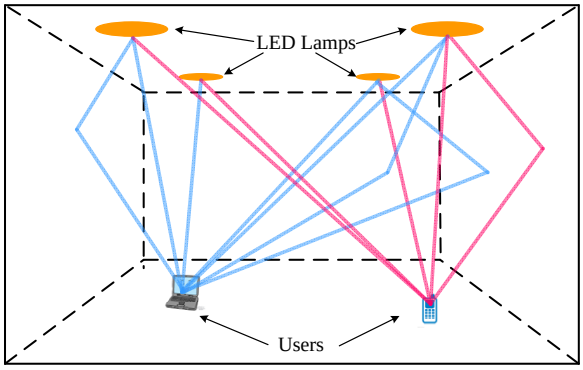

Figure 4.8: A typical indoor VLC system.

IM/DD are employed. Considering the multipath propagation in the indoor channel and bandwidth limit of the LEDs, the optical link can experience severe ISI.

In this section, we assume there are Q LED lamps and K users with one photodetector (PD) per user receiving signals, and each lamp serves to transmit downlink signals to all the users. In this work, we consider the bandwidth of the indoor channel is limited by the LED rise time. [74]. Therefore, the overall channel impulse response from LED q to user k can be modeled as

$$h_{qk}(t) = \hat{h}_{qk} h_l(t), \qquad \begin{matrix} q = 1, \ldots, Q \\ k = 1, \ldots, K \end{matrix} \tag{4.20}$$

where $h_l(t)$ is the impulse response of the LEDs, which can be modeled as a lowpass filter. We assume the impulse response of all LEDs is the same. $\hat{h}_{qk}$ is the LOS channel gain from LED q to user k, which can be calculated from (2.6). $\mathbf{h}_{qk} = (h_{qk}[1], h_{qk}[2], \cdots, h_{qk}[L_h])^T$ represents the discrete time version of the truncated channel impulse response from LED q to user k. Fig. 4.9 shows an example of a truncated channel impulse response that lasts T_h seconds. If R_c represents the sampling rate, the length of the discrete time truncated channel impulse response can be

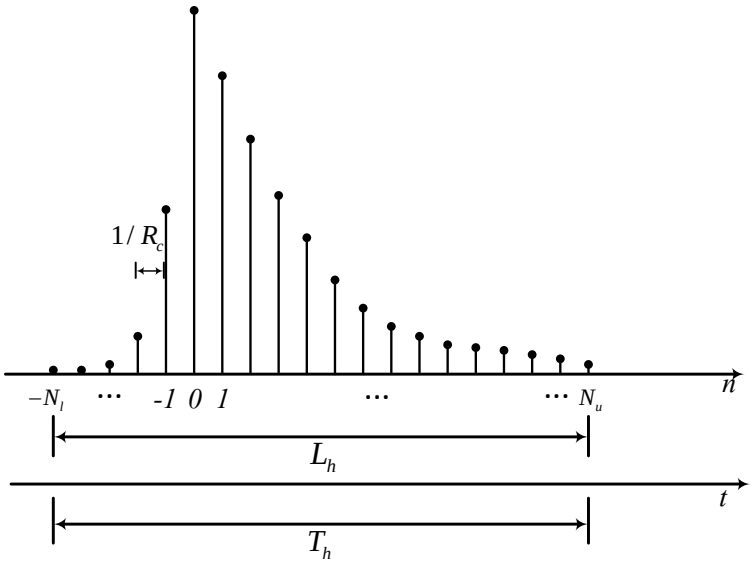

Figure 4.9: Discrete time version of a truncated LED response.

calculated as

$$L_h = T_h R_c, \tag{4.21}$$

We further assume that the impulse response of the LEDs can be modeled and estimated perfectly. However the estimation of the channel gains may be affected by shadowing, multipath, or noise. In addition, objects moving around users may interfere with the reflected light, which can introduce uncertainty in the assumed impulse response. In this chapter, we model the channel impulse response from LED q to user k as

$$\mathbf{h}_{qk}^{*} = \mathbf{h}_{qk} + \Delta\mathbf{h}_{qk}, \tag{4.22}$$

where $\Delta\mathbf{h}_{qk} = (\Delta h_{qk}[1], \Delta h_{qk}[2], \cdots, \Delta h_{qk}[L_h])^T$ is the uncertainty in modeling the channel impulse response. In this chapter, we assume the elements in $\Delta\mathbf{h}_{qk}$ are independent of each other, and each element can be modeled as a Gaussian random variable with zero mean and variance σ_h^2 [75, 76].

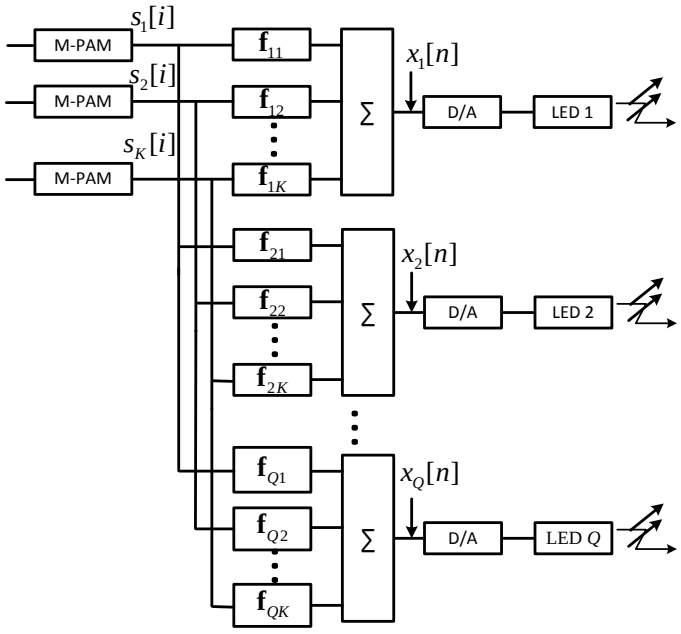

Figure 4.10: Block diagram of the transmitters for the proposed M-PAM joint optimal waveform design system.

4.2.3 M-PAM Joint Optimal Waveform Design

Transmitted and Received Signals

A block diagram of the proposed M-PAM joint optimal waveform design system is shown in Fig. 4.10. The designed transmitted waveform and MMSE filter for different users are jointly optimized. After M-PAM modulation, the M-ary amplitude symbol stream for user k at time instant i can be represented as $s_k[i] \in \{0, \frac{1}{M_k-1}, \frac{2}{M_k-1}, \cdots, 1\}$, and each symbol carries $\log_2 M_k$ bits, where M_k is the modulation constellation size for user k. We assume the $s_k[i]$ are uniformly distributed. After the waveform design, the transmitted sequence from LED q can be represented as

$$x_q[m] = \sum_{k=1}^{K} \sum_{i=-\infty}^{\infty} s_k[i] f_{qk}[m - iL_f], \tag{4.23}$$

where $\mathbf{f}_{qk} = (f_{qk}[1], f_{qk}[2], \cdots, f_{qk}[L_f])^T$ is the designed waveform for LED q and user k. L_f is the number of samples used to represent the waveform. The channel gain from each LED to each user could be different, and the waveform for each LED and user is unique.

As shown in Fig. 4.11, after chip matched filtering and sampling, the received signal for user k can be represented as

$$r_k[m] = \sum_{q=1}^{Q} \sum_{j=-\infty}^{\infty} x_q[m+j] h_{qk}[-j] + n_k[m]. \tag{4.24}$$

After applying the MMSE filter, the received signal for user k can be written in matrix form as

$$y_k[i] = \mathbf{w}_k^T \sum_{q=1}^{Q} \mathbf{H}_{qk} \mathbf{x}_q + \mathbf{w}_k^T \mathbf{n}_k + b_k, \tag{4.25}$$

where the MMSE filter for user k is represented by $\mathbf{w}_k = (w_k[1], w_k[2], \cdots, w_k[L_w])^T$ with length L_w. $\mathbf{n}_k = (n_k[1], n_k[2], \cdots, n_k[L_f])^T$ is the additive Gaussian noise for user k with zero mean and variance $\sigma_n^2 = N_0 R_c$, where N_0 is the noise spectral density. b_k is a constant needed for the MMSE estimator. $\mathbf{H}_{qk}$ is a Toeplitz matrix, which can be represented as

$$\mathbf{H}_{qk} = \left(S_L(\mathbf{h}_{qk}, \frac{L_w - 1}{2}), \cdots, \mathbf{h}_{qk}, \cdots, S_R(\mathbf{h}_{qk}, \frac{L_w - 1}{2}) \right)^T, \tag{4.26}$$

where $S_L(\mathbf{x}, m)$ and $S_R(\mathbf{x}, m)$ are two functions that operate as m circular shifts on $\mathbf{x}$, to the left and right, respectively. The vector of transmitted samples that affect $y_k[m]$ is denoted $\mathbf{x}_q = (x_q[-N_u], \cdots, x_q[0], \cdots, x_q[N_l])^T$. $N_l + N_u + 1 = L_h$, where L_h describes the length of successive samples that blur together. N_l and N_u represent past and future samples that contribute to ISI, respectively as shown in Fig. 4.9. From (4.23), the mth element of the vector $\mathbf{x}_q$ can be calculated as $\sum_k s_k[\lfloor m/L_f \rfloor] f_{qk}[$

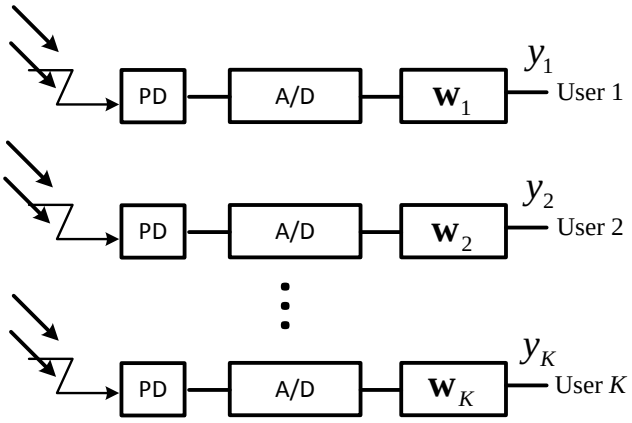

Figure 4.11: Block diagram of the receiver.

$\text{mod}(m, L_f)$], where $\lfloor m/L_f \rfloor$ represents the largest integer less than m/L_f, which is the number of successive M-PAM data that blurs together, and $\text{mod}(m, L_f)$ is the remainder of m/L_f.

Waveform Design Algorithm with Imperfect CSI

For the JOW algorithm, the CSI must be known at the transmitters. However, in practice, we cannot estimate the CSI perfectly. To account for the imperfect CSI, we substitute the imperfect channel model $\mathbf{h}_{qk}^*$ for $\mathbf{h}_{qk}$ in (4.26). The received signal for user k after the MMSE filter with channel uncertainty can be represented as

$$y_k[i] = \mathbf{w}_k^T \sum_{q=1}^{Q} (\mathbf{H}_{qk} + \Delta\mathbf{H}_{qk})\mathbf{x}_q + \mathbf{w}_k^T \mathbf{n}_k + b_k, \tag{4.27}$$

which consists of four parts: the target (intended data) for user k, the uncertainty caused by the imperfect CSI, the ISI plus MAI, and the noise. Thus, (4.27) can be

rewritten as

$$\begin{aligned} y_k[i] = & \underbrace{\mathbf{w}_k^T \sum_{q=1}^{Q} \hat{\mathbf{H}}_{qk}\hat{\mathbf{x}}_q + b_k}_{\text{Target}} + \underbrace{\mathbf{w}_k^T \sum_{q=1}^{Q} \Delta\mathbf{H}_{qk}\mathbf{x}_q}_{\text{Uncertainty}} \\ & \underbrace{+ \mathbf{w}_k^T \sum_{q=1}^{Q} \tilde{\mathbf{H}}_{qk}\hat{\mathbf{x}}_q + \mathbf{w}_k^T \sum_{q=1}^{Q} \mathbf{H}_{qk}\tilde{\mathbf{x}}_q}_{\text{ISI+MAI}} + \underbrace{\mathbf{w}_k^T \mathbf{n}_k}_{\text{Noise}}, \end{aligned} \tag{4.28}$$

where $\tilde{\mathbf{H}}_{qk} = \mathbf{H}_{qk}|_{h_{qk}[0]\to 0}$, $h_{qk}[0]$ is the peak value of $\mathbf{h}_{qk}$, $\hat{\mathbf{H}}_{qk} = \mathbf{H}_{qk} - \tilde{\mathbf{H}}_{qk}$, $\hat{\mathbf{x}}_q = \mathbf{x}_q|_{(\mathbf{f}_{qi}=0, i\neq k)}$, and $\tilde{\mathbf{x}}_q = \mathbf{x}_q|_{\mathbf{f}_{qk}=0}$.

The mean-squared error, J_k, for user k is defined as

$$J_k = E_{\mathrm{s,n},\Delta\mathrm{h}}\{(y_k[i] - s_k[i])^2\}, \tag{4.29}$$

where $E_{\mathrm{s,n},\Delta\mathrm{h}}\{\cdot\}$ represents expectation with respect to the transmitted symbols $(s_1, s_2, \cdots, s_K)$, the noise and the channel uncertainty, which are statistically independent. Substituting (4.27) into (4.29), we obtain

$$\begin{aligned} J_k = & \mathbf{w}_k^T \sum_{q=1}^{Q}\sum_{p=1}^{Q} \mathbf{H}_{qk}\boldsymbol{\Sigma}^{(qp)}\mathbf{H}_{pk}^T\mathbf{w}_k + \sigma_h^2 \mathbf{w}_k^T \sum_{q=1}^{Q}\sum_{p=1}^{Q} \boldsymbol{\Sigma}^{(qp)}\mathbf{w}_k \\ & - 2\mathbf{w}_k^T \sum_{q=1}^{Q} \mathbf{H}_{qk}\mathbf{e}_q + \sigma_n^2 \mathbf{w}_k^T\mathbf{w}_k + \frac{2M_k^2 - M_k}{6M_k - 6} \\ & - b_k + 2b_k \mathbf{w}_k^T \sum_{q=1}^{Q} \mathbf{H}_{qk}\mathbf{m}_q + b_k^2 \end{aligned} \quad , \tag{4.30}$$

where $\mathbf{\Sigma}^{(qp)} = E_{\mathrm{s}}\{\mathbf{x}_q\mathbf{x}_p^T\}$. The (m,n)th element of $\mathbf{\Sigma}^{(qp)}$ can be calculated as

$$\sigma_{mn}^{(qp)} = \begin{cases} \sum_{k=1}^{K} \dfrac{2M_k^2 - M_k}{6M_k - 6} f_{qk}[u] f_{pk}[v] & \\ \quad + \dfrac{1}{4} \sum_{k \neq z} \sum_{z \neq k} f_{qk}[u] f_{pz}[v] & , \quad i = j \\ \frac{1}{4} \sum_{k=1}^{K} \sum_{z=1}^{K} f_{qk}[u] f_{pz}[v] & , \quad i \neq j \end{cases} . \tag{4.31}$$

where $i = \lfloor m/L_f \rfloor$ and $j = \lfloor n/L_f \rfloor$; $u = \mathrm{mod}(m, L_f)$ and $v = \mathrm{mod}(n, L_f)$. $\mathbf{e}_q = E_{\mathrm{s}}\left\{s_k[i] \cdot \mathbf{x}_q\right\}$ and $\mathbf{m}_q = E_{\mathrm{s}}\left\{\mathbf{x}_q\right\}$.

Solving for $\frac{\partial J_k}{\partial b_k} = 0$ and $\frac{\partial J_k}{\partial \mathbf{f}_k} = 0$, the MMSE filter for user k can be obtained as

$$\begin{aligned} \mathbf{w}_k &= \left(\mathbf{T}_k + \sigma_n^2 \mathbf{I}\right)^{-1} \sum_{q=1}^{Q} \mathbf{H}_{qk} \mathbf{e}_q \\ b_k &= \frac{1}{2} - \mathbf{w}_k^T \sum_{q=1}^{Q} \mathbf{H}_{qk} \mathbf{m}_q, \end{aligned} \tag{4.32}$$

where

$$\mathbf{T}_k = \sum_{q=1}^{Q} \sum_{p=1}^{Q} \mathbf{H}_{qk} \mathbf{\Sigma}^{(qp)} \mathbf{H}_{pk}^T + \sigma_h^2 \mathbf{w}_k^T \sum_{q=1}^{Q} \sum_{p=1}^{Q} \mathbf{\Sigma}^{(qp)}, \tag{4.33}$$

and $\mathbf{I}$ is the identity matrix.

The signal to interference plus noise ratio (SINR) for user k can be calculated as

$$\mathrm{SINR}_k = \frac{\mathrm{Signal}}{\mathrm{Uncertainty} + \mathrm{Interference} + \mathrm{Noise}}, \tag{4.34}$$

where

$$\begin{aligned}\text{Signal} &= \mathbf{w}_k^T \sum_{q=1}^{Q}\sum_{p=1}^{Q} \mathbf{H}_{qk}\hat{\Sigma}^{(qp)}\mathbf{H}_{pk}^T\mathbf{w}_k + \left(\mathbf{w}_k^T \sum_{q=1}^{Q} \mathbf{H}_{qk}\mathbf{m}_q\right)^2 - \frac{1}{4} \\ \text{Uncertainty} &= \sigma_h^2 \mathbf{w}_k^T \sum_{q=1}^{Q}\sum_{p=1}^{Q} \mathbf{\Sigma}_{qp}\mathbf{w}_k\end{aligned} \tag{4.35}$$

$$\text{Noise} = \sigma_n^2 \mathbf{w}_k^T\mathbf{w}_k \tag{4.36}$$

$$\begin{aligned}\text{Interference} = \mathbf{w}_k^T &\sum_{q=1}^{Q}\sum_{p=1}^{Q} \tilde{\mathbf{H}}_{qk}\hat{\Sigma}^{(qp)}\tilde{\mathbf{H}}_{pk}^T\mathbf{w}_k \\ &+ \mathbf{w}_k^T \sum_{q=1}^{Q}\sum_{p=1}^{Q} \mathbf{H}_{qk}\tilde{\Sigma}^{(qp)}\mathbf{H}_{pk}^T\mathbf{w}_k \\ &+ 2\mathbf{w}_k^T \sum_{q=1}^{Q}\sum_{p=1}^{Q} \tilde{\mathbf{H}}_{qk}\bar{\Sigma}^{(qp)}\mathbf{H}_{pk}^T\mathbf{w}_k\end{aligned} \tag{4.37}$$

where $\hat{\Sigma}^{(qp)} = E_{\text{s}}\left\{\hat{\mathbf{x}}_q\hat{\mathbf{x}}_p^T\right\}$, $\tilde{\Sigma}^{(qp)} = E_{\text{s}}\left\{\tilde{\mathbf{x}}_q\tilde{\mathbf{x}}_p^T\right\}$, $\bar{\Sigma}^{(qp)} = E_{\text{s}}\left\{\hat{\mathbf{x}}_q\tilde{\mathbf{x}}_p^T\right\}$, all of which can be calculated similarly as the element of $\Sigma^{(qp)}$ in (4.31). Substituting (4.32) into (4.34), we can find that $\mathbf{F} = (\mathbf{F}_1, \mathbf{F}_2, \cdots, \mathbf{F}_Q)$, $\mathbf{M} = (M_1, M_2, \cdots, M_K)$ and R_c are the only variables needed to find the SINR_k, where $\mathbf{F}_q = (\mathbf{f}_{q1}, \mathbf{f}_{q2}, \cdots, \mathbf{f}_{qK})$. We denote $\text{SINR}_k = \gamma_k(\mathbf{F}, \mathbf{M}, R_c)$. Then, for M-PAM modulation, the BER for user k can be approximated by [34]

$$\text{BER}_{\text{k}} \approx \frac{M_k - 1}{M_k \log_2 M_k}\text{erfc}\left(\sqrt{\frac{\gamma_k(\mathbf{F}, \mathbf{M}, R_c)}{(M_k - 1)^2}}\right), \tag{4.38}$$

where $\text{erfc}(\cdot)$ is the complementary error function, which is defined as $\text{erfc}(x) = \frac{2}{\sqrt{\pi}}\int_x^\infty e^{-u^2}\text{d}u$.

For different data rates, the waveform design algorithm can adaptively adjust the waveforms for each user to minimize the ISI. For a fixed data rate and modulation

constellation size, the optimal waveforms can be obtained by maximizing the minimum SINR of all the users, through which each user can achieve a fair performance. The optimization cost function is

$$\mathbf{F}^* = \arg\max_{\mathbf{F}} \min_{k} \gamma_k(\mathbf{F}, \mathbf{M}, R_c), \tag{4.39}$$

where $\mathbf{F}^*$ is the optimal value for $\mathbf{F}$. When optimizing the waveforms, a peak transmitted power constraint must be considered, which can be represented as

$$\forall\ i,\ k \text{ and } q,\ \ \sum_{k=1}^{K} f_{qk}[i] \leq P^{max},\ \text{ and } f_{qk}[i] \geq 0, \tag{4.40}$$

where P^{max} represents the peak LED transmitted power. After the optimization process (finding the optimal waveforms in (4.39)), the SINR for all the users are similar. The transmitted data rate for user k can be calculated by $R_b^{(k)} = R_c(\log_2 M_k)/L_f$, where we assume the sampling rate, R_c, for each user is the same. R_c/L_f represents the transmitted symbol rate.

The maximum data rate for each user is constrained by the required BER, B^{max}, since the communication quality needs to be taken into account. For a fixed SINR, the modulation constellation size determines the BER and the transmitted data rate. Therefore, to maximize the data rate for each user, we need to solve the following problem:

$$\begin{aligned} &M_k^* = \max\ M_k,\ \forall\ k = 1, \cdots, K \\ &s.t.\ \ \frac{M_k - 1}{M_k \log_2 M_k} \text{erfc}\left(\sqrt{\frac{\gamma_k(\mathbf{F}^*, \mathbf{M}, R_c)}{(M_k - 1)^2}}\right) < B^{max}, \end{aligned} \tag{4.41}$$

where M_k^* is the optimal value for M_k to maximize the data rate for user k.

The steps for solving (4.41) and getting the optimal waveforms are described in

Algorithm 2. We use the genetic algorithm (GA), a powerful heuristic searching method, to find the optimal waveforms [77].

Algorithm 2: Optimal waveforms and the highest data rate

```
Initialize: R_c, L_f;
repeat
    for k = 1, 2, ..., K do
        for M_k = 2, 4, 8, 16 do
            while Constraint in (4.41) is satisfied do
                GA begins;
                Initialization for GA;
                Generate random individuals for F (1st GEN);
                repeat
                    Evaluate the fitness function, γ_k(F, M, R_b);
                    Select the individuals by checking the constraint (4.40);
                    Match, mutate and crossover;
                    Generate the next generation;
                until γ_k converges;
                Get F*;
                GA ends;
                Calculate BER using (4.38);
                Calculate R_b^(k);
            end
        end
    end
    Increase R_c;
until R_b^(k) converges;
Output: The maximum R_b^(k), optimal M, and F*
```

Illumination and Dimming Control

For VLC systems, illumination control is an important consideration. The transmitted optical power can provide wireless access as well as illumination. The maximum illumination level in the room depends on the peak transmitted power and the illumination potential, defined as the ratio of the highest average transmitted power to the peak LED power. For this work, the illumination potential using JOW can be

represented as

$$\eta_J = \frac{1}{2QKL_f P^{max}} \sum_{q=1}^{Q} \sum_{k=1}^{K} \sum_{l=1}^{L_f} f_{qk}[l]. \tag{4.42}$$

In the optimization process, η_J is an optimization constraint that can be adjusted to satisfy the specific illumination requirements by changing the values of waveforms. In (4.42), the coefficient 1/2 comes from the uniform distribution of $s_k[i]$. The illumination level can be controlled by finding the optimal waveform as shown in Algorithm **??**, inserting (4.42) as an additional constraint.

For OCDMA, the illumination potential is fixed, and depends on the codewords. The illumination potential using optical orthogonal codes (OOC) as waveforms in an OCDMA system can be calculated as

$$\eta_C = \begin{cases} W/2L_c & , \quad K \leq W \\ K/2L_c & , \quad K > W \end{cases}, \tag{4.43}$$

where W is the weight for the OCDMA codeword, and L_c is the length of the code. Therefore, if a certain OCDMA code is selected, for a certain number of active users, the illumination potential of using OCDMA cannot be changed. JOW has a more flexible illumination potential than OCDMA due to the optimally designed waveforms. When using the proposed JOW algorithm in indoor VLC systems, the illumination level can be adjusted by designing for a specific illumination potential.

For TDMA, only one user is served per time slot, and the data for each user can be sent directly. Barring any DC offset, the illumination potential for TDMA is a constant, which can be represented as $\eta_T = 1/2$. Compared with JOW, we can state that TDMA is at least as power efficient as JOW, i.e., $\eta_J \leq \eta_T$.

Off-Line Waveform Design

The proposed waveform design algorithm is a time consuming process due to the non-linear and non-convex optimization. In this section, we propose an off-line solution to make the system adapt in real-time. In the off-line method, we calculate the waveforms for multiple users in advance. Given the number of lamps in the space, a table of the waveforms for different numbers of users and channel gains can be created. In typical VLC systems, only a few users can be served by any one lamp. In practice, depending on the number of users and the channel gains, the proper waveforms for the users can be selected from the pre-established tables.

Since the LED impulse response, $h_l(t)$, can be estimated perfectly, the only factor that can affect the off-line solution's performance is the channel gains. The more channel gain choices are used to create the table, the better the performance the off-line waveforms algorithm can achieve. One table is created for each possible value of K. We assume that the initial channel gains that are used to create the table can be represented as a matrix

$$\mathbf{U}_K = \begin{pmatrix} \mu_{11} & \mu_{12} & \cdots & \mu_{1K} \\ \mu_{21} & \mu_{22} & \cdots & \mu_{2K} \\ \vdots & \vdots & \ddots & \vdots \\ \mu_{L_T 1} & \mu_{L_T 2} & \cdots & \mu_{L_T K} \end{pmatrix}, \tag{4.44}$$

where each row represents one set of the initial channel gains for the K users in the table. L_T is the number of sets of channel gains, which decides the size of the table. To create the table, μ_{ik} can be used to replace $\hat{h}_{qk},\ \forall\ q$ in (4.20). Then, the waveform lookup table can be created by using the proposed algorithm in this chapter.

During operation, the table corresponding to the number of active users K is first

Table 4.2: Parameters Used for Small Indoor Environment

Size of the small room	5 m × 5 m × 3 m
Locations of the lamps	(1.25,1.25,3),(1.25,3.75,3) (3.75,1.25,3),(3.75,3.75,3)
Responsivity	0.5 A/W
Area of the photodetector	0.01 cm^2
Radiated optical power per lamp	3 W
LED semiangle	60^o
Noise spectral density	1×10^{-9} mW/Hz
3 dB bandwidth of LEDs	20 MHz
Modulation constellation size	$2, 4, 8, 16$
BER requirement, B^{max}	10^{-4}

selected. Then, based on the real estimated channel gains for the multiple users, the proper waveforms can be selected by using the following criteria

$$i_q^* = \arg\min_i \sum_{k=1}^{K} \left(\mu_{ik} - \hat{h}_{qk}\right)^2, \quad \forall\ q, \tag{4.45}$$

where i_q^* is the index of the channel gains selected for LED q. The performance of the off-line algorithm is essentially equivalent to a channel uncertainty with

$$\sigma_h^2 = \frac{1}{K} \sum_{k=1}^{K} (\mu_{i^*k} - \hat{h}_{qk})^2. \tag{4.46}$$

4.2.4 Numerical Results and Discussions

In this section, numerical results of the performance of the proposed system are shown. To test the applicability of the system, we show results for an indoor environment with four LED lamps. This JOW does not use η_J as a constraint. Unless otherwise noted, the parameters used to obtain the numerical results are shown in Table 4.2.

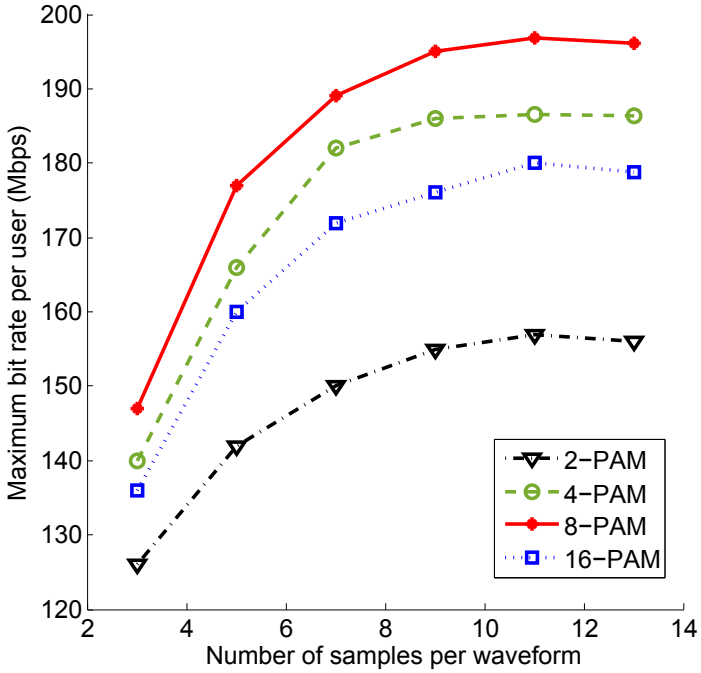

Figure 4.12: Transmitted data rate for different numbers of samples per waveform for 3 users.

Perfect CSI

In this chapter, adaptive M-PAM is used together with JOW to enhance the transmitted data rate. Only 2, 4, 8, and 16-PAM are considered in this work for our numerical results. The number of samples per waveform, L_f, is an adjustable parameter, which needs to be sufficiently large to reduce the ISI and MAI. Fig. 4.12 shows the numerical results of the optimized data rate with different numbers of samples per waveform using M-PAM to satisfy a BER 10^{-4}. The channel gains for the 3 users are 0.036, 0.032 and 0.025, respectively. In general, as the number of samples per waveform increases, a higher data rate can be supported by using M-PAM. However, the data rate achieves a limit when the number of samples per waveform is 11. Thus, considering the computational burden and design complexity, the optimal number of samples per waveform is 11 for this case. From the results, 8-PAM can provide the

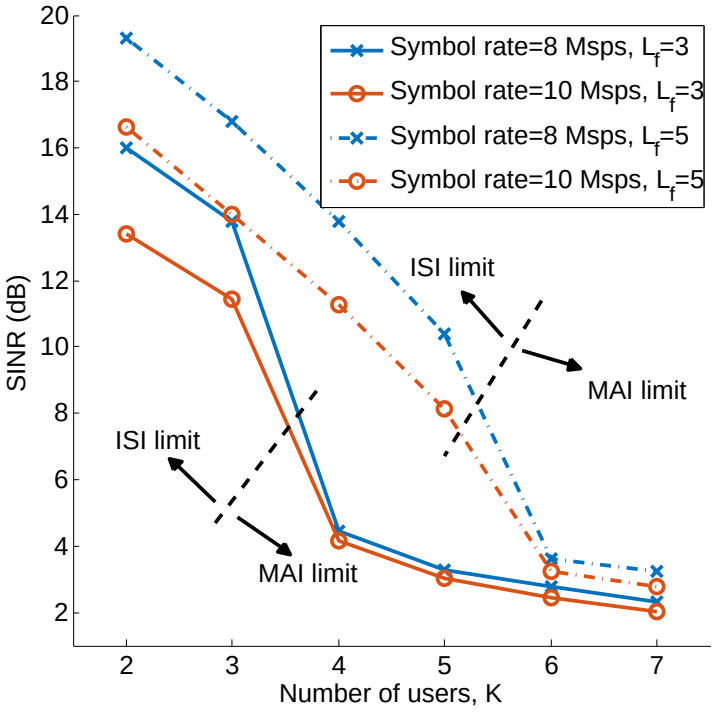

Figure 4.13: SINR for different users.

highest data rate among the other modulation schemes. Since we have a BER constraint to guarantee the communication quality, the larger modulation constellations require a higher SINR. When the system cannot provide a high enough SINR for the current M-PAM to satisfy the BER requirement, a lower level modulation needs to be used. We envision an adaptive procedure that adjusts the constellation size depending on the channel quality and received SINR.

More users can introduce more MAI. Fig. 4.13 shows the SINR for up to 7 users. The channel gains for these 7 users are 0.036, 0.032, 0.032, 0.028, 0.025, 0.021, and 0.018. If the number of users K exceeds the number of samples per waveform L_f, the MAI dominates over the ISI. In Fig. 4.13 the numerical results show that the SINR drops sharply when K is larger than L_f, and the system enters the MAI limited region. Thus, depending on the number of active users in this room, we can select the minimum number of samples per waveform.

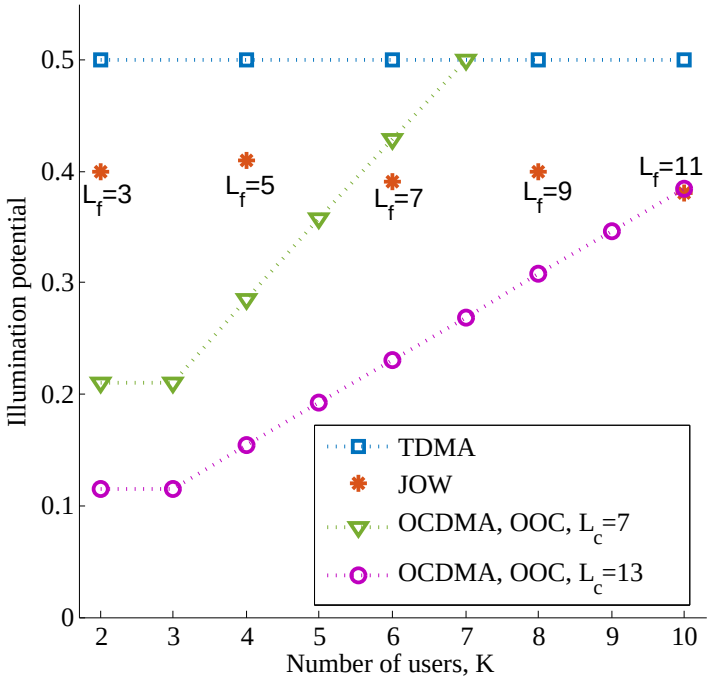

Figure 4.14: Illumination potential for different numbers of users.

The illumination potential is shown in Fig. 4.14. From the result, TDMA has the highest illumination potential since it only serves one user per time slot. The illumination potential using TDMA is the expected value of the data, which is the maximum achievable. OCDMA and JOW follow a similar principle to support multiple users. Depending on the codewords or waveforms, the power efficiencies for illumination of OCDMA and JOW are different. For OCDMA, this illumination potential is increasing as the number of users increases. Eventually, when the number of active users is equal to the length of the selected OCDMA code, the illumination potential for OCDMA can reach its maximum value since the value of the sum of the unmodulated codewords is $P^{\max}$. In Fig. 4.14, when the number of users is lower than 7, a OOC code with length $L_c = 7$ is enough. However, when the number of users is greater than 7, a length $L_c = 13$ OOC code is needed, since the length 7 OOC code cannot support that many users. Therefore, a longer code length has a lower illumination potential for OCDMA. Comparing OCDMA and JOW, JOW can

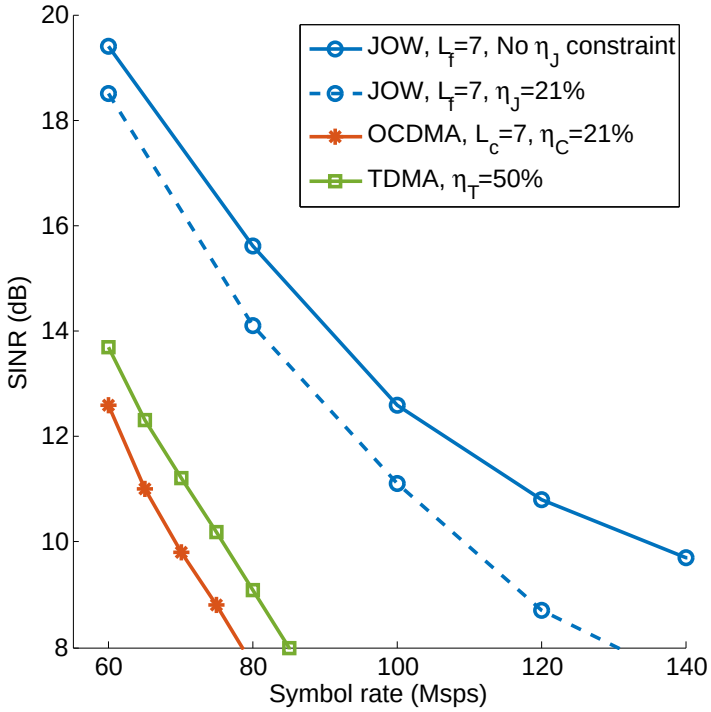

Figure 4.15: SINR comparison of JOW, OCDMA and TDMA for 3 users.

Table 4.3: Maximum data rates using M-PAM averaged over the 3 users

Data rate (Mbps)	2-PAM	4-PAM	8-PAM	16-PAM
No ISI, ideal channel	532	476	403	352
JOW, $L_f = 7$	151	180	189	172
OCDMA, $L_c = 7$	78	121	137	164
No-equalization	24	44	61	69

provide higher illumination potentials for most cases, and the illumination potential of JOW can achieve 80% of the maximum value.

Fig. 4.15 shows numerical results of SINR for JOW, OCDMA and TDMA techniques. In this result, η_J is used as an optimization constraint. For both OCDMA and TDMA, MMSE filters are applied at the receivers. For the same transmitted symbol rate, JOW has a higher SINR than TDMA and OCDMA since the optimized waveforms can reduce ISI and MAI together with the MMSE filter. Since there is

no MAI for TDMA, the SINR for TDMA is higher than OCDMA. When the JOW has the same illumination potential as OCDMA, the SINR for JOW is greater than OCDMA.

Since a higher modulation level requires a higher SINR to satisfy the communication quality (BER requirement), the larger modulation constellation size cannot always provide higher data transmission rates. In Table. 4.3, numerical results for the maximum data rate with different modulation constellation sizes are shown. 2-PAM can provide the highest data rate for the ideal channel. Since there is no ISI for the ideal channel (MAI without ISI), using higher levels modulation does not increase the throughput. For the case where the LED bandlimit is applied but no equalization is used, a higher level modulation can provide a higher transmission data rate. With the help of JOW, ISI can be reduced; therefore, the optimal modulation constellation size for JOW is 8 for this case. OCDMA has more ISI than JOW, thus, 16-PAM needs to be used for OCDMA to achieve the maximum data rate. In general, as the ISI increases, the optimal modulation constellation size increases.

Imperfect CSI

The imperfect CSI case is also considered in this chapter. Fig. 4.16 shows the comparison of the perfect and imperfect CSI cases. For the imperfect CSI case, if the channel uncertainty is known, there is about a 4 dB SINR penalty compared with the perfect CSI case when the channel uncertainty is -20 dB (the channel uncertainty is 36% of the average channel gain).

In Fig. 4.16, numerical results also show cases with and without knowing the channel uncertainty information, i.e., the uncertainty variance. From the results, the algorithm that knows the channel uncertainty variance can obtain a higher SINR than if it does not know the variance. When the variance of the channel uncertainty

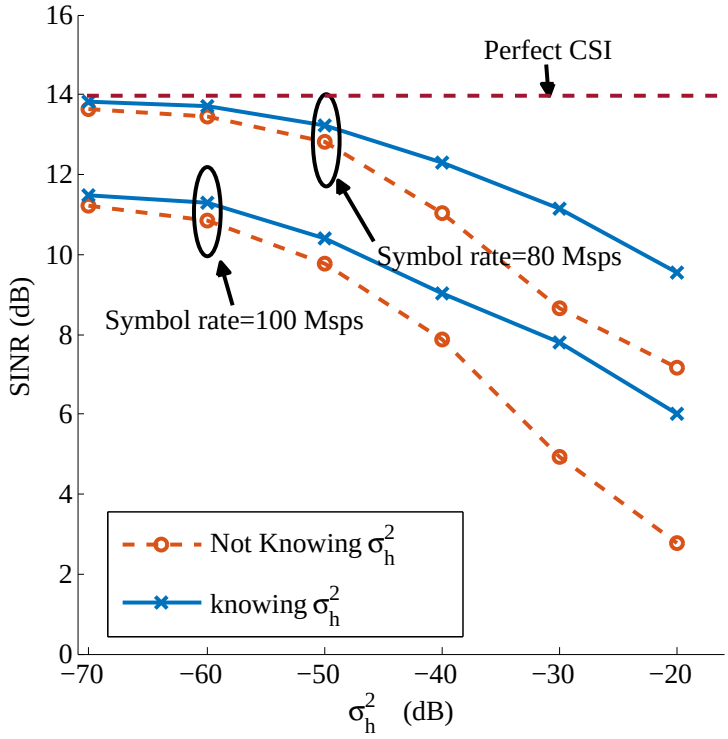

Figure 4.16: SINR for imperfect CSI with different uncertainty variance, $L_f = 7$ and 3 users.

is -20 dB, knowing the variance can provide about 2 dB SINR advantage over not knowing the variance.

The same method used to estimate the effect of imperfect CSI can be used to evaluate the off-line algorithm. The difference between $\hat{h}_{qk}$ and μ_{ik} can be regarded as a known channel uncertainty. From this results, if the variance of the difference is around -20 dB, the performance of the off-line algorithm can provide about 4 dB less SINR compared to the regular (on-line) algorithm.

4.3 Comparison of DCO-OFDM and M-PAM

4.3.1 Background

Recently, orthogonal frequency division multiplexing (OFDM) has been employed in OWC systems due to its resistance to inter-symbol interference (ISI) and high spectral efficiency [23, 24]. Since intensity modulation and direct detection are used in OWC systems, the transmitted signal should be non-negative. Therefore, the conventional OFDM cannot be applied directly in OWC. DC-biased optical OFDM (DCO-OFDM) is a popular optical OFDM technique that can be applied in OWC that use incoherent light [7]. Hermitian symmetric data is used to make the DCO-OFDM signal real. Because of the nonlinearity of LEDs, the DCO-OFDM signal must be clipped, distorting the signal.

In this section, we compare the performance of DCO-OFDM and M-PAM techniques for OWC systems. For DCO-OFDM, we consider the clipping noise caused by the LEDs' nonlinearity (clipping at both zero and peak current). We optimize the modulation index and the bits loaded on each subcarrier to maximize the transmitted bit rate. In this section, to simplify the analysis, we consider single user operation.

4.3.2 Optimized DCO-OFDM

In this section, we describe how we optimize DCO-OFDM. For VLC systems, due to the nonlinearity of the LEDs, the DCO-OFDM signals may be clipped by the LEDs. The optimized DCO-OFDM scheme maximizes the transmitted bit rate by optimizing the modulation index and the bits loaded on all subcarriers. A block diagram of the optimized DCO-OFDM is shown in Fig. 4.17. In this diagram, $X_i[m]$ is the data to be modulated by ith subcarrier at the mth time instant after M-QAM. We assume

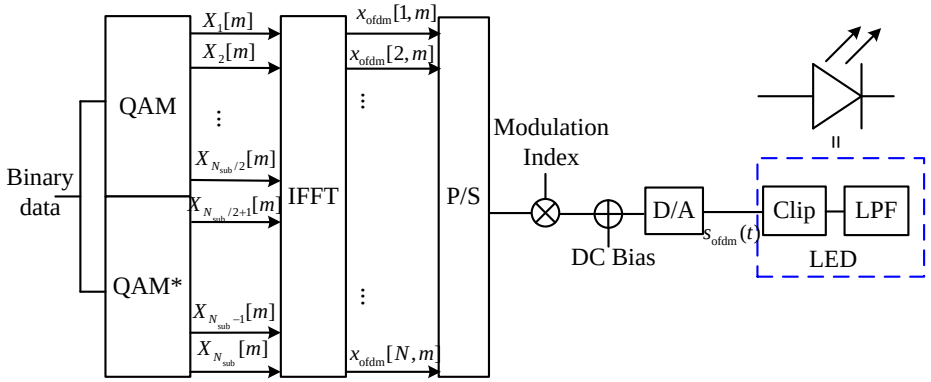

Figure 4.17: Diagram of DCO-OFDM with adjustable modulation index and loaded bits.

that there are N_{sub} subcarriers. To make the OFDM signal real, $X_{N_{\text{sub}}+1-i}[m]$ is the conjugate of $X_i[m]$, $X_{N_{\text{sub}}+1-i}[m] = X_i^*[m]$. After modulation, the real OFDM signal for the kth subcarrier component, $x_{\text{ofdm}}[k, m]$, can be represented as

$$x_{\text{ofdm}}[k, m] = \sum_{i=1}^{N_{\text{sub}}} X_i[m] e^{\frac{j2\pi ki}{N_{\text{sub}}}}, \ \forall \ k = 1, 2, \cdots, N_{\text{sub}} \tag{4.47}$$

After converting the parallel data to a serial stream, adding a DC offset and the D/A converter, the electrical signal $s_{\text{ofdm}}(t)$ can be represented as

$$s_{\text{ofdm}}(t) = \frac{\varrho}{N_{\text{sub}}} \sum_{n=-\infty}^{\infty} \sum_{k=1}^{N_{\text{sub}}} x_{\text{ofdm}}[k, m] g(t - k - mT_{\text{ofdm}}) + s_{\text{dc}}, \tag{4.48}$$

where the term ϱ/N is referred to as the modulation index. $g(t)$ is the signal pulse function, and T_{ofdm} is the duration of the pulse. s_{dc} is the DC bias, which is set to $s_{dc} = I_{\max}/2$, where $I_{\max}$ is the saturation current to drive the LEDs. When N_{sub} is large (usually greater than 64), the analog signal $s_{\text{ofdm}}(t)$ can be modeled as a Gaussian random process.

In order to prevent the LEDs from damage, the drive current should remain in the range of $[0, I_{\max}]$. Considering the bandlimited characteristic of LEDs, we model

the LED as a clipping component and a lowpass filter in series as shown in Fig. 4.17. Therefore, the signal outside the range $[0, I_{\max}]$ is clipped.

After matched filtering and sampling at the receiver, the received signal can be modeled as [78]

$$y_{\text{clip}}[m] = \alpha s_{\text{ofdm}}[m] * h[m] + n_{\text{clip}}[m], \tag{4.49}$$

where $h[m]$ is the discrete time version of the impulse response of the LED. Since the clipping effect is a non-linear operator, the constant coefficient α can be found by using the Bussagang theorem, [78]:

$$\alpha = 1 - \text{erfc}\left(\frac{I_{\max}}{\sqrt{8\sigma_s^2}}\right), \tag{4.50}$$

where $\text{erfc}(x) = 2/\sqrt{\pi}\int_x^\infty e^{-y^2}dy$, and σ_s^2 is the variance of the OFDM signal, $s_{\text{ofdm}}(t)$. We model the clipping noise, $n_{\text{clip}}[i]$, as a zero mean Gaussian variable with a variance estimated using

$$\sigma_{\text{clip}}^2 = \int_{-\infty}^{0} (\alpha x)^2 f(x)dx + \int_{I_{\max}}^{\infty} (\alpha x - I_{\max})^2 f(x)dx, \tag{4.51}$$

where $f(\cdot)$ is the probability density function (pdf) of the samples $\alpha s_{\text{ofdm}}[m]$.

In Fig. 4.18, the constellation of the clipped signal and the original signal are shown. From the plot, the clipping effect not only introduces noise, but also causes distortion. Since the clipping effect limits the peak power of the transmitted signals, the constellation of the clipped signals are shrunk. Using the model in (4.49), the constellations of the modeled clipped signals are illustrated in Figs. 4.19 and 4.20. From the results, (4.49) can perfectly model the clipping effect.

At the receiver, the signal to noise ratio (SNR) for the ith subcarrier can be

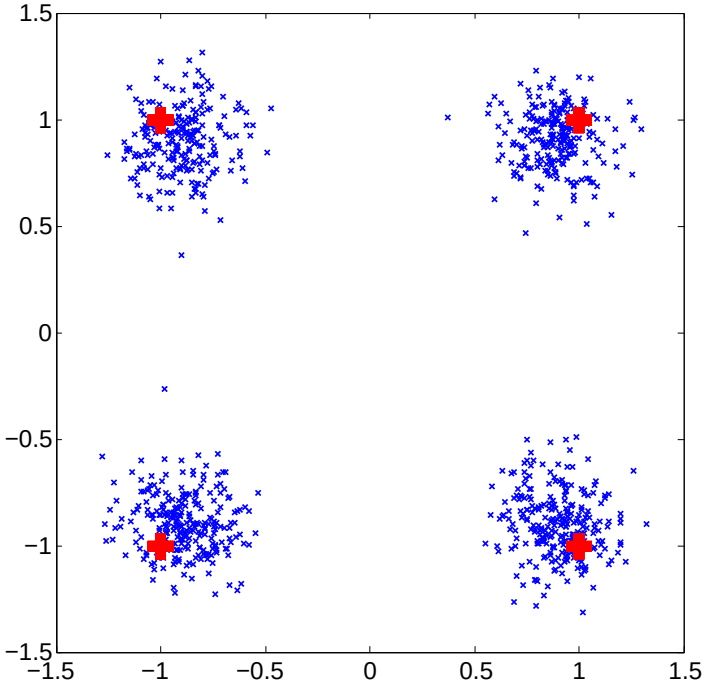

Figure 4.18: Signal constellation with clipping only, 4-QAM.

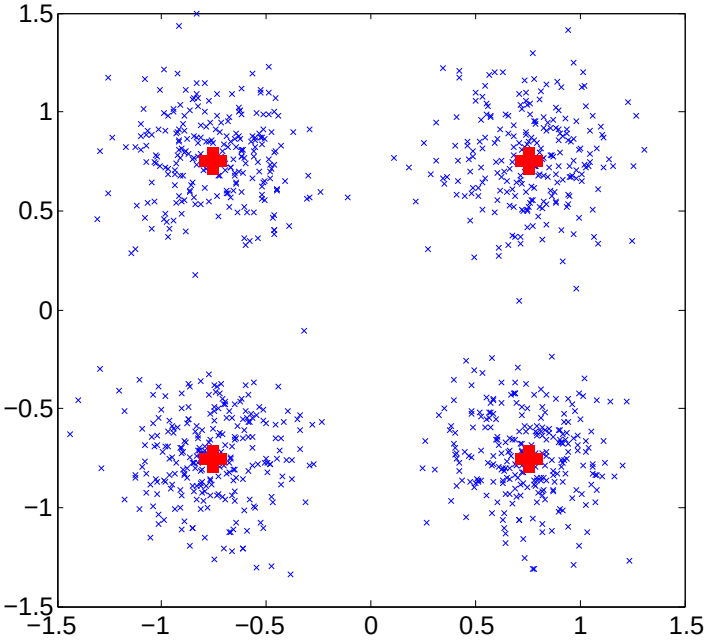

Figure 4.19: Signal constellation using (4.49), 4-QAM.

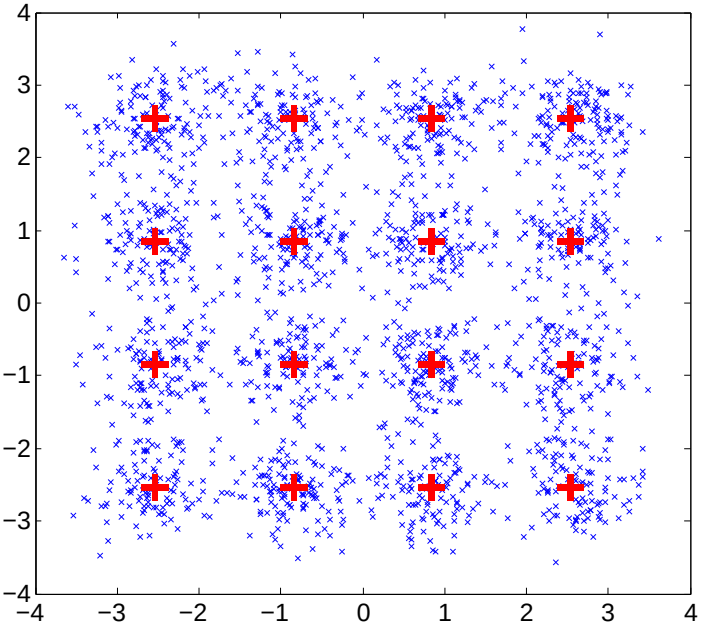

Figure 4.20: Signal constellation using (4.49), 16-QAM.

calculated as

$$\gamma_{\text{ofdm}}^{(i)} = \frac{(\varrho\alpha\mathcal{H}_i E\{|X_i|\})^2}{N\left(\sigma_{\text{ofdm}}^2 + \sigma_{\text{clip}}^2\right)}, \tag{4.52}$$

where $\mathcal{H}_i$ is the LED response for the ith subcarrier. $E\{\cdot\}$ represents the expectation operation, and σ_{ofdm}^2 is the variance of the receiver additive Gaussian noise in the ith subcarrier. Given the SNR, we can calculate the bit error rate (BER) for each subcarrier by using the approximate expression [34]

$$\text{BER}_i \approx \frac{\sqrt{M_{\text{ofdm}}^{(i)}} - 1}{\sqrt{M_{\text{ofdm}}^{(i)}}\log_2\left(\sqrt{M_{\text{ofdm}}^{(i)}}\right)}\text{erfc}\left(\sqrt{\frac{3\gamma_{\text{ofdm}}^{(i)}}{2M_{\text{ofdm}}^{(i)} - 2}}\right), \ \forall\ i, \tag{4.53}$$

where $M_{\text{ofdm}}^{(i)}$ is the modulation constellation size for the QAM used in the ith subcarrier. The simulation and theoretical results using (4.53) are shown in Fig. 4.21. With an increasing modulation index, the SNR increases, thus the BER decreases. However, when the clipping effects dominates the noise, increasing the modulation

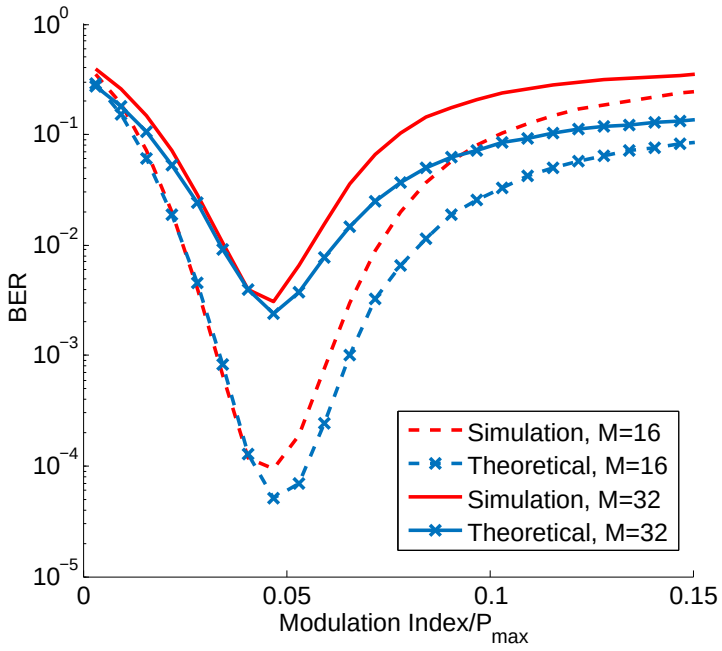

Figure 4.21: BER comparison of simulation and theoretical results using M-QAM.

index can make the BER worse, as expected.

The throughput for the DCO-OFDM can be calculated as

$$R_b = \frac{N_{\text{sub}}}{2T_{\text{ofdm}}} \sum_{i=1}^{N_{\text{sub}}/2} \log_2 M_{\text{ofdm}}^{(i)}. \tag{4.54}$$

To optimize the throughput, we can choose the optimal T_{ofdm}, ϱ, and the number of bits loaded onto each subcarrier. In this section, for each subcarrier, the subcarrier bit loading is constrained by the BER requirement and the LED bandwidth filter. Usually, with the help of forward error correction (FEC), the BER requirement for each subcarrier can be set at 10^{-3}.

4.3.3 Numerical Results and Comparison

In this section, numerical results of the comparison of DCO-OFDM and M-PAM are shown. To obtain a fair comparison, the same parameters are used for DCO-

OFDM and M-PAM. We assume that the 3 dB bandwidth of the LED, $f_{3\text{dB}} = 20$ MHz. The additive noise power spectral density is $N_o = 10^{-9}$ mW/Hz. The BER requirement for communication quality is $B^{\max} = 10^{-3}$. To simplify the problem, an ideal channel response (zero loss) is considered in this section. In addition, the forward current to optical power conversion ratio of the LED is assumed to be unity. Thus, the saturation current constraint implies the constraint on the peak transmitted optical power.

With the help of bit loading, the throughput of DCO-OFDM can be maximized. Adjusting the modulation index, a compromise is reached between the signal power and clipping noise power. In Fig. 4.22, the throughput with different modulation indexes using bit loading is shown. From the results, the number of subcarriers does not seem to affect the maximum throughput. In this result, the peak transmitted power is 10 mW.

Fig. 4.23 shows a comparison between the optimized DCO-OFDM and the optimized M-PAM using JOW. In this figure, $R_b/f_{3\text{dB}}$ is used to measure the spectral efficiency for both M-PAM and DCO-OFDM. For JOW, the waveform design algorithm and MMSE equalizer can use more than the 3 dB bandwidth of the LED, and the clipping distortion caused by the nonlinearity of the LED can affect the performance of the DCO-OFDM; therefore, using M-PAM with JOW can provide a better performance than DCO-OFDM. From the results, the M-PAM using JOW can provide an 80% higher throughput than the optimized DCO-OFDM described in Section 4.3.2. With the help of waveform design, M-PAM can achieve a higher bit rate than using only the MMSE equalizer. If there is no equalization technique for M-PAM, the optimized DCO-OFDM can support about five times higher data rate than M-PAM when the transmitted power is 8 mW.

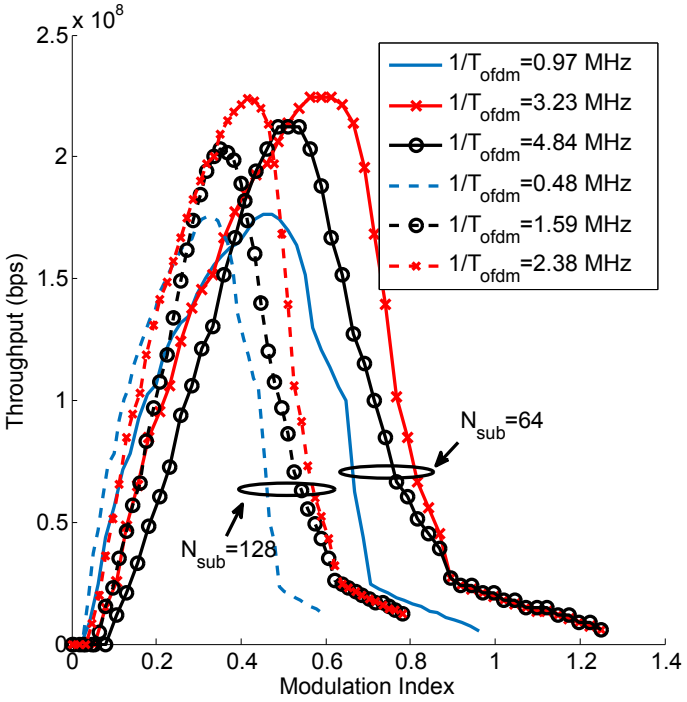

Figure 4.22: Throughput of DCO-OFDM with bit loading for different modulation indexes.

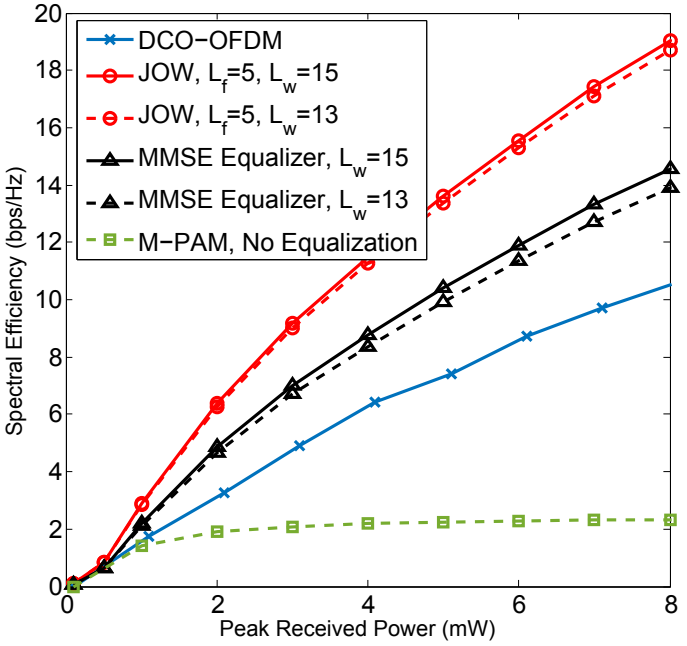

Figure 4.23: Throughput comparison of optimized DCO-OFDM and optimal M-PAM for a single user.

4.4 Summary

In this chapter, we first propose an adaptive M-PAM algorithm using OCDMA and MISO techniques to support multiple users. Depending on the SINR at the receivers, the proposed algorithm can choose the optimal power allocation and M-PAM constellation size for the users to optimize the bit rate fairly. It is able to adapt to different shadowing effects and desired BERs. Compared with the same algorithm using TDMA, the proposed algorithm using OCDMA can offer a higher bit rate when the number of users is larger than the length of the OCDMA code.

Then, a joint optimal waveform design algorithm using adaptive M-PAM modulation scheme is proposed to provide high data data transmission rates for multiple users. In this algorithm, the waveforms transmitted from each LED lamp to all the users are uniquely designed to reduce the ISI and MAI. Together with the MMSE filters at the receivers, the transmitted waveforms are optimized to provide the maximal data rates. The high level modulation can provide high data transmission rates. The modulation constellation size can be adaptively adjusted under different SINR conditions and BER requirements. In this work, the channel uncertainty and imperfect CSI cases are discussed. From numerical results, the proposed robust algorithm can get a higher SINR than the non-robust algorithm by knowing the channel uncertainty information. Compared with OOC codes, the proposed JOW can provide higher SINR. Considering the illumination and dimming control, JOW is more flexible than CDMA. The illumination level can be easily adjusted in JOW by setting a illumination constraint. The waveform length is another design parameter, we can find the optimal waveform length to maximize the data rate. In conclusion, the JOW using adaptive M-PAM can provide high data transmission rate over ISI channel for multiple users. Compared with CDMA, JOW has prominent advantages in SINR and

illumination.

In the last section, we compare the performance of DCO-OFDM and M-PAM for LED-based communication systems for a single-user operation. Considering the LED bandlimited characteristic and the constrained transmitted power, we propose an optimized DCO-OFDM by choosing the optimal modulation index with an appropriate bit loading algorithm. For M-PAM, our waveform design joint optimization algorithm is used to reduce the ISI caused by the bandlimited LED. In this section, from the simulation and theoretical results, we conclude that M-PAM with waveform design and MMSE equalization can provide an 80% higher data transmission rate than DCO-OFDM with bit loading and an optimal modulation index.

Chapter 5

Interception Vulnerability Analysis

VLC is considered as an alternative to Wi-Fi systems to provide wireless network access in indoor areas due to some critical shortcomings of Wi-Fi. A major-draw back of Wi-Fi systems is its susceptibility to eavesdropping, which has limited its use in security sensitive environments. RF signals that are used in Wi-Fi systems can penetrate through walls, and this leakage can expose the information carried by these signals to hackers. Unlike Wi-Fi systems, the signals in VLC systems are blocked by any opaque object, and therefore, the signals cannot pass through the walls. We can assume the RF leakage from the VLC modulator is controlled. As a result, 100% security against outside eavesdroppers can be guaranteed in VLC systems if no light escapes the room. However, this is usually not the case in real scenarios: the light leaks out through glass doors and windows, which can impose security risks on the VLC users.

In [79], the security risks of VLC systems due to the light leaked from under the door and through the key hole have been analyzed for various room setups. In [80], Mostafa and Lampe analyze the security of VLC systems in an indoor area against an internal hacker and, in [81], they propose a multiple input and single output MISO

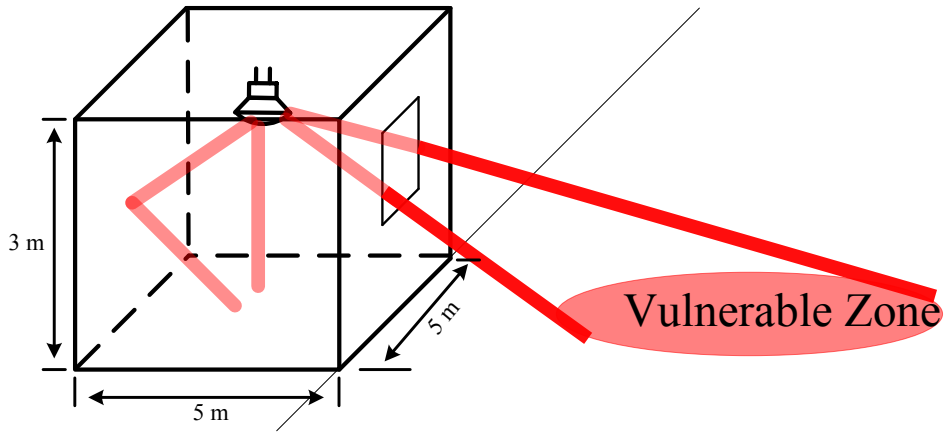

Figure 5.1: Vulnerable area outside the room

system to increase the privacy of VLC systems through pulse shaping. [82] presents a high security CDMA scheme for VLC systems, and derives an information leakage expression. Pan et. al. investigate the secrecy performance of a VLC system with a group of randomly distributed eavesdroppers in [83]. There have been more general analyses on the security of free space optical systems that can also be extended to VLC systems [84].

To the best of our knowledge, there is no study on the information leakage of VLC systems through a window and its security risks. Fig. 5.1 shows an example of the information leakage through a window. We define the area with high security risks as vulnerable zone. In this work we present an analysis for the strength of the VLC signals leaked through windows, and based on this, we calculate the specifications of devices required for eavesdropping. We divide the area outside the window into high risk and low risk regions based on the access to the line of sight (LOS) signals, and calculate the size of the minimum aperture in each region to achieve the minimum SNR required for detection of the information. We then propose a technique to reduce the size of the high-risk region by optimizing the modulation efficiency that controls the percentage of the optical power for carrying the data. This algorithm

can provide a flexible highly secure communication link for indoor users and minimize the possibility of data interception in outdoor areas.

5.1 System Performance and Security

5.1.1 System Performance

The criteria used to evaluate the performance of the VLC system are the BER and the data rate. The relationship between these two metrics is discussed in this section. Since IM/DD is employed in VLC, M-PAM can be used to increase the data rate for a fixed transmitter bandwidth. Using M-PAM, a $(\log_2 M)$-fold increase in the data rate compared with OOK can be achieved. The choice of modulation constellation size M depends on the SNR at the receiver. In this chapter, an adaptive technique is assumed, where the largest constellation size allowed by the SNR of the intended user is used to get the highest data rate [29]. No waveform optimization is included here.

We assume the desired-user SNR is determined by the channel quality, transmitted power, and the size of photo-detector (PD). For a given channel, the SNR for user k can be calculated as

$$\gamma_k = \frac{\left(\rho P^{\max} A_r \sum_{\ell=1}^{Q} \beta_\ell \hat{h}_{\ell k}\right)^2}{\sigma_n^2} \tag{5.1}$$

where ρ represents the the responsivity of the PD. $P^{\max}$ is the peak transmitted power and Q is the number of LEDs. A_r is the area of the intended receiver's PD, which is small in the VLC system, where the receiver is in the room. $\hat{h}_{\ell k}$ is the channel gain from LED ℓ to user k, which can be calculated from (2.2). β_ℓ represents the modulation efficiency that describes the percentage of the ℓth LED's optical power used for data transmission. The value of β_ℓ does not affect the total emitting power

of the LEDs. σ_n^2 represents the noise power at the receiver, which includes thermal noise and shot noise.

5.1.2 System Security

The VLC system has high security because of the characteristics of light that it cannot penetrate opaque objects like walls. It keeps the communication system secure in the wireless physical-layer. When the eavesdropper cannot have a good quality channel, the transmitted information cannot be reconstructed [79].

The size of the receiver aperture (the lens placed in front of the PD) is a significant factor to be considered by eavesdroppers. The smaller the eavesdropper receiver aperture becomes, the harder it is to expose it, since a large receiver aperture makes the eavesdropping equipment easily spotted. However, a too small size receiver aperture cannot support a sufficiently high SNR to intercept the signal. The required eavesdropper SNR depends on the desired modulation constellation size and BER.

Consider the case that the eavesdropper is outside the window during the daytime. The additional shot noise from sunlight helps to lower the received SNR, and therefore improves the security of the communications. In this chapter, we assume the sunlight illumination is sufficiently bright to make the shot noise caused by background light the dominant noise source. For this case, the eavesdropper minimum receiver aperture required to obtain a BER $= 10^{-3}$ can be calculated as

$$A_r \geq \frac{2qR_s\Phi_{\text{sun}}\gamma_k}{\rho(\varphi P^{\max}\sum_{\ell=1}^{Q}\beta_\ell\hat{h}_{\ell k})^2}, \tag{5.2}$$

where Φ_{sun} is the power density of the sunlight on the ground, which can be calculated from the sunlight illumination. φ is the transmittance percentage through normal glass. R_s is the transmitted symbol rate, the value of which is assumed to be the

same as the bandwidth. For the indoor area or the outside area at night, we assume the background light is negligible, and therefore the thermal noise is dominant. For this case, the minimum receiver aperture (for both intended and unintended users) can be calculated using

$$A_r \geq \frac{\sqrt{\gamma_k \sigma^2_{\text{thermal}}}}{\rho \varphi P^{\max} \sum_{\ell=1}^{Q} \beta_\ell \hat{h}_{\ell k}}. \tag{5.3}$$

If a very small size of receiver aperture is necessary, a high gain PD, such as an avalanche photo diode (APD), can be used. The actual PD size can be calculated roughly as

$$\hat{A}_r = \frac{A_r}{G}, \tag{5.4}$$

where G is the gain of the APD, and $\hat{A}_r$ is the effective aperture size.

5.1.3 LED Modulation Efficiency Optimization

In order to reduce the leakage of information and enhance the indoor communication performance, we can optimize the modulation efficiency of each LED. With the help of the lamp model shown in Fig. 2.1, the security and indoor data transmission quality can be considered at the same time.

We assume that the smaller the eavesdropper receiver aperture becomes, the harder it is to expose it. On the other hand, a larger aperture can collect more optical power and achieve a higher SNR to capture the data. To minimize the possibility of interception and guarantee the indoor communications, we can optimize the modulation efficiency by

$$\begin{aligned} &\max_{\beta_{\mathbf{1}}, \beta_{\mathbf{2}}, \cdots, \beta_{\mathbf{Q}}} \min_{k_{\text{in}}} \gamma_{k_{\text{in}}} \\ s.t. \quad &\max\left(\gamma_{k_{\text{out}}}\right) \leq \gamma_{\min}, \\ &0 \leq \beta_\ell \leq 1, \ \ell = 1, \cdots Q, \end{aligned} \tag{5.5}$$

where k_{in} is any user in the indoor area, and k_{out} represents any eavesdropper outside the window. $\gamma_{\min}$ is the minimum SNR for data detection. $\gamma_{k_{\text{in}}}$ and $\gamma_{k_{\text{out}}}$ represent the SNR for the any indoor user and outdoor eavesdropper, respectively, which can be calculated by using (5.1)

$$\begin{aligned} \gamma_{k_{\text{in}}} &= \frac{\left(\rho P^{\max} A_{\text{in}} \sum_{\ell=1}^{Q} \beta_\ell \hat{h}_{\ell k_{\text{in}}}\right)^2}{\sigma_{\text{in}}^2}, \\ \gamma_{k_{\text{out}}} &= \frac{\left(\rho P^{\max} \varphi A_{\text{out}} \sum_{\ell=1}^{Q} \beta_\ell \hat{h}_{\ell k_{\text{out}}}\right)^2}{\sigma_{\text{out}}^2} \end{aligned} \tag{5.6}$$

where A_{in} and A_{out} represent the desired user aperture and eavesdropper aperture, respectively. σ_{in}^2 represents the noise power for indoor users, which can be assumed as $\sigma_{\text{in}}^2 = \sigma_{\text{thermal}}^2$; σ_{out}^2 is the noise power for the outdoor eavesdropper, which is $\sigma_{\text{thermal}}^2$ at night. $\sigma_{\text{out}}^2 = \sigma_{\text{shot}}^2$ in the daytime.

To find the optimal modulation efficiency, an iterative method, the SQP algorithm, can be used. Since the maximin optimization is non-convex, only a locally optimal solution of the modulation efficiency can be obtained.

5.2 Simulation Results and Analysis

To test the system vulnerability, we set up a scenario as an empty and unfurnished room with dimensions of 5 m × 5 m × 3 m. There is only one window of 2 m × 2 m in size, and the low edge of the window is 1 m off the floor. The parameters used to obtain the simulation results are shown in Table 5.1. All measurements are simulated at the floor level.

Table 5.1: Parameters Used in Numerical Results

LED lamp placement	(2.5, 2.5, 2.9) m
Peak radiation power of each LED	500 mW
Number of LEDs per lamp	25
Semiangles of LEDs	20^o
Intended user aperture, $A_{k_{\text{in}}}$	10^{-4} m^2
Eavesdropper aperture, $A_{k_{\text{out}}}$	1 m^2
Transmittance percentage through window, φ	1
Sunlight illumination	1.2×10^5 lx
Thermal noise power, $\sigma^2_{\text{thermal}}$	6.56×10^{-15} W
Background light noise power, σ^2_{shot}	1.12×10^{-13} W

5.2.1 No LED Modulation Efficiency Optimization

In this section we consider the vulnerability of the system when all LEDs transmit data ($\beta_\ell = 1,\ \forall\ \ell$), unconcerned with security issues.

For a typical office room, the illumination level should be around 400 lx [49]. To make this requirements, the SNR distributions in the indoor area and the outdoor area are shown in Figs. 5.2 and 5.3, respectively. In these two results, we assume the size of the PD at the intended receiver is 10^{-4} m^2. For the indoor area, the thermal noise is dominant, and for the outdoor area, the shot noise caused by the background sunlight is dominant. In general, the SNR in the indoor area is more than 38 dB and is distributed symmetrically around the LED lamp. The high indoor SNR can support a reliable and high speed wireless data transmission by using a large modulation constellation size. For instance, an SNR of 38 dB allows us to use an 16-PAM.

The SNR distribution outside the room varies dramatically depending on where the receiver is placed and the background light levels. The area just outside the window has a higher SNR than other places. The high SNR area outside the window is referred to as the *vulnerable zone* in Fig. 5.3. In this plot, we choose a 20 dB SNR

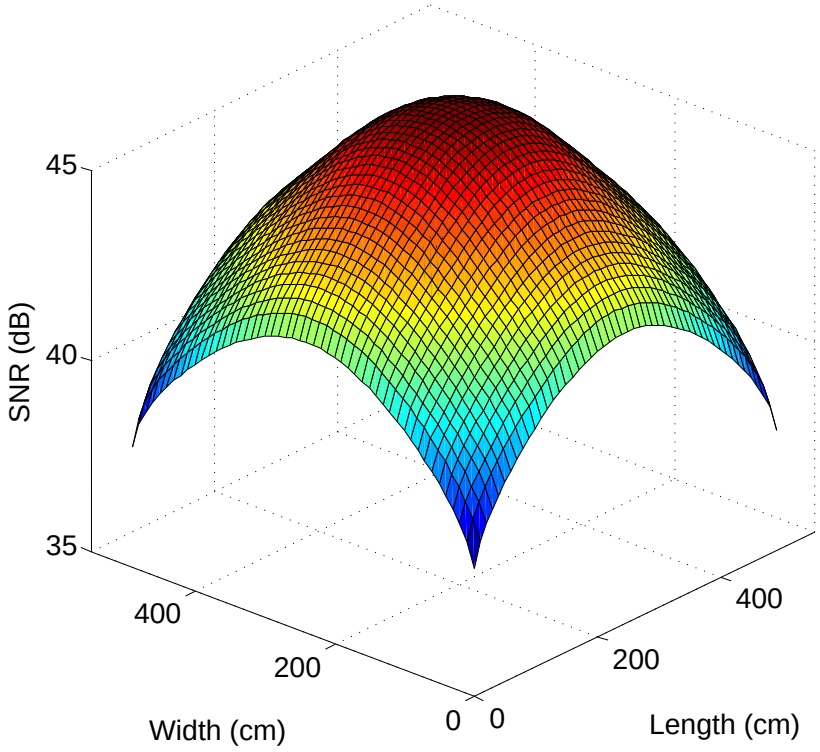

Figure 5.2: SNR distribution in the indoor area

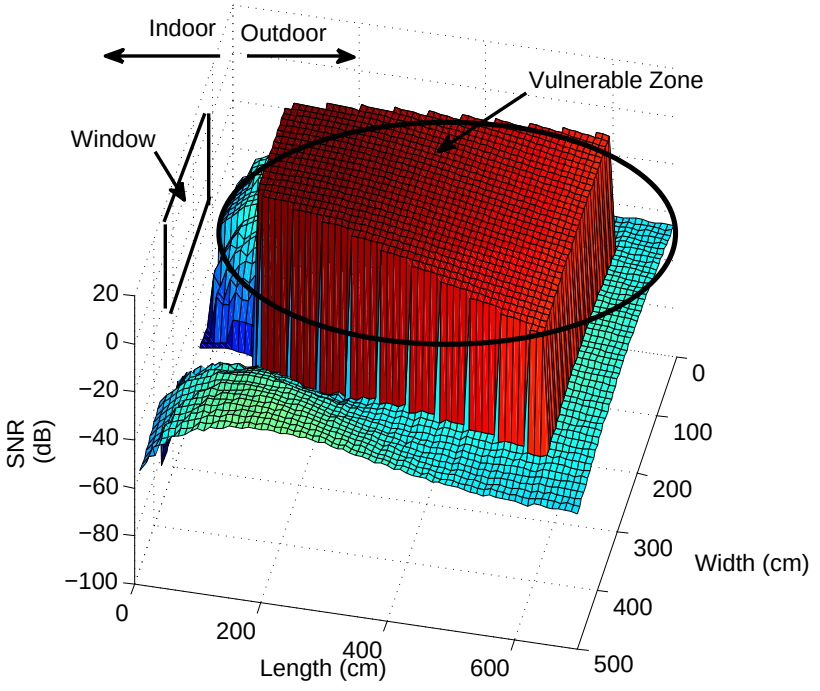

Figure 5.3: SNR distribution in the outdoor area, daytime.

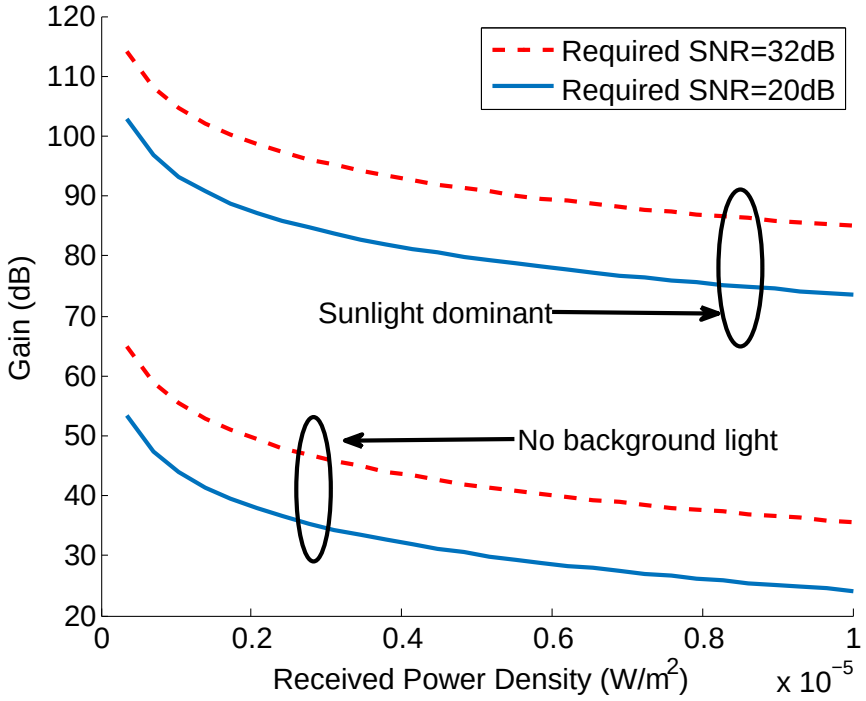

Figure 5.4: Gain of the PD requirements for different received power densities.

as a threshold, corresponding to a constellation size of $M = 8$. The area with SNR greater than 20 dB is defined as the vulnerable zone. In the vulnerable area, the LOS light dominates.

Fig. 5.4 shows the relationship between the required gain of the receiver and the received power density. Two extreme cases are compared in this result. The sunlight dominant case represents an outdoor scenario in daylight. The indoor area and the outdoor area at night can be assumed to experience no background light. From the results in Fig. 5.4, for the same received power density, the sunlight-dominant case needs around 30 dB higher gain than the no-background light case to get the same SNR. Thus, the background sunlight indeed makes it more difficult for the eavesdropper to detect the information.

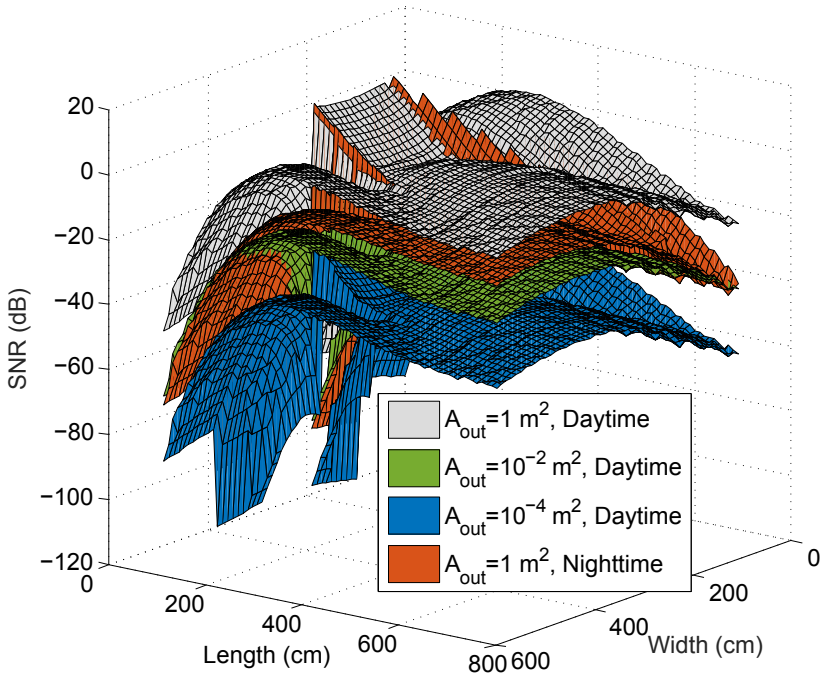

Figure 5.5: SNR distribution for outdoor areas by optimizing the LED modulation efficiency using different sizes of aperture, $\gamma_{\min} = 10$ dB.

5.2.2 LED Modulation Efficiency Optimization to Diminish Vulnerability

In this section we consider the vulnerability of the VLC system to eavesdropping when the LED modulation efficiency optimization is adjusted. In this part, we test two environment: daytime and nighttime cases. We assume that the sunlight only affects the outside background light. For the modulation efficiency optimization, we assume the detector of the eavesdropper is on the floor.

Fig. 5.5 shows the SNR distribution outside the window after applying the optimal modulation efficiency of each LED in the lamp. For the optimization results, we design $\gamma_{\min} = 10$ dB. If the eavesdropper detector uses a $A_{\text{out}} = 1$ m^2 aperture, it can only obtain up to a 10 dB SNR. However, a detector with a 1 m^2 aperture is very easily detected. From (4.38), a 10 dB SNR is the minimum value to support a

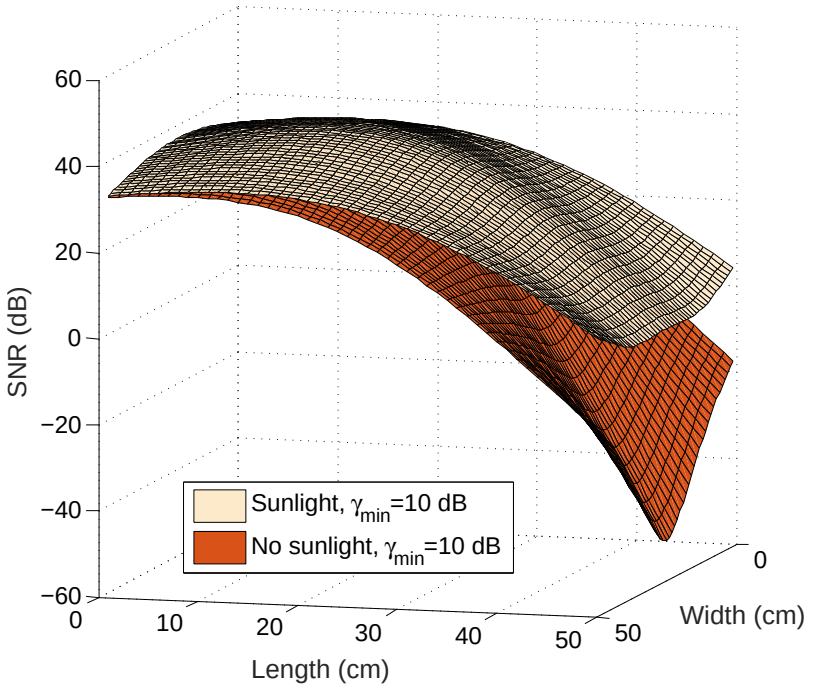

Figure 5.6: SNR distribution for indoor areas by optimizing the LED modulation efficiency, $A_{\text{out}} = 1$ m^2 and $A_r = 10^{-4}$ m^2.

communication system with a 10^{-3} BER by using 2-PAM. The outdoor eavesdropper is unable to demodulate a 16 to 32-PAM signal that is used in indoor areas. If the eavesdropper uses a detector with a smaller aperture, such as 10^{-2} m^2 or 10^{-4} m^2 as shown in Fig. 5.5, up to -10 dB and -30 dB SNR can be obtained, which are too small to recover the data. No matter whether there is sunlight or not, our algorithm can limit the outdoor SNR to a very low level. The SNR distributions of the sunlight and no sunlight cases are similar.

After optimizing the modulation efficiency, the SNR distribution in the indoor area is shown in Fig. 5.6. Although we assume the sunlight cannot affect the illumination in the indoor area, the optimization of the modulation efficiency depends on the outside sunlight. The strong sunlight can introduce more background shot noise than the case without sunlight. Thus, it is more difficult for the eavesdropper to capture the data under a strong sunlight circumstance. Compared with the nighttime case,

the sunlight can allow the system to use a higher modulation efficiency for a better indoor wireless connection. Considering the results of Fig. 5.4 and 5.5, for both the daytime and nighttime, we can guarantee a similar outdoor SNR distribution by setting the same $\gamma_{\min}$, which is secure. With the help of sunlight, daytime can allow up to a 40 dB enhancement of the indoor SNR compared with the nighttime.

5.3 Summary

In this chapter, we quantitatively analyze the potential vulnerability of the system from eavesdropping by calculating the SNR in different areas outside a window. We calculate the required gain and aperture size for the receiver in different areas in order to illustrate how big the eavesdropper equipment must be to successfully recover the signal. We show that the area where the LOS signal can be received is most vulnerable. We also show that the daytime sunlight greatly reduces the possibility of eavesdropping.

Based on our analysis, we propose a solution to improve the VLC system security by implementing a modulation efficiency optimization algorithm that can minimize the possibility of outdoor eavesdropping and maximize the minimum SNR in the indoor area to guarantee a reliable indoor data transmission. The results show that by doing this we can maintain indoor communication system performance while greatly reducing the SNR outside the room. If the eavesdropper uses small detection equipment, the SNR is not high enough to recover the data. Otherwise, to obtain an acceptable SNR, a large size equipment should be used, which makes the eavesdropper easy to detect.

Chapter 6

Conclusions and Future Work

6.1 Summary and Conclusions

In this dissertation, we investigate the multiuser MIMO indoor VLC systems. Multi-LED transmitter and multi-detector receiver models are proposed and applied. Following the Lambertian rule, the indoor VLC channel model is derived.

Then, considering multiple users cases, we propose a centralized and several decentralized power allocation algorithms. In the centralized power allocation algorithm, all the LED lamps in the room are coordinated and controlled by a central controller; each LED lamp supports all the users within the indoor area. For standard indoor office illumination level (400 lx), about 40 users can be supported with bit error rates less than 10^{-3} using on-off keying and 70 MHz bandwidth of receivers at 5×10^{-7} W/Hz spectral density. The decentralized power allocation algorithms we propose have similar bit error rate performance and less computational burden compared to the centralized algorithm. In our decentralized algorithms, users are supported by a subset of the LEDs, and so the optimization problem size of the decentralized algorithms can be reduced, by as much as 90% for the large room scenario. For each

receiver, multiple photodetectors with different orientations are employed to improve the signal to interference plus noise ratio. In addition, some practical considerations, such as shadowing effects, illumination requirements, dimming control and transmitted power quantization are taken into account. From numerical results, the proposed adaptive power allocation algorithms can adjust the transmitted power to reduce shadowing effects. Furthermore, the transmitted power can be dimmed to satisfy the illumination requirements within a range of tolerance. In this dissertation, the system uses the OCDMA technique to support multiple users. Time-space minimum mean squared error filters at the receivers are designed to diminish the effect of multiple-access interference in the indoor VLC system.

In addition, we discuss modulation schemes for VLC systems. We first propose an adaptive M-PAM algorithm to support multiple users. The proposed algorithm can adjust the modulation constellation size for each user to maximize the bit rate under different channel environments such as shadowing, light dimming, and the impact of multiple access interference. In our MISO approach, multiple LED lamps coordinate to provide users with maximum data rates. We compare OCDMA using our adaptive M-PAM with TDMA. The OCDMA technique can offer a higher bit rate when the number of users is larger than the length of the OCDMA code. Second, a joint optimal waveform design for visible light communication systems using M-ary pulse amplitude modulation is proposed to support multiple users. The transmitted waveforms and MMSE filters are jointly optimized to minimize the intersymbol and multiple access interferences. Based on different channel conditions, the designed waveforms and modulation constellation size can be adaptively adjusted to guarantee the highest data rate. When the 3 dB bandwidth of LEDs is 20 MHz and the peak transmitted power is 3 Watts, the maximum bit rate per user can be achieved about 200 Mbps using the proposed waveform design algorithm. Compared with OCDMA

and TDMA, the algorithm proposed in this dissertation can provide about 8 dB higher signal to interference plus noise ratio when the transmitted symbol rate is 80 Mb/s. In addition, the proposed algorithm can flexibly change the illumination level by adjusting the optimization constraint. From numerical results, the proposed waveform design algorithm can provide about a 20% higher illumination than OCDMA. Taking the computational complexity into account, an off-line waveform design solution is proposed, and the performance of the off-line solution can be estimated. Finally, a comparison between the optimized DCO-OFDM and M-PAM with JOW is discussed. From numerical results, the M-PAM with waveform design and MMSE equalizer can provide an 80% higher data rate than the optimized DCO-OFDM with the same BER for single user.

In the last part of the dissertation, the vulnerability of VLC systems in the physical layer is discussed. we first analyze the potential vulnerability of the system from eavesdropping outside the room. By setting up a signal to noise ratio threshold, we define a vulnerable area outside of the room through a window. We compute the receiver aperture needed to capture the signal and what portion of the space is most vulnerable to eavesdropping. Based on the analysis, we propose a solution to improve the security by optimizing the modulation efficiency of each LED in the indoor lamp. The simulation results show that the proposed solution can improve the security considerably while maintaining the indoor communication performance.

6.2 Future Work

As future work, the mobility of users should be considered. A faster way of finding the optimized power allocation for users needs to be investigated. Optical CDMA codewords reuse strategy can be explored. To reduce the clipping distortion

from LEDs, a new kind of optical OFDM technique that is suitable for LED-based communication systems can be studied.

Bibliography

[1] T. Komine and M. Nakagawa, "Adaptive detector arrays for optical communication receivers," *IEEE Trans. Consum. Electron.*, vol. 50, no. 1, pp. 100–107, 2004.

[2] Z. Chen, D. Tsonev, and H. Haas, "Improving SINR in indoor cellular visible light communication networks," in *2014 IEEE International Conf. on Commun.*, 2014, pp. 3383–3388.

[3] M. Noshad and M. Brandt-Pearce, "Application of expurgated PPM to indoor visible light communications part I: Single-user systems," *J. Lightw. Technol.*, vol. 32, no. 5, pp. 875–882, 2014.

[4] P. Luo, Z. Ghassemlooy, H. L. Minh, E. Bentley, A. Burton, and X. Tang, "Fundamental analysis of a car to car visible light communication system," in *2014 International Symposium on Commun. Systems, Networks Digital Signal Proces. (CSNDSP),*, 2014, pp. 1011–1016.

[5] S. Ucar, B. Turan, S. C. Ergen, O. Ozkasap, and M. Ergen, "Dimming support for visible light communication in intelligent transportation and traffic system," in *NOMS 2016 - 2016 IEEE/IFIP Network Operations and Management Symposium*, April 2016, pp. 1193–1196.

[6] "Free space optics (FSO) and visible light communication (VLC) / Li-Fi technology market by component (LED, photo detector, microcontroller, and software), transmission type (unidirectional and bidirectional), application, and geography - global forecast to 2022, http://www.marketsandmarkets.com/Market-Reports/visible-light-communication-market-946.html," in *Markets and Markets*, Feb. 2017.

[7] M. Zhang and Z. Zhang, "An optimum DC-biasing for DCO-OFDM system," *IEEE Commun. Lett.*, vol. 18, no. 8, pp. 1351–1354, Aug 2014.

[8] J. Armstrong and A. J. Lowery, "Power efficient optical OFDM," *Electronics Letters*, vol. 42, no. 6, pp. 370–372, March 2006.

[9] Y. Hong, J. Chen, Z. Wang, and C. Yu, "Performance of a precoding MIMO system for decentralized multiuser indoor visible light communications," *IEEE Photon. J.*, vol. 5, no. 4, 2013.

[10] Z. Yu, R. Baxley, and G. Zhou, "Multi-user MISO broadcasting for indoor visible light communication," in *IEEE International Conf. on Acoustics, Speech and Signal Processing (ICASSP) 2013*, 2013, pp. 4849–4853.

[11] J. Chen, Y. Hong, X. You, H. Zheng, and C. Yu, "On the performance of MU-MIMO indoor visible light communication system based on THP algorithm," in *2014 IEEE International Conf. on Commun. in China (ICCC)*, 2014, pp. 136–140.

[12] S. H. Chen and C. W. Chow, "Color-shift keying and code-division multiple-access transmission for RGB-LED visible light communications using mobile phone camera," *IEEE Photon. J.*, vol. 6, no. 6, pp. 1–6, 2014.

[13] C. Chen, D. Tsonev, and H. Haas, "Joint transmission in indoor visible light communication downlink cellular network," in *2013 IEEE Global Commun. Conf. (GLOBECOM)*, 2013, pp. 1127–1132.

[14] D. Bykhovsky and S. Arnon, "Multiple access resource allocation in visible light communication systems," *J. Lightw. Technol.*, vol. 32, no. 8, pp. 1594–1600, 2014.

[15] Y. Wang, L. Tao, X. Huang, J. Shi, and N. Chi, "Enhanced performance of a high-speed WDM CAP64 VLC system employing volterra series-based nonlinear equalizer," *IEEE Photonics Journal*, vol. 7, no. 3, pp. 1–7, June 2015.

[16] T. Yamazato, A. Ohmura, H. Okada, T. Fujii, T. Yendo, S. Arai, and K. Kamakura, "Range estimation scheme for integrated I2V-VLC using a high-speed image sensor," in *2016 IEEE International Conference on Communications Workshops (ICC)*, May 2016, pp. 326–330.

[17] K.-I. Ahn and J. K. Kwon, "Capacity analysis of M-PAM inverse source coding in visible light communications," *J. Lightw. Technol.*, vol. 30, no. 10, pp. 1399–1404, 2012.

[18] R. Lee, K. Yun, J.-H. Yoo, S. Y. Jung, and J. K. Kwon, "Performance analysis of M-ary PPM in dimmable visible light communications," in *2013 Fifth International Conference on Ubiquitous and Future Networks (ICUFN)*, July 2013, pp. 380–383.

[19] S. He, G. Ren, Z. Zhong, and Y. Zhao, "M-ary variable period modulation for indoor visible light communication system," *IEEE Commun. Lett.*, vol. 17, no. 7, pp. 1325–1328, 2013.

[20] T. Komine, J. Lee, S. Haruyama, and M. Nakagawa, "Adaptive equalization system for visible light wireless communication utilizing multiple white LED lighting equipment," *IEEE Trans. Wireless Commun.*, vol. 8, no. 6, pp. 2892–2900, 2009.

[21] P. Haigh, Z. Ghassemlooy, S. Rajbhandari, I. Papakonstantinou, and W. Popoola, "Visible light communications: 170 Mb/s using an artificial neural network equalizer in a low bandwidth white light configuration," *J. Lightw. Technol.*, vol. 32, no. 9, pp. 1807–1813, 2014.

[22] H. Li, X. Chen, B. Huang, D. Tang, and H. Chen, "High bandwidth visible light communications based on a post-equalization circuit," *IEEE Photon. Technol. Lett.*, vol. 26, no. 2, pp. 119–122, 2014.

[23] A. Azhar, T. Tran, and D. O'Brien, "A Gigabit/s indoor wireless transmission using MIMO-OFDM visible-light communications," *IEEE, Photon. Technol. Lett.*, vol. 25, no. 2, pp. 171–174, 2013.

[24] H. Elgala, R. Mesleh, and H. Haas, "Indoor optical wireless communication: potential and state-of-the-art," *IEEE Commun. Mag.*, vol. 49, no. 9, pp. 56–62, 2011.

[25] J. Lian and M. Brandt-Pearce, "Multiuser multidetector indoor visible light communication system," in *Opto Electron. and Commun. Conf.*, 2015.

[26] J. Lian, M. Noshad, and M. Brandt-Pearce, "Multiuser MISO indoor visible light communications," in *2014 Asilomar Conf. on Signals, Systems and Computers*, 2014 (Invited paper), pp. 1729–1733.

[27] J. Lian and M. Brandt-Pearce, "Distributed power allocation for indoor visible light communications," in *2015 IEEE Global Commun. Conf. (GLOBECOM)*, 2015.

[28] ——, "Multiuser MIMO indoor visible light communication system using spatial multiplexing," *Journal of Lightwave Technology*, vol. 35, no. 23, pp. 5024–5033, Dec 2017.

[29] ——, "Adaptive M-PAM for multiuser MISO indoor VLC systems," in *2016 IEEE Global Communications Conference (GLOBECOM)*, Dec 2016, pp. 1–6.

[30] ——, "Joint optimal waveform design for multiuser VLC systems over ISI channel," in *2016 IEEE International Conf. on Commun.*, May 2017, pp. 1–6.

[31] J. Lian, M. Noshad, and M. Brandt-Pearce, "M-PAM joint optimal waveform design for multiuser VLC systems over ISI channel," *submitted to Journal of Lightwave Technology.*

[32] ——, "Comparison of DCO-OFDM and M-PAM for LED-based communication system," *to be submitted to IEEE Commun. Lett.*

[33] J. Lian, X. Wang, M. Noshad, and M. Brandt-Pearce, "Optical wireless interception vulnerability analysis of visible light communication system," *Submitted to 2018 ICC.*

[34] Z. Ghassemlooy, W. Popoola, and Rajbhandari, *Optical Wireless Communications: System and Channel Modeling with Matlab.* CRC Press, 2013.

[35] J. Kahn and J. Barry, "Wireless infrared communications," *Proceedings of the IEEE*, vol. 85, no. 2, pp. 265–298, Aug 1997.

[36] K. Lee and H. Park, "Channel model and modulation schemes for visible light communications," in *2011 IEEE 54th International Midwest Symposium on Circuits and Systems (MWSCAS)*, July 2011, pp. 1–4.

[37] K. Ying, H. Qian, R. J. Baxley, and S. Yao, "Joint optimization of precoder and equalizer in MIMO VLC systems," *IEEE J. on Selected. Areas in Commun.*, vol. 33, no. 9, pp. 1949–1958, Sept 2015.

[38] L. Zeng, D. C. O'Brien, H. L. Minh, G. E. Faulkner, K. Lee, D. Jung, Y. Oh, and E. T. Won, "High data rate multiple input multiple output (MIMO) optical wireless communications using white LED lighting," *IEEE J. on Selected Areas in Commun.*, vol. 27, no. 9, pp. 1654–1662, December 2009.

[39] M. Biagi, A. M. Vegni, S. Pergoloni, P. M. Butala, and T. D. C. Little, "Trace-orthogonal PPM-space time block coding under rate constraints for visible light communication," *J. Lightw. Technol.*, vol. 33, no. 2, pp. 481–494, Jan 2015.

[40] H. Ma, L. Lampe, and S. Hranilovic, "Coordinated broadcasting for multiuser indoor visible light communication systems," *IEEE Trans. on Commun.*, vol. 63, no. 9, pp. 3313–3324, Sept 2015.

[41] T. V. Pham, H. Le-Minh, and A. T. Pham, "Multi-user visible light communication broadcast channels with zero-forcing precoding," *IEEE Trans. on Commun.*, vol. 65, no. 6, pp. 2509–2521, June 2017.

[42] R. Feng, M. Dai, H. Wang, B. Chen, and X. Lin, "Linear precoding for multiuser visible-light communication with field-of-view diversity," *IEEE Photon. J.*, vol. 8, no. 2, pp. 1–8, April 2016.

[43] B. Lin, X. Tang, Z. Ghassemlooy, C. Lin, and Y. Li, "Experimental demonstration of an indoor VLC positioning system based on OFDMA," *IEEE Photon. J.*, vol. 9, no. 2, pp. 1–9, April 2017.

[44] H. Kazemi and H. Haas, "Downlink cooperation with fractional frequency reuse in DCO-OFDMA optical attocell networks," in *2016 IEEE International Conference on Communications (ICC)*, May 2016, pp. 1–6.

[45] M. Guerra-Medina, O. Gonzalez, B. Rojas-Guillama, J. Martin-Gonzalez, F. Delgado, and J. Rabadan, "Ethernet-OCDMA system for multi-user visible light communications," *Electron. Lett.*, vol. 48, no. 4, pp. 227–228, 2012.

[46] C. He, L. liang Yang, P. Xiao, and M. A. Imran, "DS-CDMA assisted visible light communications systems," in *2015 IEEE International Workshop on Computer Aided Modelling and Design of Communication Links and Networks (CAMAD)*, 2015, pp. 27–32.

[47] S. Xie and C. Zhang, "Code division multiple access based visible light communication in vehicle adaptive cruise control under emergency situation," in *2013 IEEE International Conf. on Info. and Auto.*, 2013, pp. 219–224.

[48] H. Ghafouri-Shiraz and M. M. Karbassian, *Optical CDMA Network Principle, Analysis and Applications*. Wiley Press, 2012.

[49] I. E. S. of North America, *IESNA lighting handbook, 9th ed.*

[50] M. Noshad and M. Brandt-Pearce, "Hadamard-coded modulation for visible light communications," *IEEE Transactions on Communications*, vol. 64, no. 3, pp. 1167–1175, March 2016.

[51] J.-H. Jung, J. Lee, J.-H. Lee, Y.-H. Kim, and S.-C. Kim, "Ray-tracing-aided modeling of user-shadowing effects in indoor wireless channels," *IEEE Trans. Antennas and Propagation*, vol. 62, no. 6, pp. 3412–3416, 2014.

[52] D. Tsonev, H. Chun, S. Rajbhandari, J. McKendry, S. Videv, E. Gu, M. Haji, S. Watson, A. Kelly, G. Faulkner, M. Dawson, H. Haas, and D. O'Brien, "A 3 Gb/s single LED OFDM-based wireless VLC link using a gallium nitride μLED," *IEEE Photon. Technol. Lett.*, vol. 26, no. 7, pp. 637–640, 2014.

[53] J. Lian and M. Brandt-Pearce, "Adaptive M-PAM for multiuser MISO indoor VLC systems," in *2016 IEEE Global Commun. Conf. (GLOBECOM)*, 2016, pp. 1–7.

[54] Z. Zheng, T. Chen, L. Liu, and W. Hu, "Experimental demonstration of femtocell visible light communication system employing code division multiple access," in *Optical Fiber Commun. Conf. (OFC)*, 2015, pp. 1–3.

[55] Y. Chen, Y. Chang, Y. Tseng, and W. Chen, "A framework for simultaneous message broadcasting using CDMA-based visible light communications," *IEEE Sensors J.*, vol. 15, no. 12, pp. 6819–6827, 2015.

[56] Q. Wang, Z. Wang, and L. Dai, "Multiuser MIMO-OFDM for visible light communications," *IEEE Photon. J.*, vol. 7, no. 6, pp. 1–11, 2015.

[57] J. Grubor, S. Randel, K.-D. Langer, and J. Walewski, "Broadband information broadcasting using LED-based interior lighting," *J. Lightw. Technol.*, vol. 26, no. 24, pp. 3883–3892, 2008.

[58] B. Li, J. Wang, R. Zhang, H. Shen, C. Zhao, and L. Hanzo, "Multiuser MISO transceiver design for indoor downlink visible light communication under per-LED optical power constraints," *IEEE Photon. J.*, vol. 7, no. 4, pp. 1–15, 2015.

[59] L. Wu, Z. Zhang, J. Dang, and H. Liu, "Adaptive modulation schemes for visible light communications," *J. Lightw. Technol.*, vol. 33, no. 1, pp. 117–125, 2015.

[60] M. Biagi, A. M. Vegni, S. Pergoloni, P. M. Butala, and T. D. C. Little, "Trace-orthogonal PPM-space time block coding under rate constraints for visible light communication," *J. Lightw. Technol.*, vol. 33, no. 2, pp. 481–494, 2015.

[61] T. Mizuochi, Y. Miyata, T. Kobayashi, K. Ouchi, K. Kuno, K. Kubo, K. Shimizu, H. Tagami, H. Yoshida, H. Fujita, M. Akita, and K. Motoshima, "Forward error correction based on block turbo code with 3-bit soft decision for 10-Gb/s optical communication systems," *IEEE J. of Selected Topics in Quantum Electron.*, vol. 10, no. 2, pp. 376–386, 2004.

[62] Z. Chen and H. Haas, "Space division multiple access in visible light communications," in *2015 IEEE International Conf. on Commun. (ICC)*, 2015, pp. 5115–5119.

[63] K. Lee, H. Park, and J. R. Barry, "Indoor channel characteristics for visible light communications," *IEEE Commun. Lett.*, vol. 15, no. 2, pp. 217–219, February 2011.

[64] X. Huang, J. Shi, J. Li, Y. Wang, and N. Chi, "A Gb/s VLC transmission using hardware preequalization circuit," *IEEE Photon. Technol. Lett.,*, vol. 27, no. 18, pp. 1915–1918, 2015.

[65] Y. Wang, L. Tao, Y. Wang, and N. Chi, "High speed WDM VLC system based on multi-band CAP64 with weighted pre-equalization and modified CMMA based post-equalization," *IEEE Commun. Lett.,*, vol. 18, no. 10, pp. 1719–1722, 2014.

[66] A. Schmidt, R. Schober, and W. Gerstacker, "Single-carrier frequency-division multiple access transmission with physical layer network coding over ISI channels," in *2015 European Wireless Conf.*, May 2015, pp. 1–7.

[67] S. H. Song and K. B. Letaief, "Diversity analysis for linear equalizers over ISI channels," *IEEE Trans. on Commun.*, vol. 59, no. 9, pp. 2414–2423, September 2011.

[68] D. Lee and J. Kahn, "Coding and equalization for PPM on wireless infrared channels," in *1998 IEEE Global Commun. Conf. (GLOBECOM)*, 1998, pp. 201–206.

[69] M. Zhang, M. Shi, F. Wang, J. Zhao, Y. Zhou, Z. Wang, and N. Chi, "4.05-gb/s RGB LED-based VLC system utilizing PS-manchester coded nyquist PAM-8 modulation and hybrid time-frequency domain equalization," in *2017 Optical Fiber Commun. Conf. and Exhibition (OFC)*, March 2017, pp. 1–3.

[70] D. J. F. Barros, S. K. Wilson, and J. M. Kahn, "Comparison of orthogonal frequency-division multiplexing and pulse-amplitude modulation in indoor optical wireless links," *IEEE Transactions on Communications*, vol. 60, no. 1, pp. 153–163, January 2012.

[71] J. Du, W. Xu, H. Zhang, and C. Zhao, "Visible light communications using spatial summing PAM with LED array," in *2017 IEEE Wireless Communications and Networking Conference (WCNC)*, March 2017, pp. 1–6.

[72] J. M. Luna-Rivera, R. Perez-Jimenez, J. A. Rabadan-Borjes, J. F. Rufo-Torres, V. Guerra, and C. Suarez-Rodriguez, "Multiuser scheme for indoor visible light communications using RGB LEDs," in *2014 International Work Conf. Bio-inspired Intel. (IWOBI)*, 2014, pp. 119–123.

[73] M. Biagi, A. M. Vegni, and T. D. C. Little, "LAT indoor MIMO-VLC-localize, access and transmit," in *2012 International Workshop on Optical Wireless Commun. (IWOW)*, 2012, pp. 1–3.

[74] Y. Zhou, S. Liang, S. Chen, X. Huang, and N. Chi, "2.08 Gbit/s visible light communication utilizing power exponential pre-equalization," in *2016 25th Wireless and Optical Communication Conference (WOCC),*, 2016, pp. 1–3.

[75] K. Ying, H. Qian, R. J. Baxley, and S. Yao, "Joint optimization of precoder and equalizer in MIMO VLC systems," *IEEE J. Selec. Areas in Commun.*, vol. 33, no. 9, pp. 1949–1958, Sept 2015.

[76] K. H. Park, Y. C. Ko, and M. S. Alouini, "On the power and offset allocation for rate adaptation of spatial multiplexing in optical wireless MIMO channels," *IEEE Trans. on Commun.*, vol. 61, no. 4, pp. 1535–1543, April 2013.

[77] K. Deb, A. Pratap, S. Agarwal, and T. Meyarivan, "A fast and elitist multiobjective genetic algorithm: NSGA-II," *IEEE Transactions on Evolutionary Computation*, vol. 6, no. 2, pp. 182–197, Apr 2002.

[78] J. Armstrong, "OFDM for optical communications," *Journal of Lightwave Technology*, vol. 27, no. 3, pp. 189–204, Feb 2009.

[79] J. Classen, J. Chen, D. Steinmetzer, M. Hollick, and E. Knightly, "The spy next door: Eavesdropping on high throughput visible light communications," in *Proceedings of the 2nd International Workshop on Visible Light Communications Systems. ACM*, Sep 2015, pp. 9–14.

[80] A. Mostafa and L. Lampe, "Physical-layer security for indoor visible light communications," in *2014 IEEE International Conference on Communications (ICC)*, June 2014, pp. 3342–3347.

[81] ——, "Pattern synthesis of massive LED arrays for secure visible light communication links," in *2015 IEEE International Conference on Communication Workshop (ICCW)*, June 2015, pp. 1350–1355.

[82] D. Li, L. Zhang, and J. Qiu, "High security chaotic multiple access scheme for VLC systems," in *2016 26th International Telecommunication Networks and Applications Conference (ITNAC)*, Dec 2016, pp. 133–135.

[83] G. Pan, J. Ye, and Z. Ding, "On secure VLC systems with spatially random terminals," *IEEE Communications Letters*, vol. 21, no. 3, pp. 492–495, March 2017.

[84] F. J. Lopez-Martinez, G. Gomez, and J. M. Garrido-Balsells, "Physical-layer security in free-space optical communications," *IEEE Photonics Journal*, vol. 7, no. 2, pp. 1–14, April 2015.